Aus dem Institut für Chirurgische Forschung
im Walter-Brendel-Zentrum für Experimentelle Medizin
Klinik der Universität München
Leiterin: Prof. Dr. Daphne Merkus
ehem. Leiter: Prof. Dr. Ulrich Pohl

Maturation of human induced pluripotent stem cell based myocardium by biomechanical stimulation of three-dimensional tissue cultures

Dissertation
zum Erwerb des Doktorgrades der Medizin
an der Medizinischen Fakultät der
Ludwig-Maximilians-Universität zu München

vorgelegt von

Lu, Kun

aus

Shaanxi, China

2023

Mit Genehmigung der Medizinischen Fakultät
der Universität München

Berichterstatter:	Prof. Dr. Andreas Dendorfer
Mitberichterstatter:	Prof. Dr. Sabine Steffens Prof. Dr. Dominik Paquet Prof. Dr. Annette Müller-Taubenberger
Mitbetreuung durch den promovierten Mitarbeiter:	Prof. Dr. Christian Schulz
Dekan:	Prof. Dr. med. Thomas Gudermann
Tag der mündlichen Prüfung:	15.06.2023

Meinen Eltern und meiner Frau Shi Wei

in Dankbarkeit gewidmet

CONTENTS

Zusammenfassung

Künstlich hergestellte Herzgewebe (Engineered heart tissues, EHTs) aus menschlichen induzierten pluripotenten Stammzellen (hiPSC-CMs) haben ein großes Potenzial für die Erforschung von Herzmuskelphysiologie und -krankheiten, aber die strukturelle und funktionelle Unreife bringt immer noch Einschränkungen mit sich. Eine physiologische, biomechanische Stimulation ist für die Aufrechterhaltung der Funktion und Lebensfähigkeit des Herzmuskelgewebes über lange Zeiträume sowie für die Entwicklung und Reifung des Herzmuskels während der Wachstumsphase unerlässlich. In Vorarbeiten unserer Arbeitsgruppe wurde ein Bioreaktor entwickelt, der eine umfassende Simulation der kardialen Biomechanik ermöglicht (Fischer et al., 2019). Es wird untersucht, inwieweit die damit mögliche biomimetische Gewebekultur die Kontraktilität und Struktur des adulten menschlichen Myokards bewahren kann und ob aus Stammzellen gewonnenes künstliches Myokardgewebe unter diesen Bedingungen die Struktur und physiologische Funktion des adulten Myokards besser erreicht.

Auf dieser technischen Grundlage ermöglichte der eingesetzte Bioreaktor eine kontrollierte Einwirkung von externen Kräften auch bei Wachstum des Herzmuskels und eine kontinuierliche elektrische Stimulation. Daher wurde dieses biomimetische Modell mit mechanischer Simulation auf der Grundlage der ersten Arbeiten auch auf künstliches Herzgewebe (EHTs) angewendet.

Frühere Studien zur mechanischen Konditionierung von EHTs berücksichtigten selten die Anpassungsfähigkeit der Gewebeausdehnung. Daher konnten diese Studien das postnatale hypertrophe Wachstum des Herzmuskels nur unzureichend rekonstruieren. Aus diesem Grund wurde eine neue Methode der Gewebebildung mit einer höheren Zelldichte und einer natürlicheren extrazellulären Matrix entwickelt.

Die auf diese Weise aus humanen induzierten pluripotenten Stammzellen (iPSCs) erzeugten EHTs wurden einer mechanischen Stimulation und einer sukzessiven Dehnung in einer biometrischen Kultur unterzogen, die an das Wachstum des menschlichen Herzmuskels angepasst ist. Während der dreiwöchigen Konditionierung entwickelten die EHTs eine signifikante Verbesserung der Muskelstruktur und eine robuste Kontraktionskraft, die mit der des menschlichen Herzmuskels vergleichbar ist. Dies führte auch zu dynamischen funktionellen Eigenschaften, die für menschliches Myokard charakteristisch sind, einschließlich eines positiven Kraft-Frequenz- und Kraft-Dehnungs-Ver-

hältnisses (Frank-Starling-Mechanismus). Darüber hinaus führte die progressive Dehnung auch zu einem Längenwachstum und einer linearen Ausrichtung der Kardiomyozyten. Sie verbesserte die Dichte und Reifung der Sarkomere und beeinflusste auch die Genexpression.

Zusammenfassend zeigt diese Dissertation, wie wichtig eine biomimetische Kultur mit mechanischer Konditionierung für die Erhaltung und Entwicklung von Herzgewebe *in vitro* ist. Progressive Dehnung fördert die mechanische, elektrische und strukturelle Reifung von auf hiPSC-CMs basierenden EHTs, möglicherweise durch Rekapitulation der postnatalen Herzentwicklung. Die Einbeziehung der Dehnung in die biomimetische Gewebekultur führt zu EHTs mit zunehmender Größe und biomechanischer Leistung, die der des erwachsenen menschlichen Myokards nahekommt. Der neuartige Tissue-Engineering-Ansatz erfüllt wichtige Anforderungen der Krankheitsmodellierung und des therapeutischen Gewebeersatzes.

Die integrierte biomimetische Methode mit der Funktion der mechanischen Konditionierung beschleunigt nicht nur die Herstellung fortschrittlicher menschlicher EHTs, sondern hat auch das Potenzial, Erkenntnisse über die Biomechanik des Herzens zu liefern. Daher kann die biomimetische Kultur die Möglichkeiten der Grundlageforschung der angewandte Zelltherapie bedeutend erweitern.

Summary

Engineered heart tissues (EHTs) from human induced pluripotent stem-cell-derived cardiomyocytes (hiPSC-CMs) show considerable potential in myocardial physiology and disease research, yet structural and functional immaturity still entails restrictions. Physiological, biomechanical stimulation is essential for maintaining the function and viability of cardiac muscle tissue over long periods of time and governs the development and maturation of cardiac muscle during the growth phase. In the preliminary work of our group, we have developed a bioreactor that provides a comprehensive simulation of cardiac biomechanics (Fischer et al., 2019). It is investigated the extent to which the biomimetic tissue culture that this allows can preserve the contractility and structure of adult human myocardium, and whether stem cell-derived artificial myocardial tissue better approximates the structure and physiological function of adult myocardium under these conditions.

On this technical basis, the applied bioreactor allowed the controllable application of external forces with the growth of the myocardium and continuous electrical stimulation. Therefore, based on the initial work, this biomimetic model with mechanical simulation was also applied to engineered heart tissue (EHT).

Previous studies on mechanical conditioning of EHTs rarely considered the adaptability of tissue expansion. Therefore, these studies could inadequately reconstruct postnatal hypertrophic growth of the myocardium. To address this, a new method of tissue formation was developed with a higher cell density and a more natural extracellular matrix.

EHTs generated in this approach using human induced pluripotent stem cells (iPSCs) were subjected to mechanical stimulation and successive elongation in biomimetic culture, adapted to the growth of human myocardium. During three weeks of conditioning, the EHTs developed significant improvement in muscle structure and robust contractile force comparable to that of adult human myocardium. This also resulted in dynamic functional properties characteristic of the adult human cardiac muscle, including positive force-frequency (i.e. FFR) and force-stretch relationships. In addition, progressive stretch also induced length growth along with linear alignment of cardiomyocytes. It improved sarcomere density, maturation, and affected gene expression.

In conclusion, this dissertation demonstrates the importance of biomimetic culture with mechanical conditioning for the maintenance and development of heart tissue in vitro. Progressive stretch promotes mechanical, electrical, and structural maturation of

hiPSC-CMs based EHTs potentially by recapitulation of postnatal heart development. Inclusion of stretch in biomimetic tissue culture yields EHTs with increased size and biomechanical performance close to that of adult human myocardium. The innovative tissue-engineering technique accommodates essential requirements for disease modeling or even therapeutic tissue replacement.

This integrated biomimetic method with the feature of mechanical conditioning not only accelerates the production of advanced human EHTs, but also has the potential to provide insights into cardiac biomechanics. Therefore, biomimetic culture may significantly expand the possibilities of basic research of applied cell therapy.

List of figures

List of tables

List of abbreviations

AP	Action potential
Akt1	Rho family - alpha serine/threonine-protein kinase
ANP	Atrial natriuretic peptide
BNP	Brain natriuretic peptide
BMCCs	Biomimetic culture chambers
Ca^{2+}	Calcium
cTNT	Cardiac troponin
CM	Cardiomyocyte
Cx43	Connexin 43
DF	Diastolic force
EHT	Engineered heart tissue
ESC-CM	Embryonic stem cell-derived cardiomyocyte
FFR	Force-frequency-relationship
GAPDH	Glyceraldehyde-3-phosphate-dehydrogenase
hiPSC-CM	Human induced pluripotent stem cell-derived cardiomyocyte
iPSC	Induced pluripotent stem cell
iPSC-CM	Induced pluripotent stem cell-derived cardiomyocyte
LDH	Lactate dehydrogenase
MHC	Myosin heavy chain
MYH7	Myosin Heavy Chain 7
PPAR-alpha	Peroxisome proliferator activated receptor alpha
PDMS	Polydimethylsiloxane
PV-loop	Pressure-volume loop
RMP	Resting membrane potential
SD	Standard deviation
SEM	Standard error of the mean
SERCA2a	Sarcoplasmic/endoplasmic reticulum Ca^{2+} - ATPase 2a

1. INTRODUCTION

1.1 Background

Cardiovascular diseases remain the leading cause of death worldwide. Chronic manifestations of the disease typically affect the pumping function of the heart and drive the myocardium into a vicious circle of overload and remodeling. Research on the pathomechanisms of heart failure requires experimental models with various grades of complexity, among which multi-factorial *in vitro* models of human myocardium (e.g., myocardial tissue slices and engineered myocardium) may ideally complement animal experiments. Artificial myocardium, engineered from induced pluripotent stem cells in particular, holds great promises to promote heart failure diagnostics and therapy, and may even provide tissue substitutes to support the pumping action of the diseased myocardium. There is no doubt that the clinical translational research and development of cardiac cell graft-based treatment strategies will greatly benefit from the further development of these *in vitro* approaches. Scientists will be able to evaluate the viability, phenotype, maturation level, and contractility of cardiomyocytes ever more reliably, the better the experimental conditions are able to mimic the *in vivo* environment.

Since iPSC-CMs and EHT are one of the most potential future treatment strategies, significant efforts should be made to understand their biology and experimental applications. Any advances to improve the maturation of the fetal-like iPSC-CM to an adult phenotype would significantly help researchers to utilize iPSC-CMs as cell sources in the field of tissue engineering and regenerative medicine, including developing of organs-on-a-chip systems.

A suitable biomechanical environment is considered to be a crucial factor for cardiomyocyte maturation. The heart develops under a certain biomechanical impact. It functions optimally within a particular hemodynamic load range, and it fails in situations of acute or chronic overload. Previous studies have shown that insufficient mechanical load can cause abnormal cardiogenesis, which provides further evidence for the importance of biomechanical stimuli during heart development and maturation (Hove et al. (2003). As such, a multifactorial bioreactor system that mimics the *in vivo* biomechanical environment may be a key factor for the maturation of engineering myocardium and may also lay a foundation for its scale-up and clinical application.

In the present dissertation, the importance and technical implementation of biomechanical conditions for the tissue culture of stem cell-derived myocardium were investigated. The development of a custom-made biomimetic cultivation chamber (BMCC) enabled the optimization of biomechanical conditions for the long-term maintenance of adult myocardium *in vitro*, and the modification of these conditions permitted the improvement of iPSC-CMs' maturation by progressive mechanical loading.

1.2 Physiology of cardiac biomechanics

Cardiac biomechanics describe the myocardial properties and conditions under which the heart performs its pumping function. Biomechanical factors such as wall stress, tissue compliance, and cardiomyocyte distension typically determine the contractile performance of the heart. The myocardium adapts to changes in these factors by altering the cellular structure, gene expression, and tissue composition. The aim of the present studies is to generate biomechanical conditions *in vitro* to maintain the physiological function and structure of the cultured myocardium. For the design of an appropriate *in vitro* environment, it is necessary to understand the mechanical stimuli to which the myocardium is subjected *in vivo*. The major external mechanical stimuli of interest to the heart are typically described as preload (volume load) and afterload (pressure load). Preload is defined as the ventricular wall stress at the end of the ventricular filling during diastole (i.e., the forces applied on the distended cardiac muscle wall). These forces are directly related to the extent of ventricular filling and myocardial diastolic compliance. Preload affects contractile forces by determining the sarcomere length of cardiac myofibrils prior to contraction. Afterload is the stress that the heart generates to eject blood during systole (ventricular contraction). As such, afterload is determined by the individual arterial blood pressures and the muscle mass of the left and right ventricles, respectively. Afterload, in concert with systolic shortening, represents the external physical work of the heart muscle. The entire contraction period is most effectively represented by a pressure-volume loop (PV-loop) with distinct stages of isotonic and isovolumetric contraction through systole, and relaxation through diastole. Abnormal changes in preload or afterload will cause pathological changes of the myocardium, which in turn will lead to heart disease (Toischer et al., 2010).

Cardiac myocytes generate contraction force by the interaction of their thick and thin myofilaments. The interaction is critically dependent on the physical overlap of the myofilaments and the number of actin-myosin cross-bridges established between them. The latter parameter is determined by the Ca^{2+}-related activation of troponin C, and is promoted when thick and thin filaments are at short distance (Huxley, 1969). Hence, the contraction force produced by a single myocardial fiber is directly related to the sarcomere length. Shorter sarcomere length causes calcium sensitivity to decrease, while longer sarcomeres impede myofilament overlap (Allen and Kentish, 1985, Huxley and Hanson, 1954, Huxley and Niedergerke, 1954). Since the average sarcomere distances determine the length of a cardiomyocyte, it can generate its highest active tension when contraction is evoked at optimum diastolic length.

In vivo, diastolic filling of the ventricle (end-diastolic volume) stretches the cardiomyocytes and determines the sarcomere length of fibers. This results in length-dependent activation (Frank-Starling Law) (Kobirumaki-Shimozawa et al., 2014), which is a central factor in determining the overall myocardial contractile force (Stephenson et al., 1989, Allen and Kentish, 1985, Stephenson and Williams, 1982). Thanks to this mechanism, the native heart can intrinsically accommodate an increase in venous return, at any heart rate (Moss and Fitzsimons, 2002). *In vitro*, length-dependent activation importantly influences the contractility of cardiomyocytes. Early studies showed that the Frank-Starling Law is still present and maintained in isolated human left ventricular myocardium from healthy as well as diseased hearts. An increase in sarcomere length also leads to a sensitization of contractile proteins (Vahl et al., 1997, Holubarsch et al., 1996). Our own results obtained in human heart slice preparations indicate a well-preserved Frank-Starling Law within the physiological range of strain (i.e. ≤ 1 mm of stretch, corresponding to ≤ 20 % of distension). The actively developed systolic force (twitch force, TF) reaches the 6-fold value of the diastolic force (DF) (Fischer et al., 2019). This ratio resembles the physiological conditions of systolic and diastolic wall stress, and can be interpreted as an indicator of myocardial function. A reduction of the TF: DT ratio may be caused be impairment of contraction force or increased muscle stiffness, which both are pathophysiological features observed in heart failure.

As for the growth and differentiation of engineered myocardium, the importance of appropriate preload has been noticeable since the early advents of cardiac tissue engineering. Despite that, the TF: DT ratio even of highly elaborated EHTs does not reach the levels of mature myocardium (e.g., TF: DT = 2:1, (Ruan et al., 2016)). This reflects

shortcomings in the tissue structure of EHTs and of the cellular maturation of iPSC-derived cardiomyocytes, and thus, has been chosen as a primary parameter for the evaluation of tissue maturation in our studies. Another hallmark mechanism of healthy adult myocardium is the Bowditch-effect (known as the positive force-frequency relationship), which is an autoregulation mechanism by which myocardial contractility increases when the heart rate increases (Usman et al., 2020, Endoh, 2004). This response reflects a well-coordinated excitation-contraction coupling, and depends on a highly compartmentalized cycle of intracellular cytosolic Ca^{2+} release and sequestration. Myocardium with immature characteristic or pathological changes, on the other hand, displays a suppressed maximum or even a decline of contraction force at higher beating rates (Wiegerinck et al., 2009, Crozatier, 1998, Alpert et al., 1998, Mulieri et al., 1992).

The present studies are based on close imitations of the natural biomechanical environment, provided by a technically feasible bioreactor. To account for the importance of pre-and afterload, a model of elastic muscle contraction was established that determined afterload by a fixed relationship of contraction force and muscle shortening, and that generated preload by application of an adjustable stretch to the cultured tissue.

1.3 Biomechanics for cardiogenesis and postnatal hypertrophy

The *in vitro* generation of artificial myocardium follows the general concept of replicating cardiogenesis and postnatal hypertrophy, with the aim to drive the differentiation of dedicated stem cells to that of mature cardiomyocytes. Since mechanical forces govern almost all steps of this process, the present study assumes that proper biomechanical conditions might improve the maturation of artificial stem cell-derived myocardium. Here, the impact of biomechanics on heart development is described as a rationale for this hypothesis and as an explanation for the particular biomechanical stimulation employed in this study.

A primitive heart tube establishes when two separate masses of cardiac mesoderm migrate to the ventral midline and meet to form a sunken structure. The actin microfilaments contract asymmetrically to form a cylindrical bend of the epithelial cells leading to a hollow tube (Bartman and Hove, 2005, Taber, 1998). Way before the sarcomeres develop and blood flow is established, fetal cardiomyocytes in the early heart tube start to contract spontaneously and asynchronously (Lindsey et al., 2014). Although the mechanism behind this spontaneous contraction has not yet been discovered, studies

have shown that the early contractions drive sarcomere-genesis and cause hemodynamic forces to develop. Geach et al. reported that suppressing muscular contraction *in vivo* utilizing either small-molecule inhibitors or a mutation of the UNC45B (Unc-45 Myosin Chaperone B, a co-chaperone required for the folding and accumulation of type II myosins) induces comparable abnormalities in Z-disc formation, highlighting the great importance of contractility in very early phases of sarcomere development (Geach et al., 2015). Bartman et al. evaluated the various contributions of myocardial contraction as well as blood flow-induced shear strain in zebrafish embryos' cardiogenesis. They experimented with different concentrations of 2,3-butanedione monoxime in order to modify the level of myofibril inhibition and then analyzed the resulting effect that had on blood flow. Cardiac muscle function declined significantly in a dose-dependent fashion with myofiber inhibition, and also the proportion of embryos that formed endocardial rings at 48 hours post-fertilization furthermore decreased, which indicates that shear stress and myocardial contraction both contribute to the process of cardiogenesis (Mironov et al., 2005, Bartman et al., 2004).

As soon as the initial cardiac contractions are established, the looping process ensues immediately. Actin polymerization, myosin II activation, and nodal-mediated cell shape changes further take part in the bending and looping procedure (Noel et al., 2013, Latacha et al., 2005). An increase in hemodynamic force, as an extrinsic mechanical stimulus, further causes the heart loop to twist and rotate (Wyczalkowski et al., 2012). Undergoing a complex process that continuously changes the topography and physically alters the cellular architecture, the heart then transforms from a simple linear tubular structure to a four-chambered heart (Manner, 2009, Bartman and Hove, 2005). The looping process and chamber expansion resulted in the cells on the outer surface formation of elongated convex architectures, whereas the cells on the internal surface continued to take on a cuboidal form (Auman et al., 2007, Manasek et al., 1972), indicating that cell shape-changing by mechanical forces are crucial in cell fate decisions and already happen prior to cardiomyocyte maturation.

During the late fetal cardiomyocyte stage of heart chamber formation involving trabeculation and compaction of the myocardium, the influence of mechanical tension is more prominent. The myocardial wall is subjected to a gradient of tension decreasing from the highest tension at the inner layer across the myocardial wall (Damon et al., 2009). With the increase of hemodynamics, transmural pressure gradually triggers myocardial

growth which includes myocardial wall thickening, fibroblast proliferation, and extracellular matrix production (Ivey et al., 2018, Kowalski et al., 2014, Tao et al., 2012, Intengan et al., 1999). Chick embryonic hearts exposed to left atrial ligation (elevated preload in the right ventricle and reduced preload in the left ventricle) demonstrate hypoplasia of the left heart constructions with compensating overdevelopment on the right side, suggesting that appropriate mechanical loading is crucial for proper cardiac morphogenesis and also the transformation of natural myocardial patterns (Sedmera et al., 1999). After birth, the further development and maturation of the myocardium are mainly characterized by an early cessation of myocyte proliferation and prolonged physiological hypertrophy, which also leads to multinucleation in human cardiomyocytes (Nakamura and Sadoshima, 2018, Paradis et al., 2014, Tiburcy et al., 2011).

In general, mechanical stimuli play a vital role in every stage of cardiomyocyte and heart development. From the perspective of tissue engineering, it is supposed to generate "realistic" heart muscle models and also surrogate tissue for myocardial repair. EHTs should exhibit characteristics of natural hearts for all of these applications, which include terminal differentiation, organotypic maturation, and physiological hypertrophic growth.

1.4 Biomechanical approaches to promote cardiomyocytes maturation

The spontaneous differentiation of stem cells *in vitro* yields – among others - cardiomyocytes, which - to date - do not develop an adult phenotype and resemble the differentiation and structure of fetal myocardium. The many attempts to improve maturation including nutrition, growth factors, electrical stimulation, and the optimization of biomechanical conditions have already yielded tremendous advances.

In monolayer cultures of cardiomyocytes, the only possible way to manipulate mechanical conditions is the use of adhesion substrates with different mechanical properties. Studies on isolated cardiomyocytes showed that modifications in substrate stiffness co-occur with adaptations in cellular function and growth (Gershlak et al., 2013, Jacot et al., 2010). Obviously, isolated cardiomyocytes coated on substrates of different material characters sense the physical properties of their attachment substrate and modify their cellular phenotype and gene expression, enabling the use of stiffness as a tunable property for *in vitro* manipulating CM function.

A greater potential for the simulation of accurate biomechanics is provided by three-dimensional engineered heart tissue (EHT) that develops directed forces via cell-cell and cell-matrix interactions. It more closely resembles intact myocardium in terms of the cytoskeletal arrangement, availability of nutrients, and excitation conduction. For the exploitation of these prospects, scientists have developed many different *in vitro* systems with a variety of methodologies.

The most studied concept is based on the cyclic passive mechanical distension of an EHT. This method imitates the geometry of muscle contraction using a motorized rod that forces the EHTs to change their length periodically. Eschenhagen's group designed one of the first heart tissue bioreactors capable of cyclic mechanical stretching twenty years ago (Zimmermann et al., 2000, Fink et al., 2000). Utilizing isolated neonatal rat cardiomyocytes, they generated a primitive engineered tissue construct with a maximum twitch force of 0.5 mN. The rhythmically stretched EHTs demonstrated an increased contraction force with prolonged culture duration and exhibited distinct force-length and force-frequency relationships, which can be considered as a big step forward to tissue maturation. Subsequent studies with varying cell sources, tissue matrix, and bioreactor design demonstrated an increased cell and myofilament length, and improvements in cellular structures such as myofibril alignment, mitochondrial density, and cell-cell junctions (Zimmermann et al., 2002, Akhyari et al., 2002).

The next step toward more physiological biomechanics was taken with the introduction of active contraction of artificial muscle against stiff or elastic resistances. Suitable EHTs were based on cardiomyocytes suspended in a hydrogel of extracellular matrix proteins that was poured into a model groove containing two sagittal attached rods. Within some days, the cells interact with the matrix, and the tissue condensed and detached from the inner wall of the gutter. Embedded in the compact tissue, two rods function as the fulcrum of mechanical contraction.

If the two rods cannot deform, then the contraction will be isometric, while rods of lower stiffness (e.g., based on PDMS - Polydimethylsiloxane) will define an elastic contraction. Since the diastolic tension of the tissue is generated spontaneously by tissue compaction, this mode of preload generation can be considered as constant stretch or static loading. Based on this concept, the maturation of EHTs made significant progress. Groups like Legant et al.; Bouduo et al., and Galie et al. fabricated small-size EHTs with the help of two PDMS posts which permitted measurement of contraction forces through

the determination of their deflection (Galie et al., 2015, Boudou et al., 2012, Legant et al., 2009).

Cultivation of EHTs under static load improved maturation of the tissues (Abilez et al., 2018) and enabled investigation of the tissue response to various intensities of afterload. Hirt et al. replaced the soft PDMS posts with metal braces to mimic increased afterload, and thereby provoked myocyte hypertrophy (Hirt et al., 2012).

Murry's group adjusted afterload over two orders of magnitude by increasing the flexible post resistance and demonstrated that twitch forces of EHTs raised in accordance with the degree of afterload, whilst twitch velocities declined (Leonard et al., 2018). Moreover, a progressive increase of afterload also caused improvement of cardiomyocyte maturation, in terms of morphology, calcium transients, expression of several decisive markers, including a shift from fetal to adult ventricular myosin heavy chain (MYH) isoforms. Nonetheless, when afterload exceeded an optimum level, gene expression gradually showed the trend of pathological hypertrophy.

These studies evidenced that flexible loading is superior to the other less physiological loading regimes. However, the biological behaviors of static or cyclic stretch differ fundamentally from that of the myocardium in cardiogenesis, which grows in size, continuously. These studies settled conditions of fixed diastolic length and contraction against an elastic resistance as the state-of-the-art of EHT cultivation. While systolic force development (i.e., afterload) is determined by the elastic modulus, the diastolic tension (i.e. preload) is poorly defined. Since the final constructs have a fixed size, passive static or cyclic stretching will cause the tissue to stretch accordingly without increasing in size. This is of particular relevance for the maturation of iPSC-CM which cannot grow in length and volume, as they physiologically do in postnatal development.

So far, there is no method that considers the progressive growth in the size of the myocardium and at the same time precisely regulates the preload. The methodological difficulty is to accommodate the biomechanical load to the developmental stage-specific intrinsic contractile properties of ETHs to enable rather elastic to auxotonic contractions within the optimal range of the Frank-Starling curve.

1.5 Objective

It is evident that a multi-modal simulation of the physiological environment would be desired for myocardial tissue engineering. Naturally, each of the multiple bioreactor approaches to date has focused on specific technological features and tissue sources. The present thesis tries to combine key elements of these endeavors - biomechanical pre- and afterload, electrical pacing, and medium agitation in particular - in a unified approach of biomimetic tissue culture. Such a development is of high interest because suitable conditions might not only elucidate the growth pattern of myocardial tissue *in vitro* but could also be extended to stem cells, providing significant assistance in the production and maturation of artificial myocardium. A requirement for this versatility would be a free control and adaptation of the conditions to the tissue models, given the changes of heart rate and hemodynamic load that occur during heart development. Most importantly, the maturation of embryonal to adult myocardium proceeds in parallel to extensive growth and cellular hypertrophy which have to be accounted for by a model that is intended to replicate this process *in vitro*.

In the previous work of our group (Fischer et al., 2019), we already showed that modeling tissue mechanics by application of uni-directional forces was a substantial requirement for the maintenance of adult human myocardium in culture. Identically prepared myocardial slices exhibited severe functional degeneration when cultured in the absence of mechanical stress and electrical stimulation. By fine-tuning biomechanical parameters to resemble a moderate diastolic ventricular pressure, slack tissues' sarcomere length could be maintained. Assessment of sarcomere length in slices under the specified preload suggested that diastolic strain was within the physiologic range. Furthermore, the conditions of biomimetic culture were optimized for the maintenance of physiological cardiac contractility.

Thus, the following questions were addressed:

1. How could tissue growth-adapted biomimetic stimulation be implemented? What is the best way to implement favorable biomimetic and mechanical conditions for the maturation of EHT and which parameters will be optimized?
2. How to generate EHTs accommodated this type of stimulation, or what specifications may the new methodology have for EHT generation?
3. How will the EHT's maturity be impacted, and what parameters would be optimized?

2. MATERIALS AND METHODS

2.1 Materials

2.1.1 General Laboratory Devices and Equipments

Laminar flow	Thermo Fisher Scientific, USA
Cell culture incubator	
Centrifuge, Heraeus Megafuge 40R	
Cell culture incubator, BINDER CB160	BINDER, Germany
Centrifuge, Rotina 35R	Hettich, Germany
Shaking water bath, SWB25	Thermo Haake, USA
Shaking air bath, UNIMAX 1010	Heidolph, Germany
Digital Vortex Mixer	VWR, USA
Countess Cell Counter	Life Technologies, USA
+4°C fridge	LIEBHERR, Germany
-20°C fridge	Privileg, Germany
-80°C fridge	Heraeus Holding GmbH, Germany
Thermo-Shaker, PCMT	Grant Instruments, UK
Flow cytometer, BD FACS Canto II	BD, USA
Inverted microscope	Zeiss, Germany
Rolera EM-C2 camera	Teledyne QImaging, Canada
Horizontal organ baths, Mayflower	Hugo Sachs Elektronik, Germany
BA-01X amplifier	NPI electronic, Germany
Simplinano Spectrophotometer	Biochrom, USA
StepOnePlus Real-Time PCR System	Applied Biosystems, USA
Cryostat, Leica CM3050 S	Leica, Germany

Confocal microscope, Leica SP8X WLL	Leica, Germany
Confocal microscope, Zeiss LSM780	Zeiss, Germany
Agilent 2100 Bioanalyzer System	Agilent, USA
Illumina HighSeq-2000 platform	Illumina, USA

2.1.2 hiPSC cell line

Cell line name	MRIi-004-A
Accession	CVCL_A8QA
Species of origin	Homo sapiens (NCBI Taxonomy: 9606)
Category	Induced pluripotent stem cell
Cell line databases/resources	hPSC-reg; MRIi-004-A
Comments	Klinikum rechts der Isar, Technical University of Munich; Munich; Germany. Derived from sampling site: Skin. Cell type=Fibroblast.

2.1.3 Cell culture medium and other supplements

IMDM	Gibco, USA
DMEM	Gibco, USA
DMEM X10	Gibco, USA
DMEM/F-12	Gibco, USA
Essential 8™ Medium	Gibco, USA
RPMI 1640	Gibco, USA
EHT culture medium	Custom made
EB6 medium	Custom made
B27 minus Insulin	Gibco, USA
MEM non-essential amino acids	Gibco, USA
Penicillin G sodium salt, P3032	Sigma Aldrich, USA
Streptomycin sulfate salt, S9137	Sigma Aldrich, USA
Penicillin-Streptomycin (10,000 U/mL)	Gibco, USA
Dexamethasone	Sigma Aldrich, USA
FGF-2, fibroblast growth factor-2	PEPROTECH, USA
IGF-1, insulin-like growth factor 1	PEPROTECH, USA
TGF-β1, transforming growth factor-β1	PEPROTECH, USA
VEGF165, vascular endothelial growth factor 165	PEPROTECH, USA
FBS Premium South America	PAN ™ Biotech, USA
beta-mercaptoethanol	Sigma Aldrich, USA
3,3`,5-triiodo-L-thyronine	Sigma-Aldrich, USA

Table 1. Custom made medium formulations

Medium name	Supplement	
EHT culture medium (base medium is IMDM, Gibco TM No. 12440061)	B27 minus Insulin (Gibco, A1895601), %	2
	MEM non-essential amino acids solution (Gibco™,11140050), %	1
	penicillin, U/mL	50
	streptomycin, µg/mL	50
	dexamethasone (Sigma Aldrich, D4902), µmol/L	1
	IGF-1 (PEPROTECH ,100-11), ng/mL	100
	FGF-2 (PEPROTECH, 100-18B), ng/mL	10
	VEGF165 (PEPROTECH, 100-20), ng/mL	5
	TGF-ß1 (PEPROTECH,100-21), ng/mL	5
EB6 medium (base medium is DMEM/F-12, Gibco ™ No. 11320033)	MEM non-essential amino acids (Gibco™,11140050), %	1
	penicillin, U/mL	50
	streptomycin, µg/mL	50
	fetal bovine serum, % FBS Premium South America; PAN ™ Biotech	6 (v/w)
	beta-mercaptoethanol, mmol/L	0.1

*Table adapted from Lu et al., 2021 with permission.

2.1.4 Chemical reagents

EDTA Versene solution	Gibco, USA
TrypLE Select Enzyme	Gibco, USA
Collagenase II	Sigma-Aldrich, USA
Bovine collagen I	Gibco, USA
Geltrex®, LDEV-Free	Gibco, USA
RevitaCell supplement	Gibco, USA
DPBS	Gibco, USA
4% paraformaldehyde	Sigma-Aldrich, USA
1% Triton X-100	Thermo Fisher Scientific, USA
Fetal bovine serum	Gibco,USA
Fluo-4, 5 µmol/L AM cell permeant (F14201)	Invitrogen, USA
Isoproterenol	Sigma-Aldrich, USA
HEPES-buffered Earle' s-salt solution	Sigma-Aldrich, USA
30% Sucrose solution	Sigma-Aldrich, USA
7.5% gelatin	Sigma-Aldrich, USA
Isopentane	Sigma-Aldrich, USA
Glycerol solution	Sigma-Aldrich, USA
Blocking solution (3% bovine serum albumin, + 1% fetal calf serum in PBS)	Custom made
DAPI, 2 µmol/L	Invitrogen, USA
CF™ Dye Wheat Germ Agglutinin (WGA) Conjugates 29024-1 CF™633	BioTium CF, USA
Fluoromount-G	Invitrogen, USA
Trizol	Life Technologies, USA
NaOH	Sigma-Aldrich, USA
MatriGel	Dow Corning, USA

2.1.5 Commercial kits

Essential 8™ Medium Kit	Gibco, USA
PSC Cardiomyocyte Differentiation Kit	Thermo Fisher Scientific, USA
RNeasy Mini Kit	Qiagen, Netherlands
QuantiTect ReverseTranscription Kit	Qiagen, Netherlands
SENSE Total RNA-Seq Library Prep Kit	Lexogen, Austria

2.1.6 Antibodies

First Antibodies	
cardiac troponin T, ab45932	Abcam, USA
Monoclonal anti-α-actinin, sarcomeric, 1:100, A7811	Sigma-Aldrich, USA
rabbit polyclonal MT-CO2 antibody, 1:50	Invitrogen, USA
rabbit anti-Connexin-43 antibody,1:100	Sigma-Aldrich, USA
Second Antibodies	
Alexa Fluor 488 anti-Rabbit IgG, A-21441, 1:100	Invitrogen, USA
Alexa Fluor 546 anti-Mouse IgG, A-11030, 1:100	Invitrogen, USA

2.1.7 Software

GraphPad Prism 7	California, USA
FlowJo	Treestar Inc., USA
Micro-Manager Studio Version 1.4	University of California San Francisco, USA
ImageJ	National Institute of Health, USA
WinEDR v3.8.6	University of Strathclyde, UK
PowerLab 4/20; LabChart Reader	ADInstruments, Dunedin, New Zealand
Zeiss ZEN Imaging Software	Zeiss, Germany
Leica LAS X Life Science	Leica, Germany
Illumina software BaseCaller	Illumina, USA

2.2 Methods

2.2.1 hiPSC-CMs cultivation and differentiation

Following the previously reported methodologies (Moretti et al., 2013) , the skin fibroblasts from a healthy human donor were reprogrammed in order to induce pluripotent stem cells (hiPSC). Here we appreciate Prof. Moretti and her group who provided this cell line (ID MRIi004-A). hiPSCs are cultured in 12-well plates (Costar, Corning) that have been pre-coated with basement membrane extract (Geltrex LDEV-Free, Gibco). Using E8 culture medium (Gibco), the hiPSCs reached appropriate confluency at 80%-85% after 4-5 days to perform the subsequent differentiation. A simplified differentiation strategy for hiPSC-CMs was modified from Chen and colleagues' work (Chen et al., 2011) by applying two types of chemically defined mediums (medium A for the first 24h of differentiation and medium B for subsequent 48h, PSC Cardiomyocyte Differentiation Kit; Gibco). After that, the hiPSC-CMs were continued to be cultured with Maintenance Medium (PSC Cardiomyocyte Differentiation Kit; Gibco) for another 8 days to achieve the beating state of monolayer cells. Refer to Figure 1 for detail workflow.

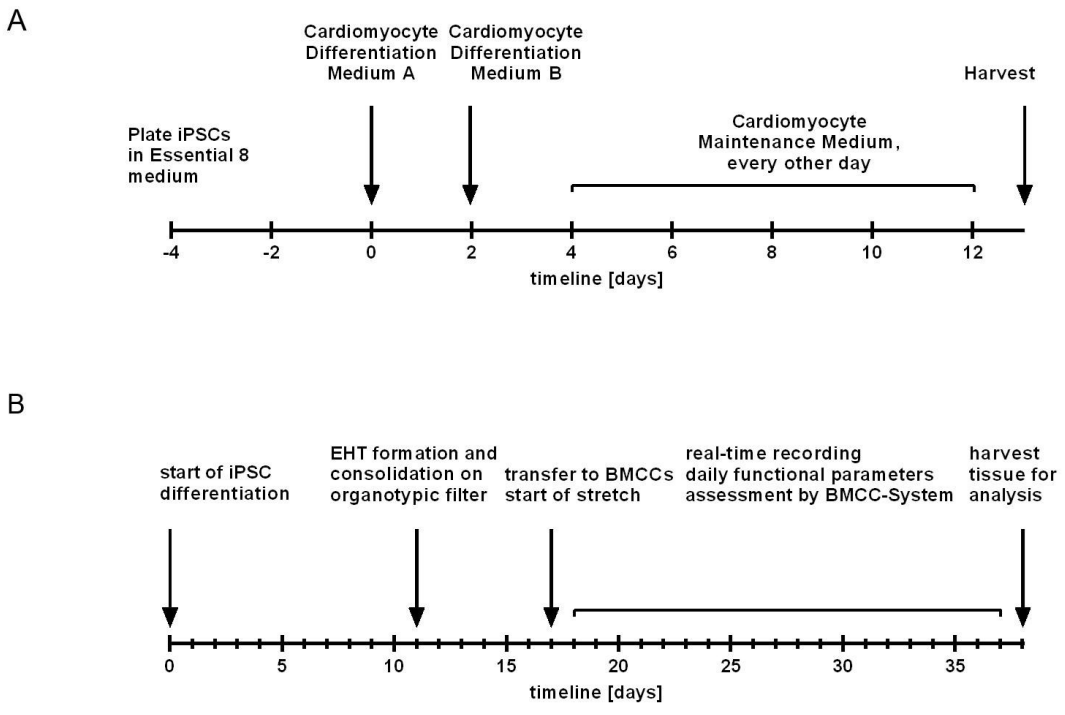

Figure 1. Experimental design

(A) The workflow of hiPSC-CMs cultivation and differentiation. (B) Experimental procedure. Adapted from Lu et al., 2021, with permission.

2.2.2 Formation of the primary tissue disc

Beating monolayers of hiPSC-CMs were successively dissociated with TrypLE™ (Tryp LE Select Enzyme, Gibco) for 8 mins and collagenase II for 7 mins (1.5 mg/mL, Sigma-Aldrich). Single cells were then resuspended in EB6 medium (Table 1. Custom-made medium formulations) to remove the collagenase II effects and then subjected to centrifugation for 5 min at 390 xg. The supernatant was then decanted, and a small amount of EB6 medium was added to re-solubilize the cell pellet. The high-density cell suspension was mixed with 0.55 mg/mL bovine collagen I (Gibco™) in a 1 ml Eppendorf capsule, following adding 0.08 mg/mL Geltrex (LDEV-Free, Gibco) and 1% Revita Cell supplement (modified from (Cashman et al., 2016)) to finally form a cell-matrix mixture with a cell concentration of 1.1×10^5 cells/µL. This mixture was then immediately pipetted onto a sterile 30 mm organotypic filter (PICMORG50, Merck Millipore). At this point, it is important that no air bubbles are produced, and that the disc-like structure formed is as close as possible to 8 mm in diameter and 2 mm in thickness. After the tissue disc's solidification, which took 30 minutes at 37 °C, 1 mL of EB-6 medium was pipetted below the filter. The medium was replaced every two days for a total of 5 days (Figure 1B and Figure 2).

2.2.3 Biomimetic culture chamber system (BMCC)

The biomimetic culture system developed by our group (biomimetic culture chambers, BMCCs) has already been applied to long-term maintain adult human ventricular myocardial slices *in vitro* in our previous work (Fischer et al., 2019). We implemented the established criteria as standardized conditions for EHT maturation because it had been proven that all biomimetic characteristics of the BMCCs, including defined preload, systolic tension, continuous electrical field stimulation, and medium agitation, are all vital for the consistent function of cultured adult human ventricular myocardial slices (Fischer et al., 2019).

As previously mentioned, (Fischer et al., 2019), the BMCCs offer elasticity attachment, length modification, bipolar field electrical stimulation, as well as continuous force monitoring through magnetic positioning measurement. Based on the unique properties of the EHT, such as the lower stiffness, and the special shape, we have re-adapted the BMCC to accommodate the incubation conditions. The modified BMCC chambers were constructed via injection-formed polystyrene (Proto Labs, Feldkirchen). A spring wire composed of stainless-steel (grade 1.4401) with a diameter of 0.16 mm was used to

produce an elastic compliance (elasticity) of 71 mm/N (Figure 2A). The contraction force generated by the EHTs was detected through the movement of a tiny magnet at the free end of the spring wire, whose magnetic field was sensed by an integrated three-D sensor (FXOS8700, NXP Semiconductors, USA). According to the spring wire constant, the value of contraction was computed. The two mounting posts for the EHT were coated with polyethylene tubes which had a flattened bottom end for convenient support of the tissues to prevent being cut off. These tubes had an outer diameter of 0.96 mm and were manufactured by Smiths Medical in Dublin, United States. EHTs in the BMCCs were electrically stimulated using bipolar, current-controlled electro pulse with a duration of 2 ms and a frequency of 1 Hz. These pulses were delivered by two graphite electrodes (6 x 8 mm^2, CG1290, CGC Klein, Germany), which were positioned on both longitudinal sides of the EHTs (Figure 2A). For the purpose of automatic stimulation and force acquisition, eight BMCCs were mounted on a rocking plate powered by a gearless stepper motor. These BMCCs were then controlled by a specialized microcontroller (NXP K22F) for operation (Figure 3A). By rotating the BMCCs at a speed of 60 rpm while tilting them at an angle of 12° relative to their longitudinal axis, the integrated rocker was able to enhance the oxygen uptake and reduce the heat that was lost within the CO_2 incubator. By applying this system, the oxygen level (measured by blood gas analysis, 75-100 mmHg) in the culture medium reaches the regular level of human arterial blood in vivo.

The BMCCs culture system was operated inside a conventional incubator with the following parameters: 37 °C, 3% CO_2, and 80% humidity. The incubators were connected through a USB cable to external computers running customized software for raw data collection and stimulation management (Figure 3 A-B). With a signal interval of 2 ms, forces generated by EHTs were registered and uploaded into LabChart Reader software (AD Instruments) for further study.

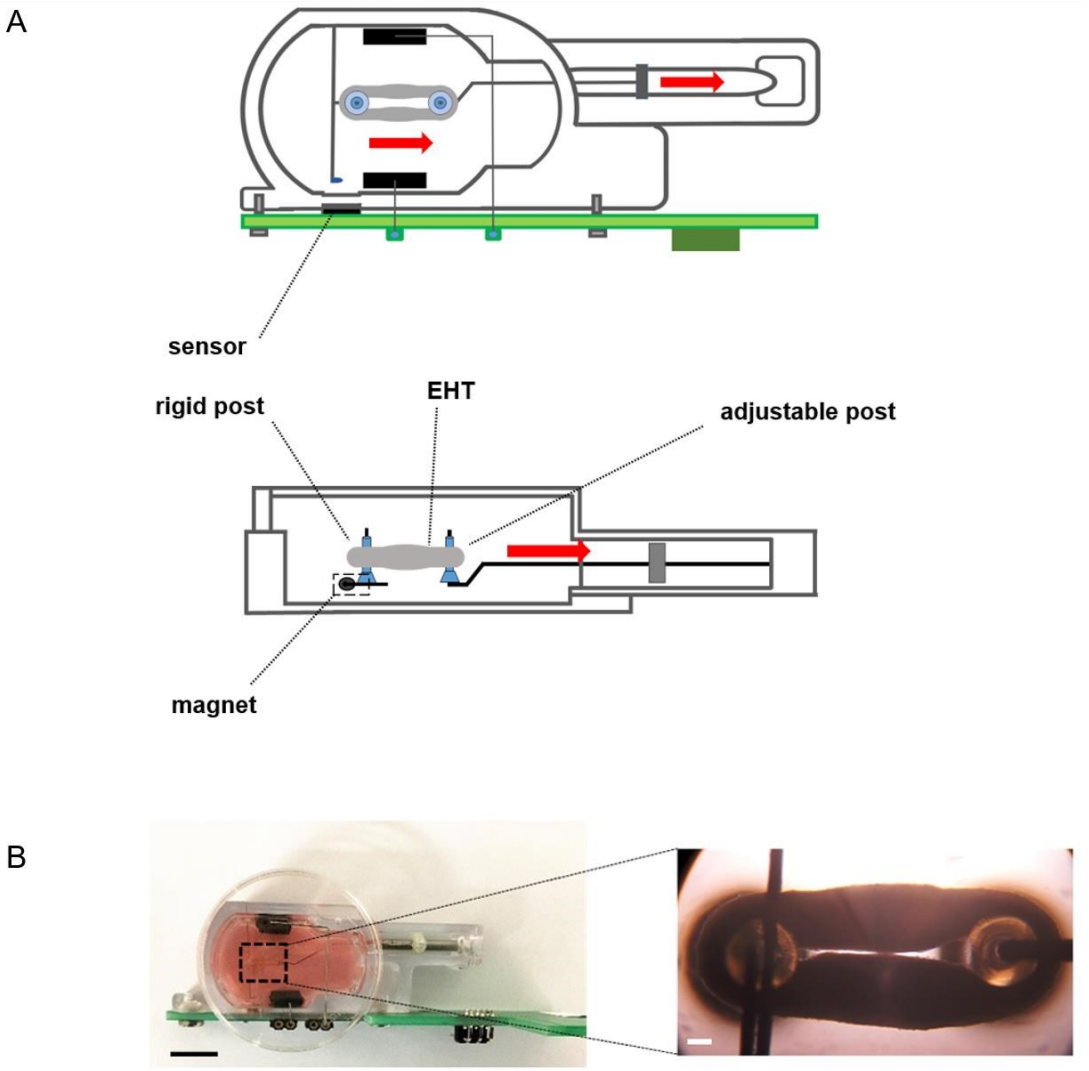

Figure 2. Assembly of biomimetic culture chambers (BMCCs)

(A) Schematic drawing of EHT attachment in a biomimetic culture chamber (BMCC) with annotation. The grey oval structure represents EHT. The red arrow refers to the stretching force direction. (B) Closed view of EHT anchored in a BMCC. scale bar left: 10 mm; scale bar right: 0.5 mm. Photos and schematics adapted from Lu et al., 2021, with permission.

A

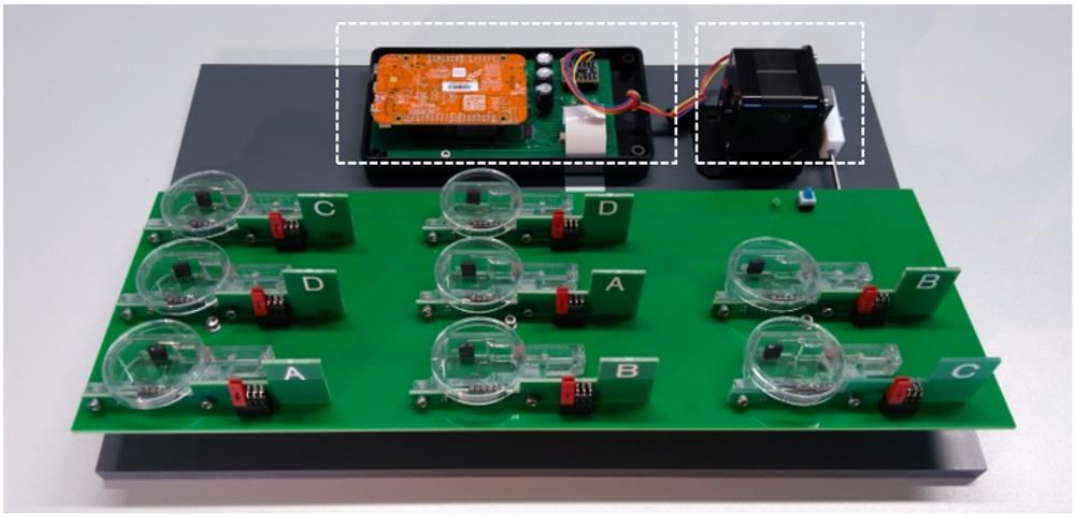

B

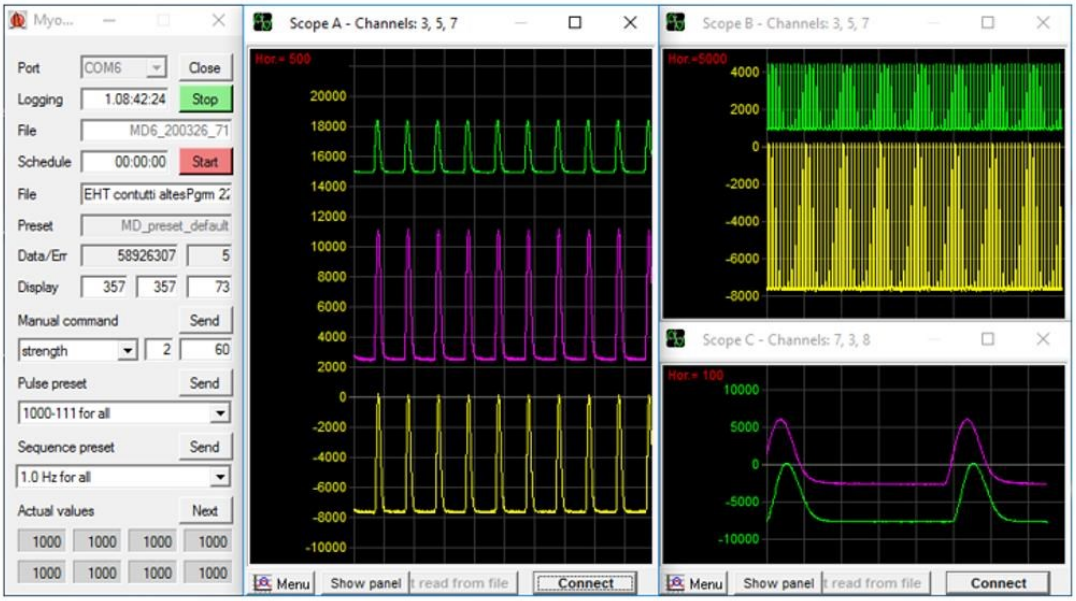

Figure 3. BMCC-setup and operating software

(A) The configuration of a BMCC platform. A microcontroller (the left box with dashes) is responsible for collecting data regarding contractions, outputting electrical stimulation pulses, and regulating the rocking of the BMCC-platform, which is accomplished by a stepper motor (the right box with dashes). (B) The software interface of the BMCC system. Datastore and stimulation parameters are defined at the left control panel. Contraction forces are visualized on the freely configurable monitor oscillograph window (middle/right panels). Each peak indicates a single contraction. Photos adapted from Lu et al., 2021, with permission.

2.2.4 Stretch conditioning and biomechanical analysis

After about five days on the organotypic filter, primary tissue discs (compacted) were transferred to the BMCCs using special transfer tools (Figure 6, A-B). Starting from this point on, each BMCC was supplied with 2,4 ml customized EHT culture medium (modified from (Tiburcy et al., 2017), Table 1), which was partially (2/3, 1.6 mL) changed every two days with the supplementation of 0.1 nM liothyronine (Sigma-Aldrich). By perforating the centrum of the discs, ring-shaped EHTs were installed in the BMCCs attached to two holding posts with an initial distance of 3mm. They were then directly subjected to field electrical stimulation at 1 Hz frequency, 50 mA current intensity, and stretch conditioning (Figure 2 and Figure 6). EHTs transferred to BMCCs were randomized into four groups (S0-S3) according to the daily stretching intensity: a control group with static stretching (S0 = 0 mm/day), and three different experimental groups with different speeds (S3 = 0.32 mm/day, S2 = 0.16 mm/day, S1 = 0.08 mm/day). EHTs in three experimental groups (S1-S3) were manually stretched once daily by shifting the adjustable post at different increments (Figure 2A). A total of 20 independent experiments were performed for the entire duration of the progressive stretching. During these 21 days, the EHT contractility, including the progression of systolic and diastolic force, and the electrophysiological characteristics (e.g., alteration of the stimulation threshold) were continuously recorded. After the experimental period, we removed the EHTs from the BMCCs and subjected them to an organ bath for endpoint data measurements, as previously described (Brandenburger et al., 2012). The specific contraction force (Figure 9C) of EHTs were calculated based on the alpha-actinin^{+} cross-section area (which considered to be the area where the cardiomyocytes located, Figure 26C).

2.2.5 Calcium transient

Under electromechanical stimulus at 1 Hz, EHTs inside BMCCs were loaded with 5 mol/L Fluo-4, AM (Invitrogen) for 30 minutes at 37 °C and followed by a subsequent washout period for 15 min. Videos were obtained on an inverted microscope using a Rolera EM-C^2 camera (Teledyne QImaging, Canada) under continuous stimulation at a rate of 50 frames per second. Data was collected using Micro-Manager (V1.4.23, UCSF, USA). ImageJ (National Institute of Health in the United States of America) was implemented to extract statistical results, and WinEDR Version 3.8.6 (University of Strathclyde, UK) was used to evaluate calcium kinetics. In each sample, a number of regions

of interest were chosen for the purpose of calculating the average fluorescence intensity. The calcium transient signal duration, transient amplitude, and transient decay rate were determined.

2.2.6 Electrophysiology

As previously described, action potentials were acquired utilizing conventional sharp microelectrodes from entire EHTs after 21 days of cultivation (Fischer et al., 2019). Briefly, an EHT in relaxed length is exposed to a modified, thermostatically controlled, and continuously perfused BMCC chamber (with HEPES-buffered Earle' s-salt solution), which is continuously stimulated with a 1 Hz current monopolar of 3 ms duration. A sharp electrode was used and carefully poked on the surface of the EHT to obtain data on the membrane potential, which was magnified by a BA-01X bridge amplifier (NPI electronic GmbH, Germany), and registered with PowerLab 4/20 ML840 (ADInstruments, Australia). LabChart software (ADInstruments, Australia) was used to perform analyses on standard parameters such as the resting membrane potential (RMP), upstroke velocity, amplitude, and action potential duration.

2.2.7 Quantitative PCR analysis

The RNeasy Mini Kit (Qiagen) was applied in order to extract RNA from the sample. The Simplinano Spectrophotometer (Biochrom) was utilized in order to ascertain the RNA integrity number (RIN). An equal quantity of RNA was then subjected to reverse transcription utilizing the QuantiTect Reverse Transcription Kit (Qiagen) following the instructions provided by the manufacturer. All qRT-PCR tests were carried out in duplicate on a StepOnePlus Real-Time PCR System (Applied Biosystems). Cycling conditions: holding stage (95°C) for 10 min, cycling stage 40 cycles at 95 °C for 15 s, 60 °C for 1 min, and 72 °C for 15 s. For the purpose of analyzing, the fold change was standardized to the level of expression of the glyceraldehyde-3-phosphate dehydrogenase (GAPDH) gene. A primer list is presented in Table 2.

2.2.8 Quantitative morphology

For morphology analysis, EHTs were fixed with 4% paraformaldehyde under sustained strain for one hour. In order to perform immunostaining, the EHTs were cryo-sectioned to a thickness of 20 mm. Detailed steps are presented next. After three washes with PBS, EHTs were kept overnight at 4 °C in 1 mL of a 30% sucrose solution in PBS. The

next day, the EHTs were immersed in a 30% sucrose solution which contains 7.5% (w/v) gelatin. Several small cubes of dry ice were dropped into an isopentane bath until the temperature reached between -50 ° and -30 °C. The gelatin block was then submerged in the cold isopentane bath and frozen for two minutes. 20mm sections were cut in a standard cryostat (Leica CM3050 S) for immunostaining. The sections were washed in PBS for 30 minutes, permeabilized in PBS with 1% Triton X-100 for 60 minutes, and then blocked in PBS for an hour with 3% bovine serum albumin and 1% fetal calf serum. The sections were then incubated sequentially in the primary antibody solution (monoclonal Anti-α-Actinin (Sarcomeric) antibody produced in mouse, 1:100; A7811 Sigma-Aldrich) overnight at 4 °C and in the secondary antibody solution (goat anti-Mouse IgG (H+L) Highly Cross-Adsorbed Secondary Antibody, Alexa Fluor™ 546,1:100; A-11030 Invitrogen) for 2 hours. Following this, tissue sections were washed in PBS for 10 min three times and incubated with 2 µmol/L DAPI (Invitrogen), and 40 µg/mL wheat germ agglutinin (WGA) conjugated to CF633 (BioTium CF) overnight at 4 °C. Additionally, the primary antibody to the cytochrome c oxidase component (rabbit polyclonal MT-CO2 antibody, 1:50; PA5-75199 Invitrogen) and the appropriate secondary antibody (Alexa Fluor 488 anti-Rabbit IgG 1:500; A-21441 Invitrogen) were used to identify the mitochondria. A confocal microscope was utilized to visualize the immunostained tissue sections (inverted Leica SP8X WLL). The sarcomere length was determined along the cell's long axis which displayed distinct striations by utilizing the Cell Counter (plugin of Image J, University of Sheffield). At least five measurements were acquired for each individual cell using eleven different duplicates. A minimum of 50 actinin-positive cells from each sample were used to conduct the measurement of the cardiomyocyte cross-section. Using the second harmonic generation technique, myofibril alignment was assessed based on an earlier described method (Dietzel et al., 2014).

2.2.9 Cell morphology and alignment

Anti-alpha actinin (A7811, Sigma), WGA-AF647 conjugate (Thermo Fisher), and DAPI (Thermo Fisher) were used to stain paraformaldehyde-fixed EHTs, after which they were embedded in Fluoromount on a conventional microscope slide. A confocal microscope (Zeiss LSM780) with a 63x oil immersion lens and a pixel size of 0.1x 0.1 μm^2 was used for image acquisition. 10% tile overlap was implemented to collect two-dimensional scans covering an area of 1-3 mm^2, and the scans were then automatically

stitched together (Zeiss ZEN Imaging Software). Myocyte nuclei were identified from the DAPI signal using morphological closure operators and histogram-based thresholds. The WGA intensity was then employed as gradient imaging, and nuclei were used as seeds to perform a morphological watershed segmentation. The generated segments highlighted the EHT cells (Figure 30). The signal for alpha-actinin was segmented using a histogram-based threshold (mode + 1 SD) (Seidel et al., 2017). For morphological examination, only segments with a defined alpha-actinin area fraction (≥ 0.07) and nucleus size (≥ 5 μm^2) were included in order to limit the evaluation to hiPSC-CM with their centers within the optical section. The morphological assessment was carried out using custom-written Matlab programs (version 2019a) and included the determination of cell area, cell length, and major axis orientation (principal component analysis). Local cell alignment was assessed using the standard deviation of the main axis orientation of each cell and its first- and second-degree neighbors (dispersion). (This part was performed by collaborator Thomas Seidel in my own published work (Lu et al., 2021). To ensure the consistency and integrity of the data for this study, he approved that this part of the data could be used as part of this doctoral thesis.)

2.2.10 Simulated hypoxia

In order to induce oxidative stress (tissue hypoxia), the normal condition of medium agitation (BMCCs tilting at a 12° angle at 1 Hz) was paused for two minutes. 1 Hz electrical stimulation and contraction force recording were maintained.

2.2.11 Flow cytometry

Flow cytometry was first applied to analyze the purity of hiPSC-CM for EHT formation after differentiation. A portion of the dissociated cells (0.5×106) were fixed and resuspended in 4% paraformaldehyde solution for about 15min to be used for intracellular labeling of alpha-actinin and cardiac troponin T (cTnT). Cells were then centrifuged at 200 xg for 5min, permeabilized in 1% Triton X-100 PBS solution, and washed twice with 1% BSA (Sigma). After that, the cells were stained for 45 min at a temperature of 4 °C with unconjugated primary antibodies labeling cTnT (ab45932, Abcam) and alpha-actinin (A7811, Sigma) in FACS buffer composed of 1% fetal bovine serum (FBS, Gibco). The first antibodies were then removed. Cells were subsequently incubated at 4 °C for 30 mins with secondary antibodies (Alexa Fluor 488 anti-Rabbit IgG,1:500; Invitrogen A-21441 and Alexa Fluor 546 anti-Mouse IgG, 1:500; Invitrogen A-11030). Afterward,

the cells were washed with PBS and processed utilizing a BD FACSCanto™ II Flow Cytometer (BD Biosciences, USA) in association with the software FlowJo (Tree-star Inc., USA). For the assessment of hiPSC-CM volumes, a FACS analysis was performed on the resuspended cells from dissociated EHTs. EHTs after 21 days were manually broken down into tiny pieces, which were then incubated with a dissociation solution containing collagenase II (2,2 mg/mL, Sigma Aldrich) and TrypLE Select Enzyme (Gibco) for 20 minutes at 37 °C on a thermostated shaker. EHTs were gradually dissociated into single-cell suspensions by repeated mechanical dispensing with a 1 ml pipette. The remaining tissue pieces and strips were discarded. Subsequently, the suspensions of these single cells were stained for cardiac troponin T (cTNT), as previously described.

2.2.12 Isometric contraction performance in organ bath

As previously mentioned, the EHTs contractility was measured under isometric settings in a horizontal organ bath (Mayflower, Hugo Sachs Elektronik, Germany) (Brandenburger et al., 2012). EHTs were mounted to isometric force transducers (F30, HSE) with a 1 mN preload together with 1 Hz electrical stimulation (pulse duration 3 ms, 2-fold stimulation threshold) and constantly perfused using oxygenated Tyrode solution (23 mmol/L bicarbonate and 1.8 mmol/L $CaCl_2$, pH 7.4) for approximately 10 minutes before any assessment. Under optimal preload conditions, the maximal twitch force achievable was then recorded. In order to access the Frank-Starling relationship, the EHTs were stepwise stretched by increments of 0.25 mm. The reference line (or baseline), also known as the slack or relaxation length, was defined to be the length that did not result in any diastolic force. Continuous recordings of both active and passive forces were obtained and then evaluated 15 seconds after each stretch. In order to assess the force-frequency relationship (FFR), the stimulation frequency was gradually increased from 1 Hz up to 6 Hz. By using the diastolic force slope (related to the length and actinin positive cross-section area) just before the maximal contractility state, the elastic modulus was calculated.

2.2.13 RNA sequencing and bioinformatical analysis

RNA was extracted using Trizol (Life Technologies), and the RNA integrity was acquired with the Agilent Bioanalyzer 2100, as instructed by the manufacturer. Total RNA was processed to RNA-sequencing on an Illumina HighSeq-2000 platform (SR 50 bp; > 25

Mio reads/sample) and library preparation using the SENSE Total RNA-Seq Library Prep Kit from Lexogen. The software BaseCaller from Illumina was used to convert sequence pictures into bcl files, which CASAVA (v1.8.2) was then used to demultiplex into fastq files. Salmon (v0.14.1) was used to determine the read counts of genes and transcripts. EdgeR (v3.28.1) was used to normalize the counts (TMM), and limma was used to analyze the differential expression (v3.42.2, voom with quality weights). With the assistance of topGO (v2.38.1), gene ontology (GO) analysis was carried out for those differentially expressed genes (adj p-value 0.1). (This part was performed by collaborator Aarif Mohamed Nazeer Batcha in my own published work (Lu et al., 2021).To ensure the consistency and integrity of the data for this study, he approved that this part of the data could be used as part of this doctoral thesis.)

2.2.14 Quantitation and statistical analysis

Data are presented as mean ± standard error of the mean (SEM). As applicable, one-way ANOVA or two-way ANOVA was employed to confirm treatment effects. Dunnett's multiple comparison test and Tukey's Honest Significant Difference test were applied to the post-hoc pairwise analyzation. GraphPad Prism 7 was used for all statistical testing. A threshold of error of p-value less than 0.05 was considered statistically acceptable for significance. The number of individual experiments completed for each data set is specified in the related figure legends.

3. RESULTS

3.1 Cell culture and construction of three-dimensional tissue

3.1.1 Two-dimensional cell culture

Standard techniques for stem cell culture and CM development resulted in a monolayer structure that exhibited earliest contractile activity on day 8-9 of differentiation (Figure 4). Flow cytometric examination revealed this cell population was composed of 69 ± 1% cells that were positive for both cardiac troponin (c-TNT) and alpha-actinin and were therefore considered hiPSC-CMs (Figure 5).

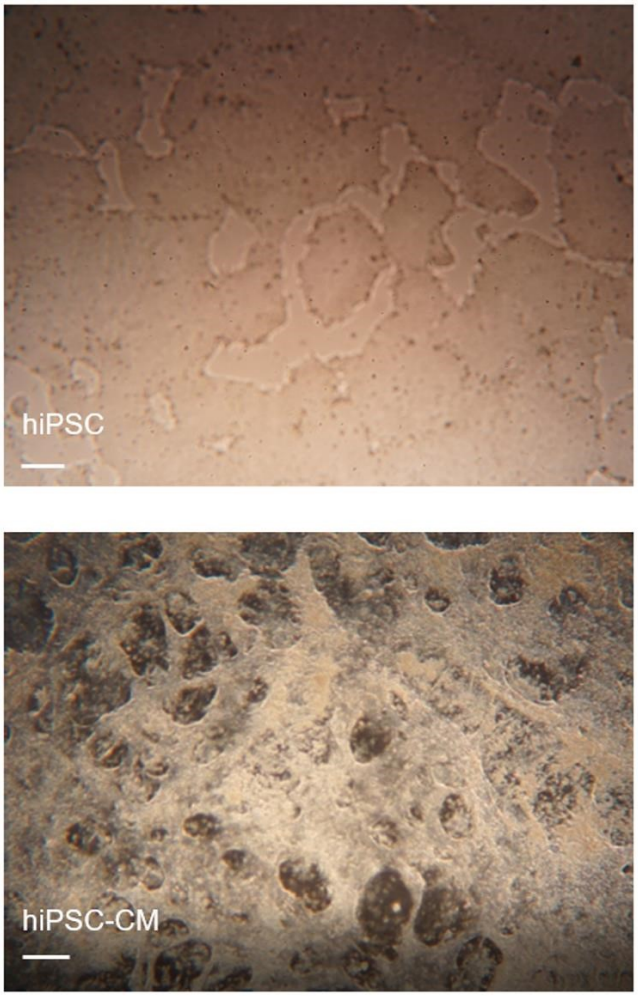

Figure 4. Monolayer cell culture

Confluent cultures of hiPSC before differentiation (upper picture) and beating hiPSC-cardiomyocytes (bottom picture), scale bar: 300 µm.

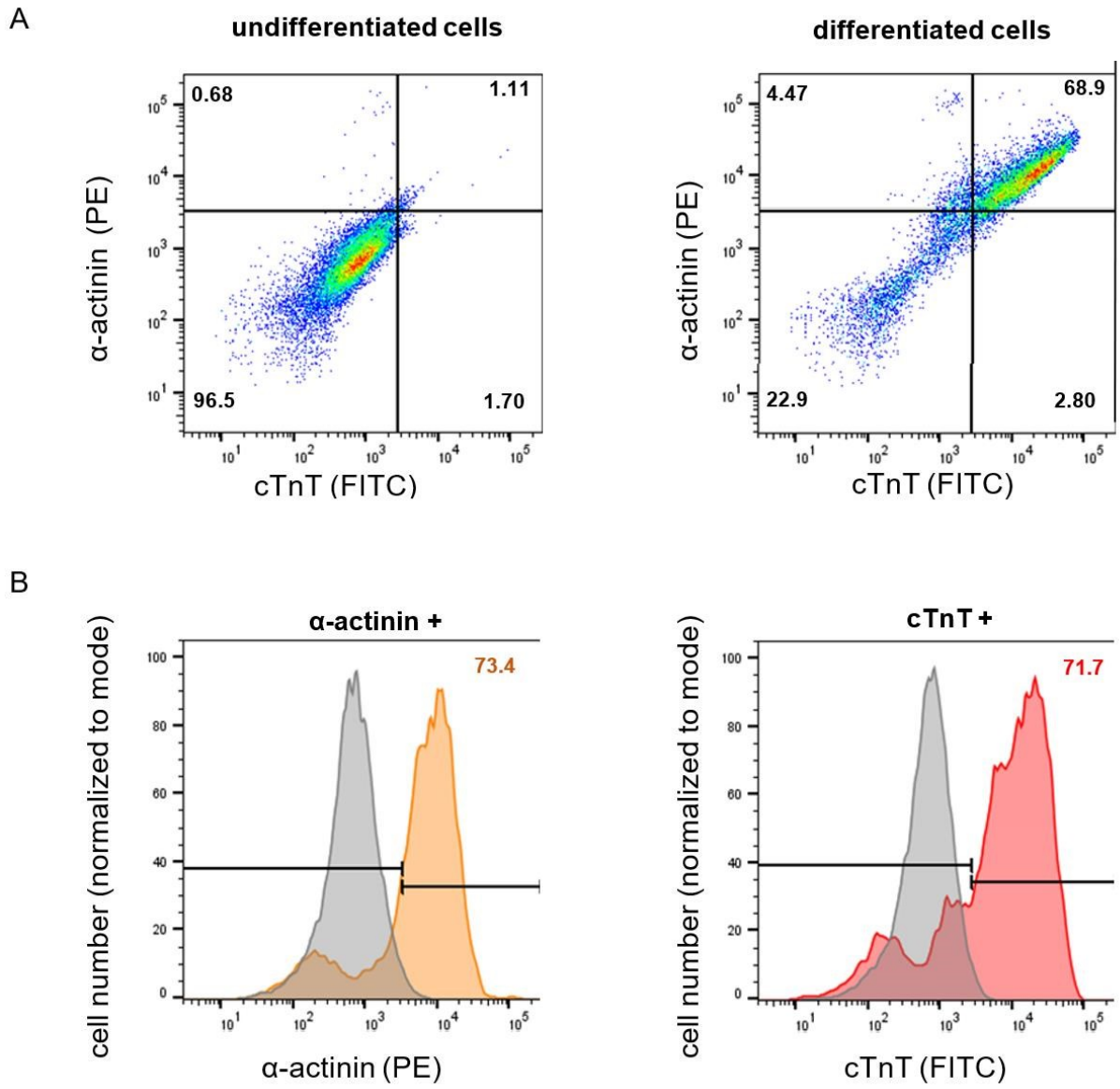

Figure 5. Flow cytometric characterization of hiPSC-CMs differentiation

(A) Flow cytogram of stem cells (undifferentiated hiPSC, MRIi004-A) and differentiated cells (cells after differentiation procedure as used for EHT fabrication). Cardiac muscle troponin T (cTnT) and alpha-actinin were used to label both cell suspensions. cTnT and alpha-actinin double-positive labeled cells were identified as cardiomyocytes. (B) Distribution of alpha-actinin (orange peak) and cTnT (red peak) in hiPSC-CMs and in undifferentiated stem cells (both grey peaks). Figure modified from Lu et al., 2021 with permission.

3.1.2 Two-step tissue formation and fixation

Since our previous efforts to construct EHTs were unsuccessful due to the high stiffness or delayed compaction of the primary tissues, a reliable strategy for EHT formation was established with a two-step process of cell assembly as well as biomimetic conditioning (Figure 1). The monolayer adhering cells were first dissociated, then combined with a collagen-based matrix, and finally reassembled on the surface of an organotypic filter in order to facilitate the fastest and most efficient creation of EHTs that are mechanically stable (Figure 6, Figure 7). This technique encouraged cellular connections by rapidly removing excessive media, which led to the creation of a flat disc that started synchronous spontaneous contraction within only twenty-four hours. The tissue continued to condense and compacted itself from an 8 mm diameter to a diameter of 5 mm over the course of following 5 days, achieving the necessary mechanical stability for the subsequent transfer to BMCC chambers and subsequent application of stretch.

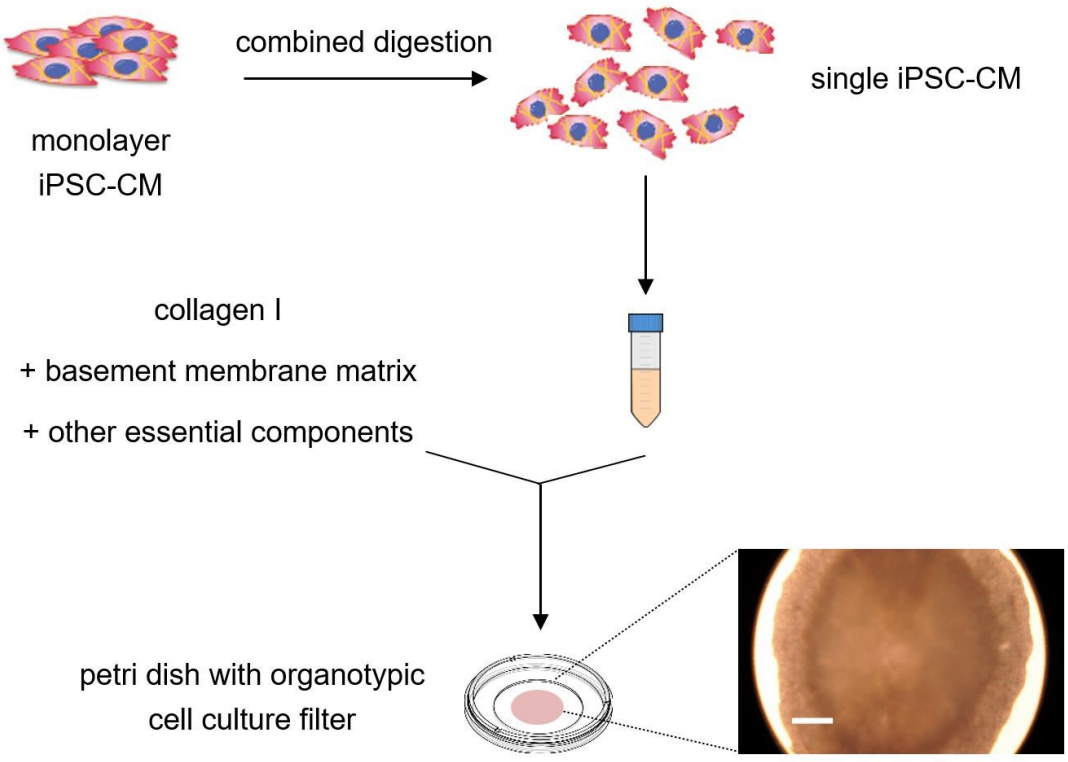

Figure 6. Primary EHT formation

Schematic diagram of primary EHT disc formation. Bottom right: a close view of the discoid EHT acquired from an optical microscope (scale bar 0.5 mm). Reproduced from Lu et al., 2021 with permission.

The physical attachment to the two supporting poles was accomplished by drilling a hole through the middle of the disc and widening the 3 mm distance between them (Figure 7, Figure 2A). Tissue discs often adhered to the screen underneath them during the first step of compaction and must first be removed with medium to maintain the disc integrity. In the second step, the tissue disc was carefully scooped up with a special transfer tool and carefully placed in the BMCC, where the center of the disc needs to be pierced by two supporting poles. This transfer process requires a certain mechanical rigidity of the tissue, so the cell density and the compaction process in the previous first step were crucial.

This mounting method succeeded in making ring-shaped EHTs whose immediate generation of contractile force indicated minimization of mechanical injury to the puncture site. Special attention should be paid to the fact that both supporting poles must be pierced as close as possible from the center of the tissue disc during the transfer in order to ensure a balanced stretching effect afterward.

In the following 3 weeks of stretch conditioning, the CMs organized with force orientations between the posts to create elongated loops whose dimensions were mostly dictated by the external stretching (Figure 2B, Figure 7).

Because mechanical forces in a single direction are constantly applied during tissue growth, tissue fracture has also been studied as an indicator. At low to moderate distension rates (S0-S2), no EHTs ruptured, whereas seven of twenty EHTs ruptured spontaneously following stretch application in the most intense stretch group (S3). These results also demonstrate that the tissue stretching speed has reached its maximum at S3.

In rare instances, the two sides of an EHT touched and merged. This did not appear to impede the EHT performance.

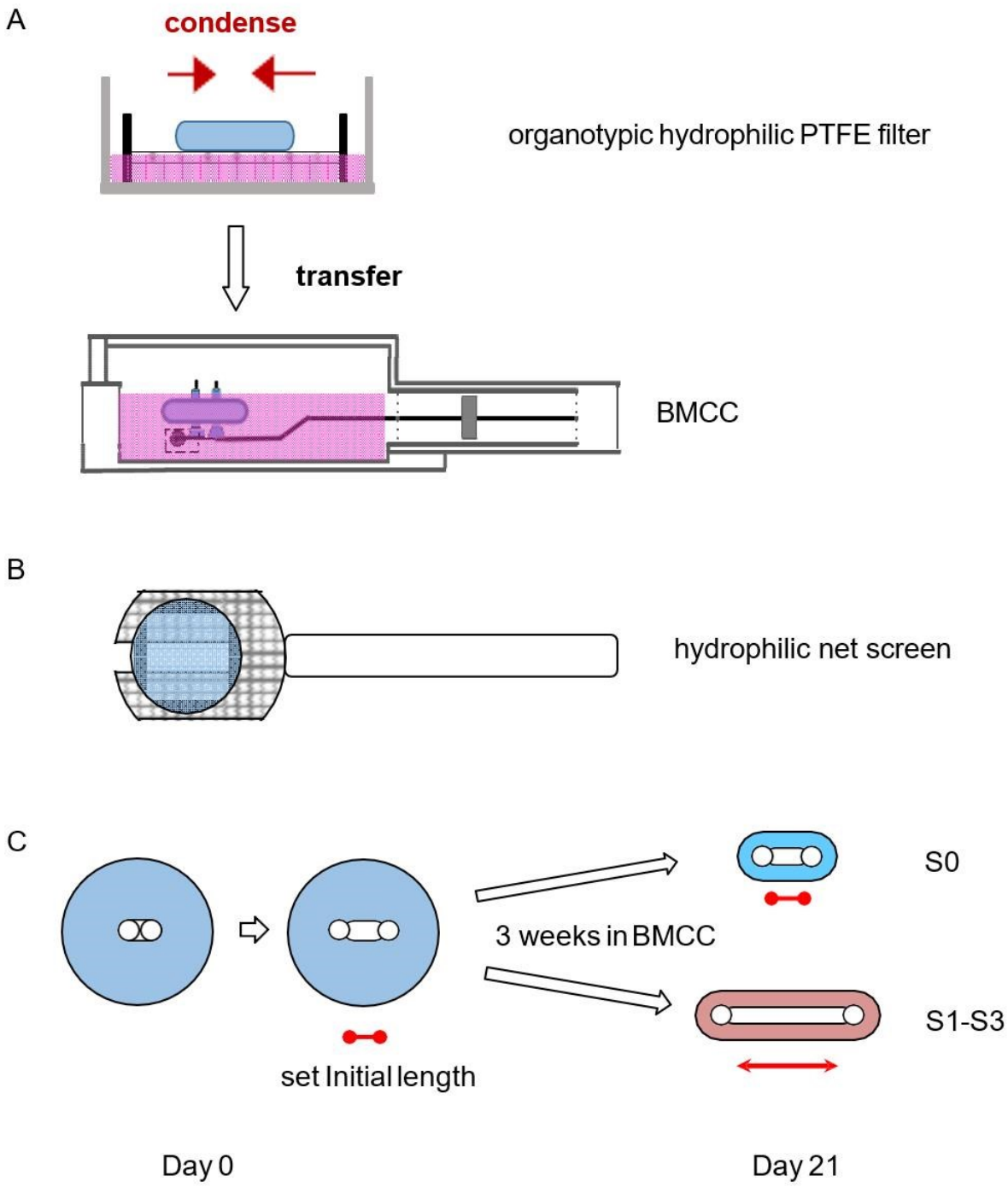

Figure 7. Transfer and stretch implementation

(A) Transition of the disc-shaped construction to a biomimetic culture chamber (BMCC) with a custom-made hydrophilic net (B) to support the vulnerable tissue. (C) Demonstration of the stretching process depicts a daily extension of EHTs by steadily extending the distance between EHT holding posts. The direction of loading forces is shown by red arrows. Reproduced from Lu et al., 2021 with permission.

3.2 EHT properties development during stretch conditioning

3.2.1 Contractility development

During 3 weeks of stretch training, the force generated by each tissue was constantly monitored using a 500 Hz sampling rate (Figure 3B). The medium was changed every 36-48 hours, depending on the needs.

We noticed that the impact of progressive stretching could be described as either acute or chronic effects. As the screw was tightened with a screwdriver, one of the two posts on the tissue loop moved outward, resulting in a single direction of tension. This procedure typically lasts 1-2 seconds. The increase in contractile force can be clearly seen in the real-time recording (Figure 8A).

At the end of this 1-2 second period, an immediate fallback occurred. The rate of contraction fallback is positively correlated with the stretching intensity (S1-S3) and the number of days in culture (for instance, the fallback of S3 is more obvious than that of S2, and the fallback of day 20 exceeds that of day 10, etc.).

Nevertheless, the rise in contractility is always larger than the fallback value. Thus, contractility accumulates after each acute episode. This buildup of contractile power is enhanced by everyday stretching permanently. By studying at the contractility curves several hours after each stretching, we found that there was another slow increase, which indicates the chronic effect of the stretch. All systematic distension contributed to an increase in the amplitude of the contraction; however, the maximum rate of stretch (S3) seems to be the only condition that created diastolic preload accumulations (Figure 9).

Spontaneous contractions occurred throughout the incubation process. However, the proportion of spontaneous contractions gradually decreases with increasing culture time. After about 7-10 days of incubation, the pronounced and persistent spontaneous contractions largely disappear. It was also occasionally observed that acute stretching causes irregular contractions of the tissue, i.e., spontaneous contractions. Such behavior disappears on its own when the tissue stabilized.

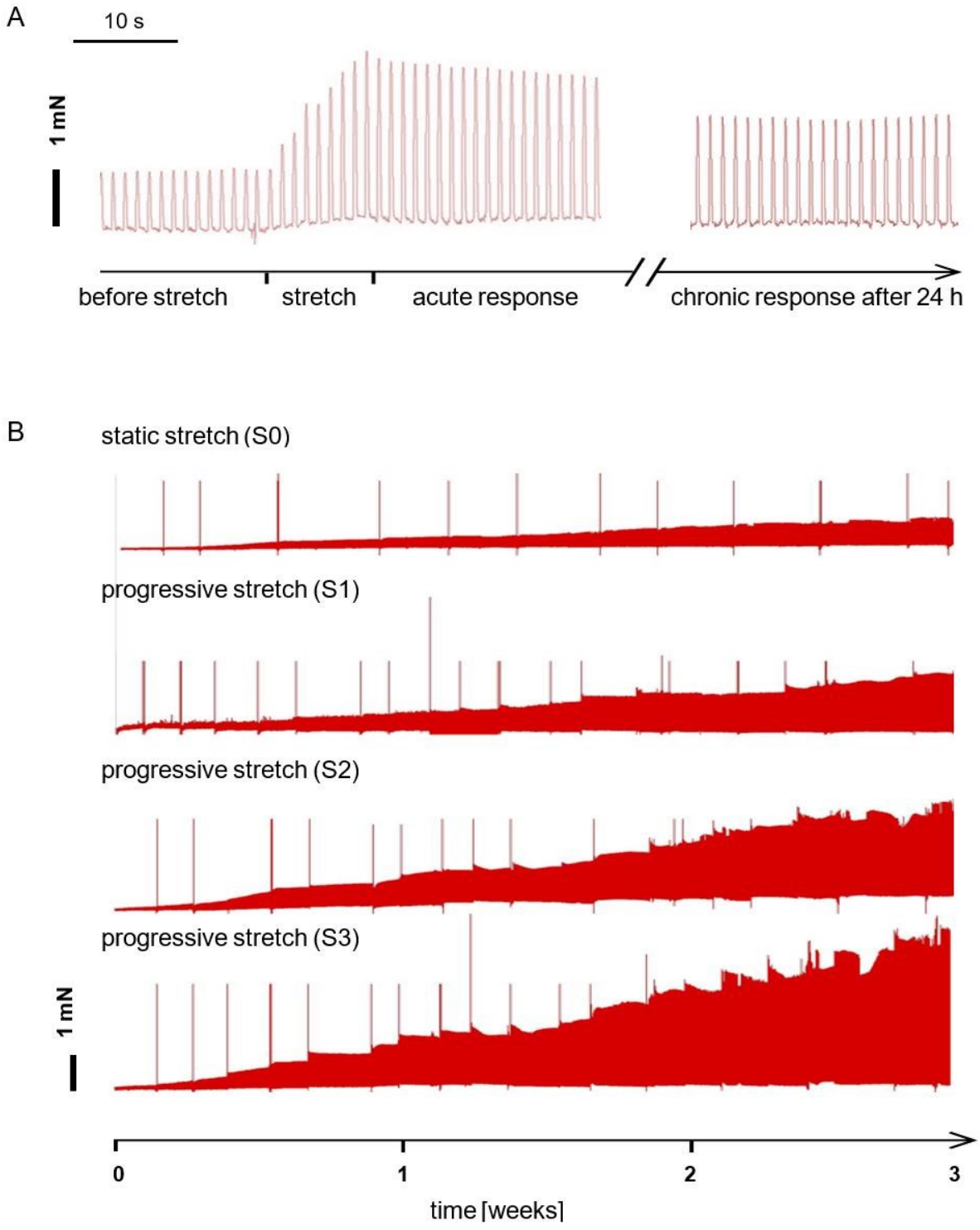

Figure 8. Contraction force recording

(A) A typical recording of a single stretch maneuver in real time, with each peak denoting a single contraction. (B) Exemplary three-week recordings of twitch forces (from top to bottom: S0-S3). Medium exchange intervals correspond to cyclical interruptions (36 - 48 h). Based on Lu et al., 2021 with permission.

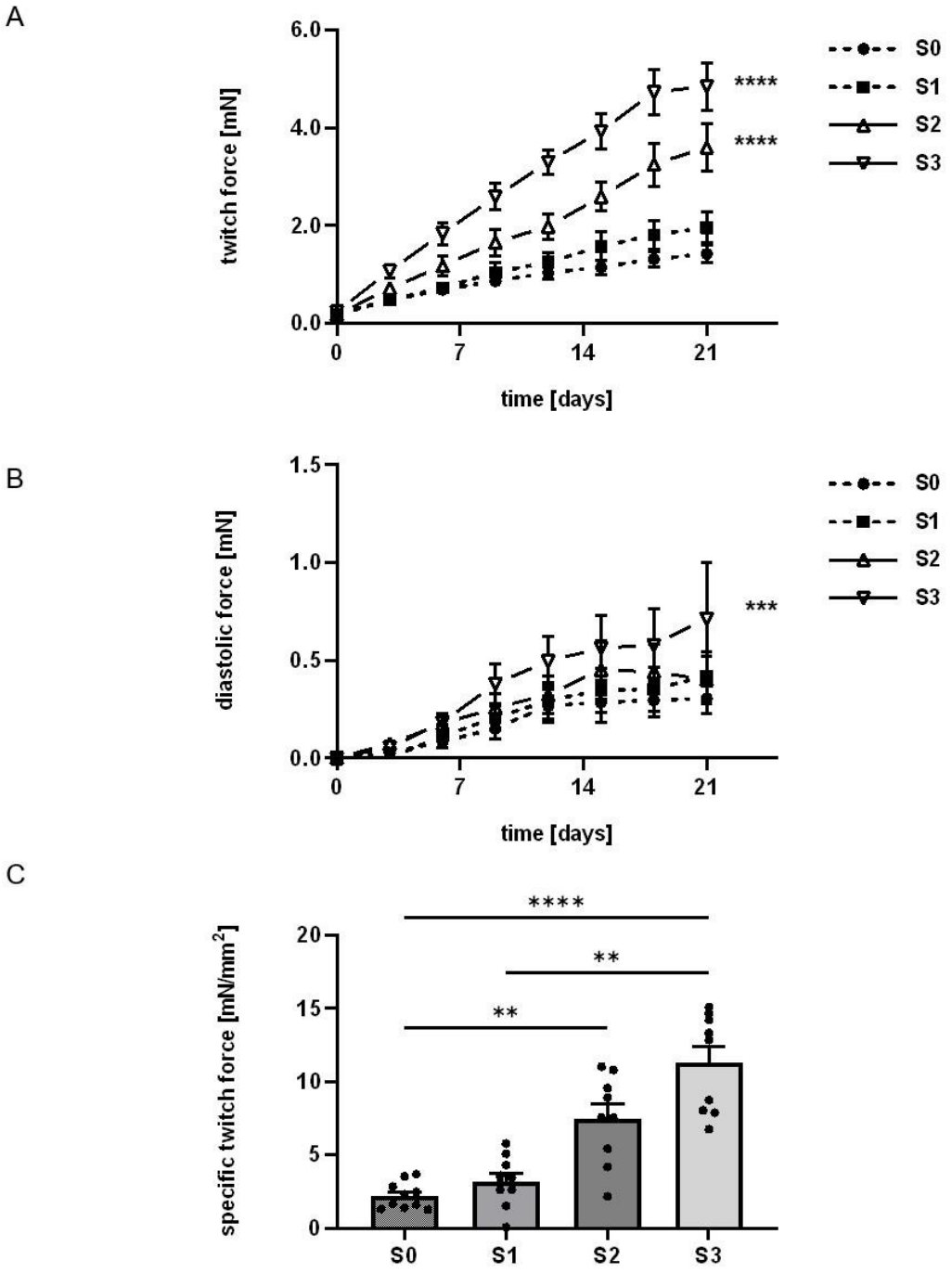

Figure 9. Contractility and preload were enhanced under stretch conditioning

(A) and (B): The development of twitch force (A) and diastolic force (B) in groups subjected to various stretch intensities. (C) Specific twitch force at different stretch intensities after a three-week cultivation period. (A-C): S0 for static, S1 for low, S2 for moderate and S3 for high stretch; n = 10 per group. (A) - (B) Two Way ANOVA, Tukey's multiple comparison tests (vs. static stretch) (C) One-way ANOVA, Tukey's multiple comparison test. (*p < 0.05, **p<0.01, ***p<0.001, ****p<0.0001). Based on Lu et al., 2021 with permission.

3.2.2 Electrical stimulation threshold development

Immediately after transfer into BMCCs, more than half of the EHTs exhibited stimulability, indicating that they had completed a considerable degree of electrical maturation previously on the 2D filter. Since all EHTs exhibited stimulability after 3 days, the stimulation threshold on day 3 was taken as the initial value (Figure 10). EHTs acquired an all-or-none force response to electrical stimulation, and this response occurred in conjunction with a steady lowering of the stimulation threshold (Figure 10). This phenomenon did not have a substantial relationship to the applied stretch intensities.

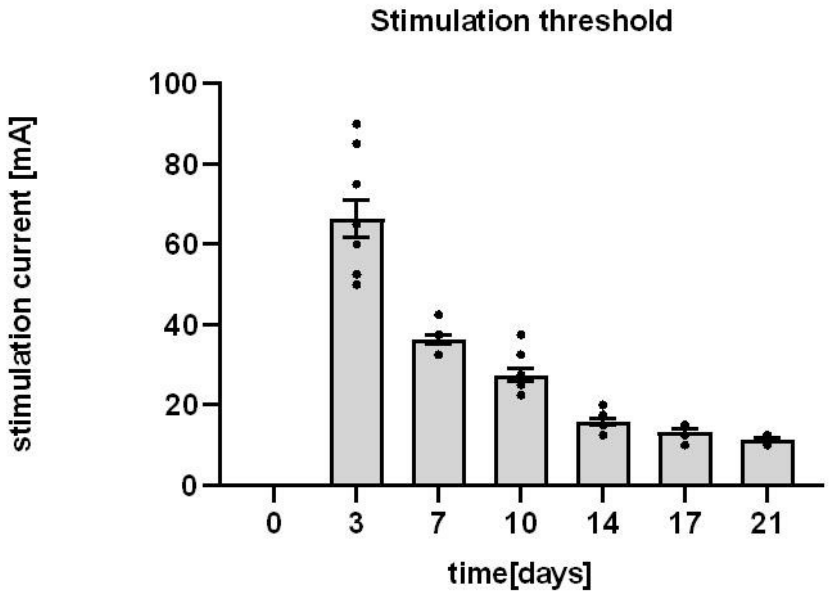

Figure 10. Electrical stimulation threshold development

The threshold intensity for EHT stimulation decreases during culture period. There was no discernible difference between the various stretching intensities. The graph depicts exemplary data from EHTs subjected to various stretch conditions (S0 - S3, n = 6). Based on Lu et al., 2021 with permission.

3.2.3 Oxidative metabolism

Stretched EHTs also exhibit more mature characteristics in terms of metabolism. Based on experience on human adult myocardial slices, agitation of the culture medium is essential for the oxygen supply to human myocardial slices (Fischer et al., 2019). Human myocardial slices that ceased culture medium shaking immediately exhibited a decrease in contractility, i.e., signs of hypoxia.

Therefore, we measured here the oxygen dependence of EHT based on the same principle, which can be approximated by the contraction force decrease during stoppage of medium agitation for 2 mins.

It is clear that all EHTs showed a decrease in contractility after stopping agitation. The lowest relative decrease was observed in static cultured EHTs (S0, 77.6 ± 2.5% residual force, Figure 11B). The decrease rate was also shown to be positiv correlated with the degree of stretch conditioning with a maximal decrease in high stretched group (S3, 64 ± 2.4% residual force, Figure 11B). This correlation suggests that progressively stretched tissues encounter an increase in contraction force in conjunction with an increase in their oxygen capacity.

In addition, immunohistochemistry staining offered excellent evidence to support this view. The figure demonstrates that the stretched tissues included a greater number of mitochondria in a more defined order (Figure 12).

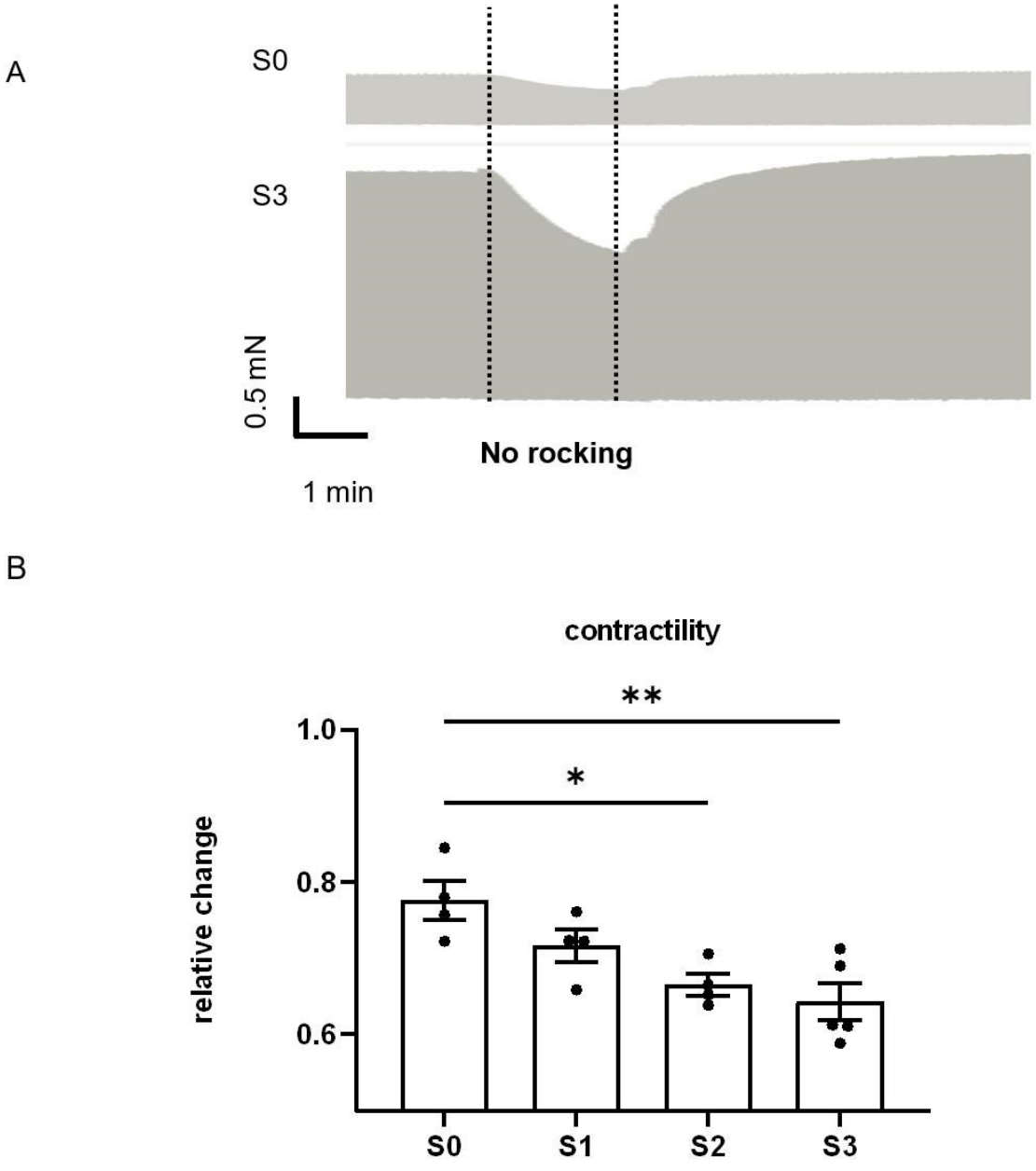

Figure 11. Stretch conditioning improves oxidative metabolism

(A) Exemplary recording of twitch force during O2 depletion (hypoxia) induced by the stoppage of medium agitation for 2 minutes. S0 for static stretch, S3 for high stretch. (B) The proportional loss of twitch force triggered by simulated hypoxia in EHTs under different stretch speeds (S0–S3, n = 5). One Way ANOVA, Kruskal-Walli's test (vs. static stretch), *p < 0.05. **p < 0.01. Based on Lu et al., 2021 with permission.

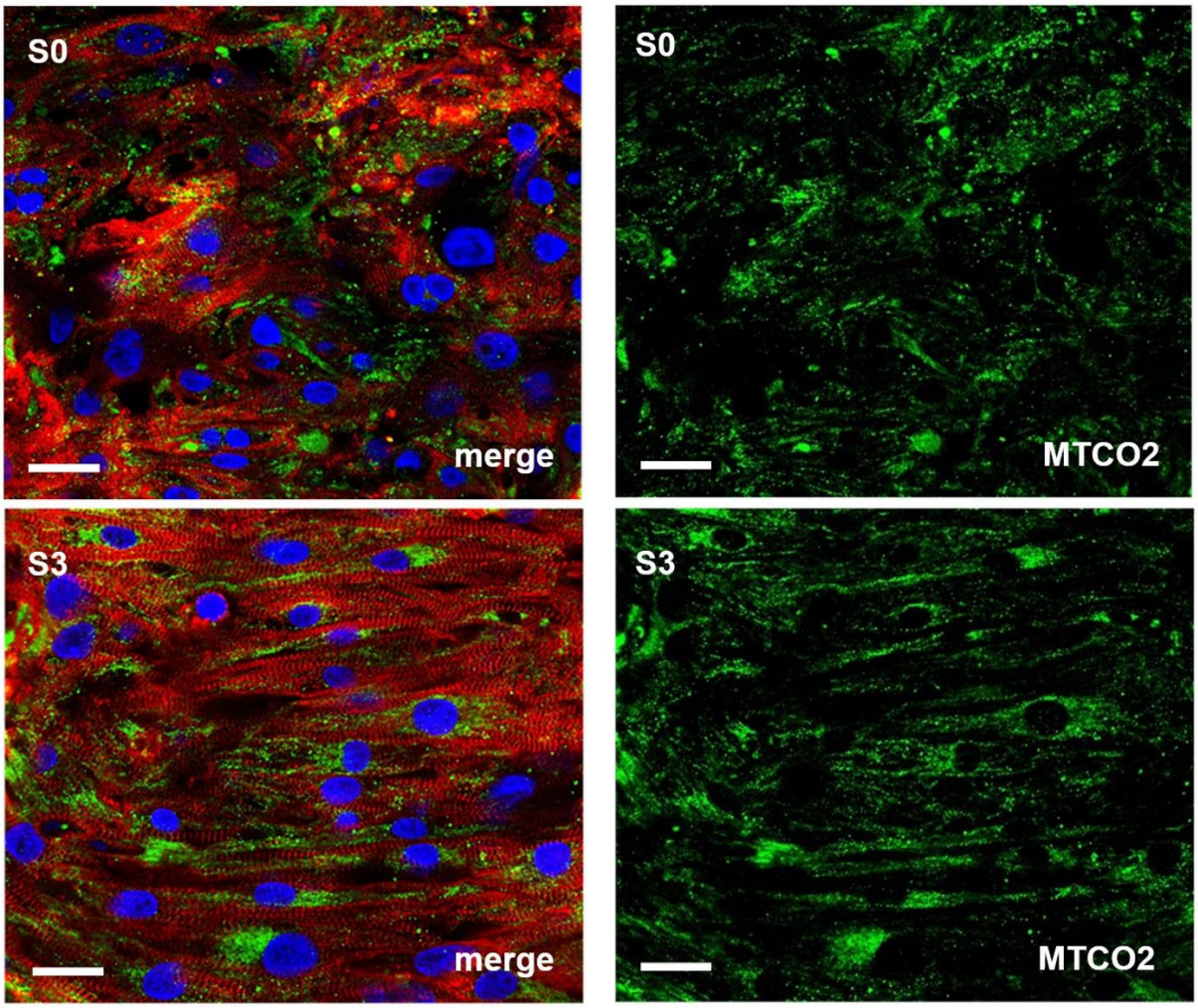

Figure 12. Immunofluorescence detection of mitochondria abundance

Immunofluorescence images of longitudinal EHT section (S0 for static stretched and S3 for high stretched EHTs). Immunohistochemical staining for MTCO2 (a subunit of the cytochrome c oxidase in mitochondria, appears green in left and right images), alpha-actinin (red), and nuclei (blue). Adapted from Lu et al., 2021 with permission.

3.3 Stretch improves contractility and passive elasticity of EHTs

All EHTs obtained stable mechanical structures after three weeks of biomimetic incubation, which made the endpoint experiments of transfer possible. To test the optimal contractility and elasticity, EHTs were transferred to a horizontal organ bath and subjected to acute distension as well as different pacing frequencies under isometric settings. Tissues were able to sustain an extension of up to 1.8 times their slack length, and exhibited enhanced diastolic and systolic contractility (Figure 14).

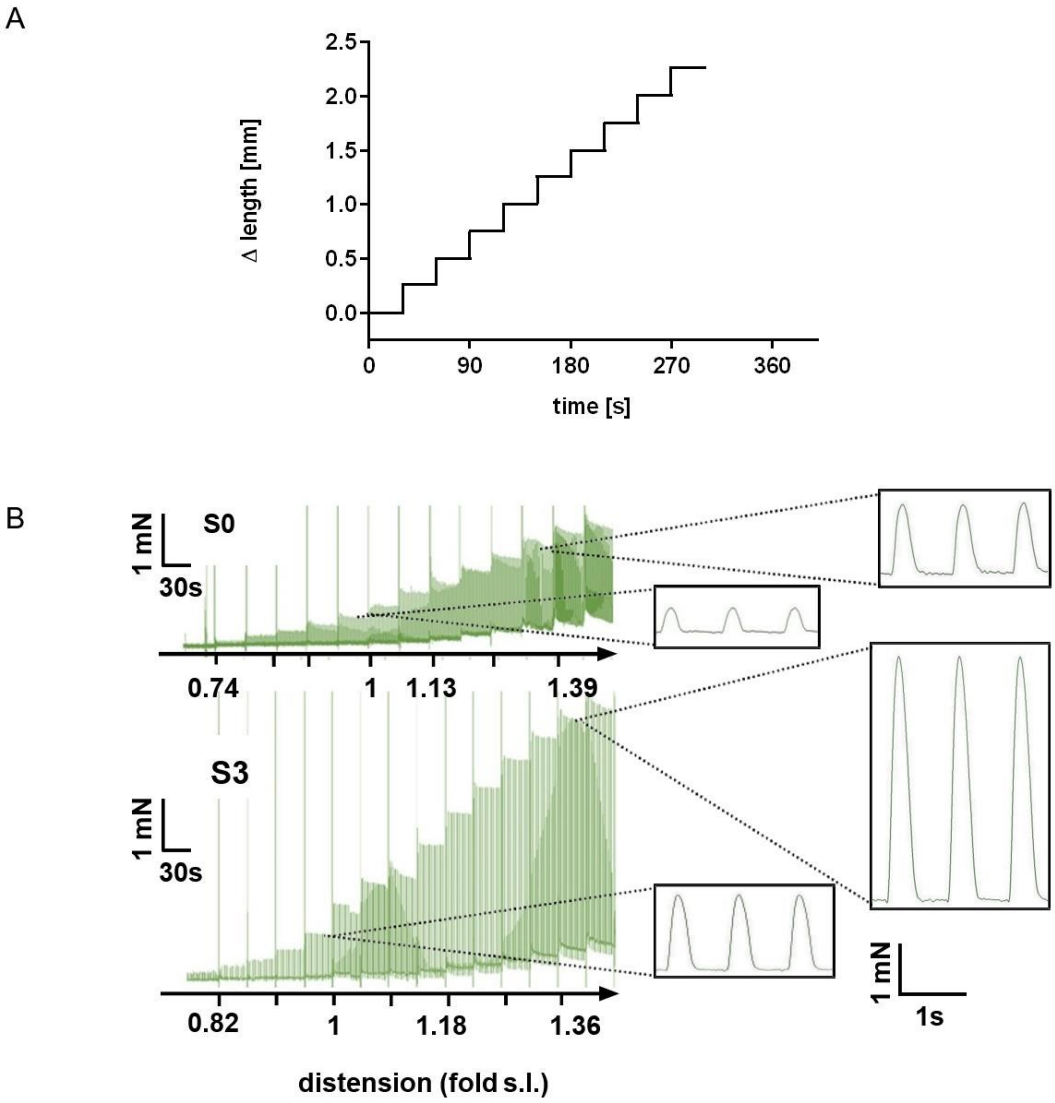

Figure 13. Frank-Starling relationship assessment

The behavior of EHTs after 3 weeks stretch period to stepwise escalating distension (illustrated as (A)) under isometric conditions is exemplarily demonstrated in a force trace recording (B) (S0 for static stretched and S3 for high stretched), which together reflect a correlation between the Frank-Starling relationship. Adapted from Lu et al., 2021 with permission.

With increasing stretch conditioning, the contraction force which responded to rapid distension as well as the twitching force at optimal preload increased both. Compared to tissues subjected to static stretch, EHTs stretched at the greatest rate (S3) not only exhibited 5.1-fold greater contractility but also a 2.6-fold increment in modulus of elasticity (Young's modulus) (Figure 15). Importantly, training with the highest stretch allowed EHTs to create a maximal ratio of systolic to diastolic wall stress reaching 9.47 ± 0.84 (Figure 15), therefore reaching the biomechanical properties of a healthy human left ventricle (ratio of systolic to diastolic:10.5, (Hood et al., 1968)).

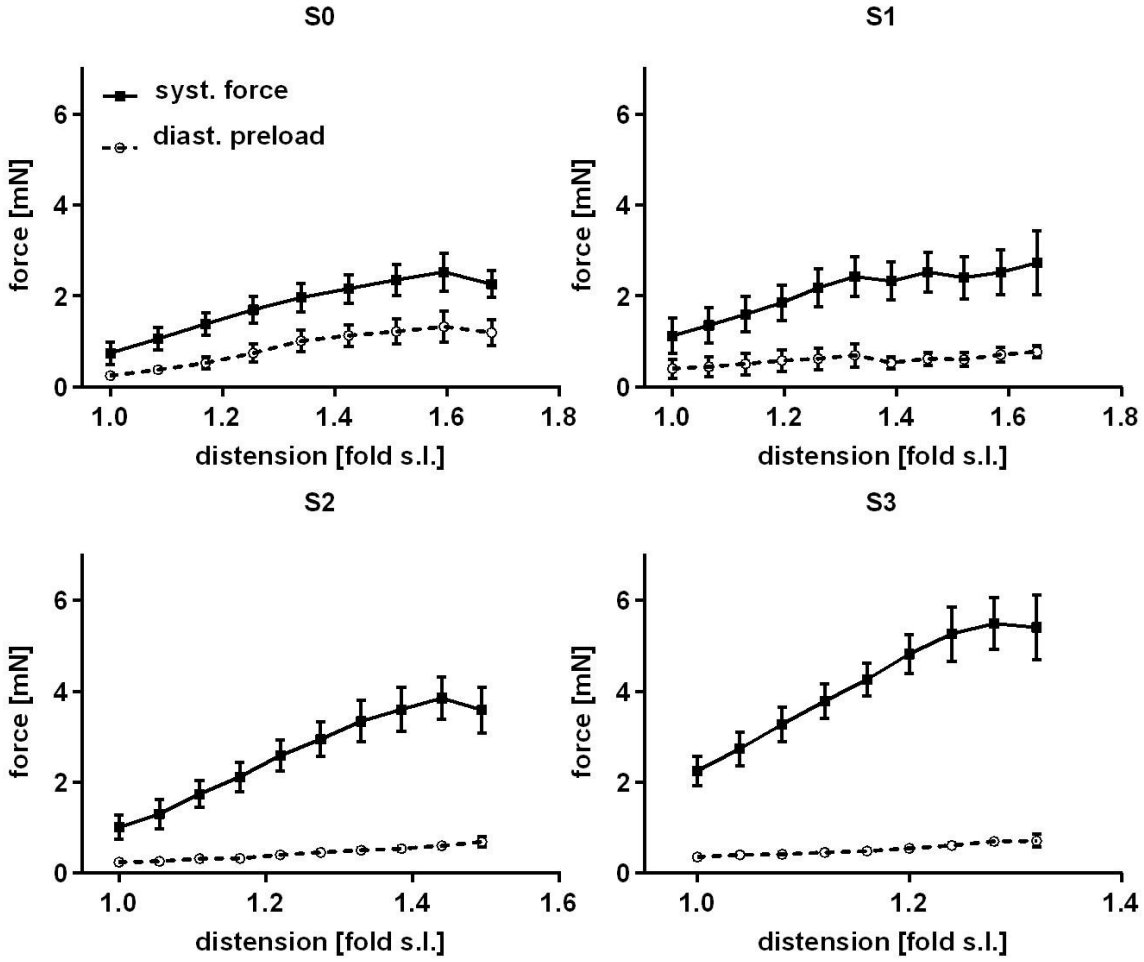

Figure 14. Frank-Starling relationship analysis of EHTs

Response of different stretched EHTs (S0 - S3, after 3 weeks stretch period) to acute stepwise distension (systolic and diastolic forces) (n = 7 per group, s.l. for slack length). Figure modified from Lu et al., 2021 with permission.

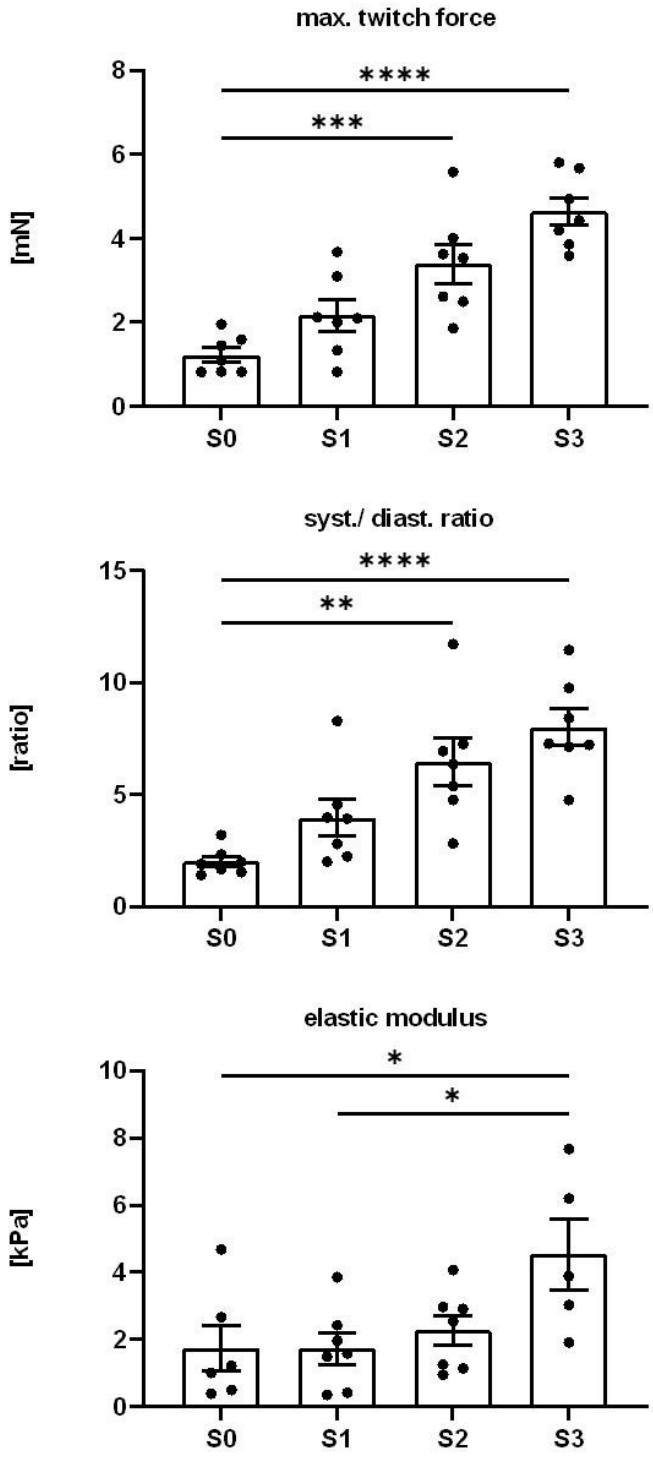

Figure 15. EHTs after stretch exhibit mature biomechanical characteristics

From top to bottom: the maximum contraction force, the ratio of systolic/diastolic force, and the modulus of elasticity of different stretched EHTs after 3 weeks period (S0 for static, S1 for low, S2 for moderate, and S3 for high stretch; n = 7 per group). Two Way ANOVA, Tukey's multiple comparison tests (vs. static stretch), **p < 0.01, ***p < 0.001, ****p < 0.0001. Figure modified from Lu et al., 2021 with permission.

3.4 Excitation/contraction coupling in stretched EHTs

3.4.1 EHTs approach the physiological Force-frequency relation

The force-frequency relationship (FFR) is one fundamental intrinsic cardiac contractility regulating mechanism. In the majority of the mammalian ventricular myocardium, the FFR is positive; that is, an increase in contractile force, together with an enhancement in the amplitude of Ca^{2+}- transients, is generated by an increase in stimulation frequency, which indicates the cardiac contractile reserve (Endoh, 2004).

For this reason, positive FFR is considered as one of the important hallmarks of cardiomyocyte maturation. EHTs grown under static stretch demonstrated a significant reduction in contraction force as the pacing rate increased, which indicates a negative FFR. In comparison, stretch-conditioned EHTs, specifically group S2 and S3, reacted to rapid pacing with a force increase with optimum performance at 4 Hz (1.25 times greater than 1 Hz), which indicates a positive FFR (Figure 16). Although the contraction force rather decreases with a further increase in stimulation frequency (5-6 Hz), the whole relationship is closer to the physiological situation.

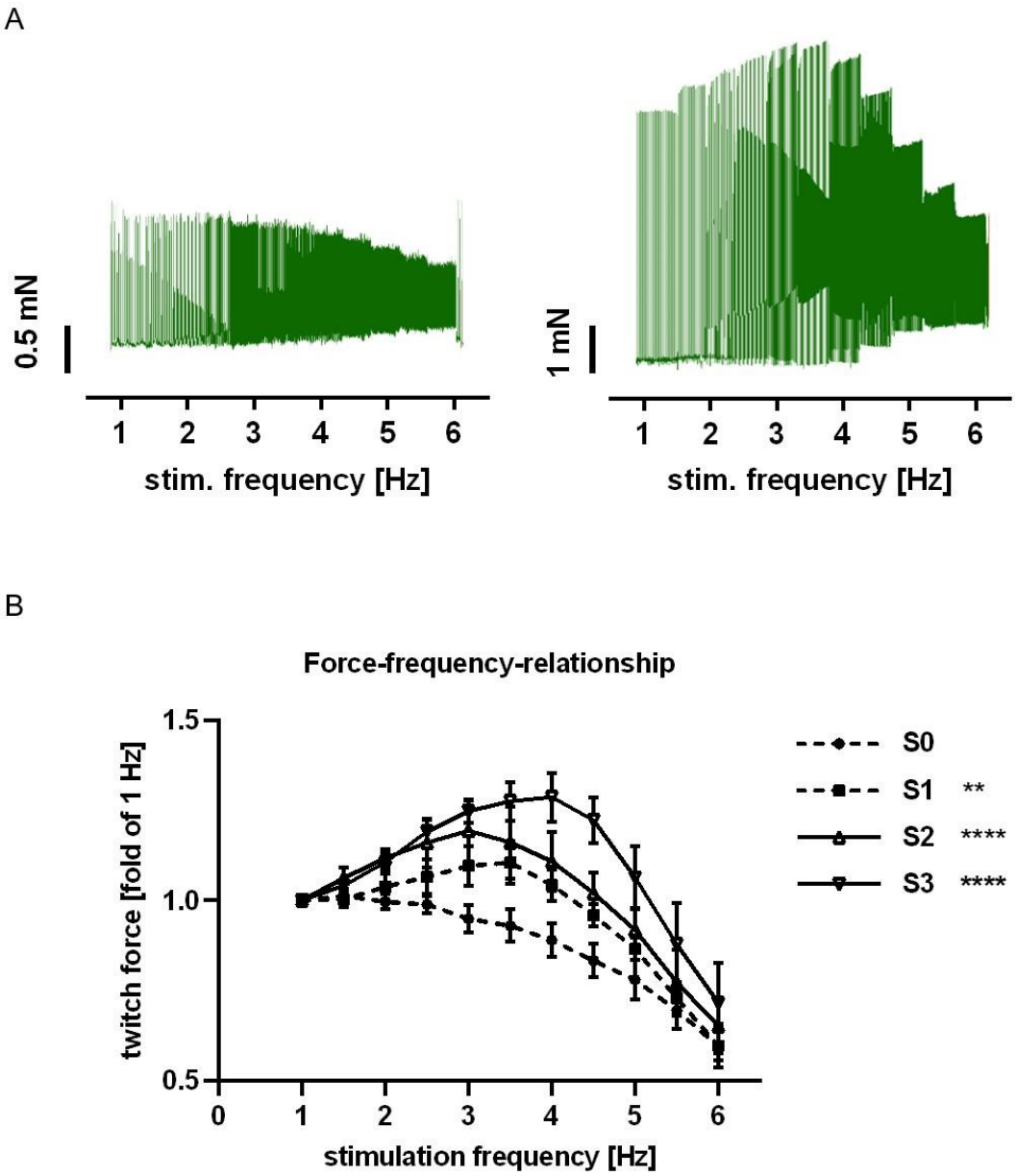

Figure 16. Force-frequency-relationship (FFR)

(A) Exemplary force-frequency-relationship recording of EHTs after three weeks of static (S0) or high (S3) stretch. (B) FFR analysis in four groups of EHTs (S0-S3, n = 7 per group). Two Way ANOVA, Tukey's multiple comparison tests (vs. static stretch), **p < 0.01, ***p < 0.001, ****p < 0.0001. Figure modified from Lu et al., 2021 with permission.

3.4.2 Calcium transients analysis

The proper expression pattern of calcium transients is a crucial component of cardiomyocyte function. At the end of 3 weeks of biomimetic culture, EHTs were loaded with the fluorescence calcium dye Fluo-4 to evaluate the effect of stretch on Ca^{2+}-signaling. The two photographs in Figure 17 (relaxed and contracted) show the relatively homogenous distribution of the calcium dye and the variation in brightness. As anticipated, higher levels of progressive stretch led to greater amplitudes of the systolic Ca^{2+}- transients. Shorter Ca^{2+} - transient duration and faster exponential Ca^{2+}- transient decay (τ) also suggest that the Ca^{2+}- cycling is becoming accelerated in the stretched group (Figure 18).

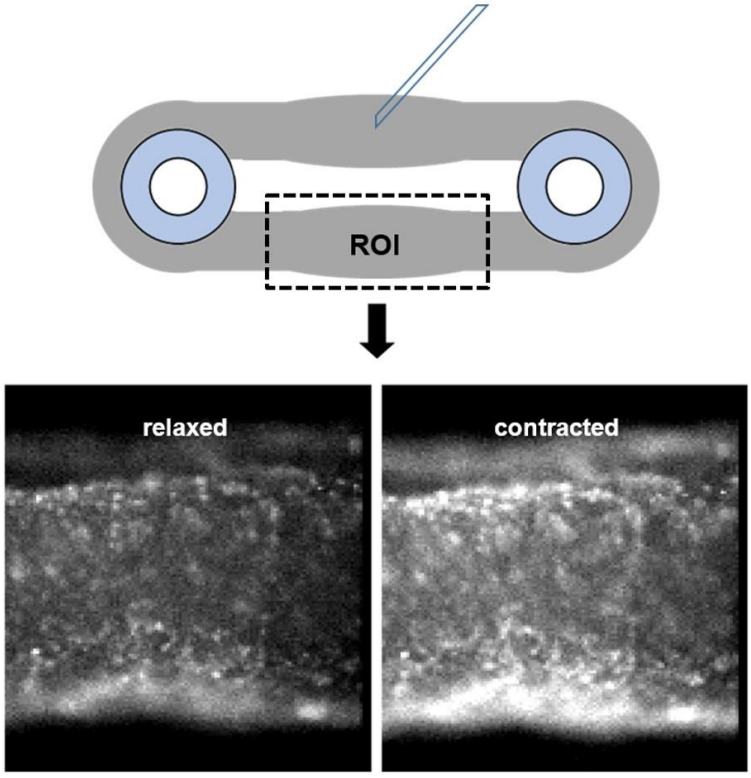

Figure 17. Representative Ca^{2+} - transient

Image capture of Ca^{2+}- transient signals with Fluo-4 loading (ROI: region of interest). Adapted from Lu et al., 2021 with permission.

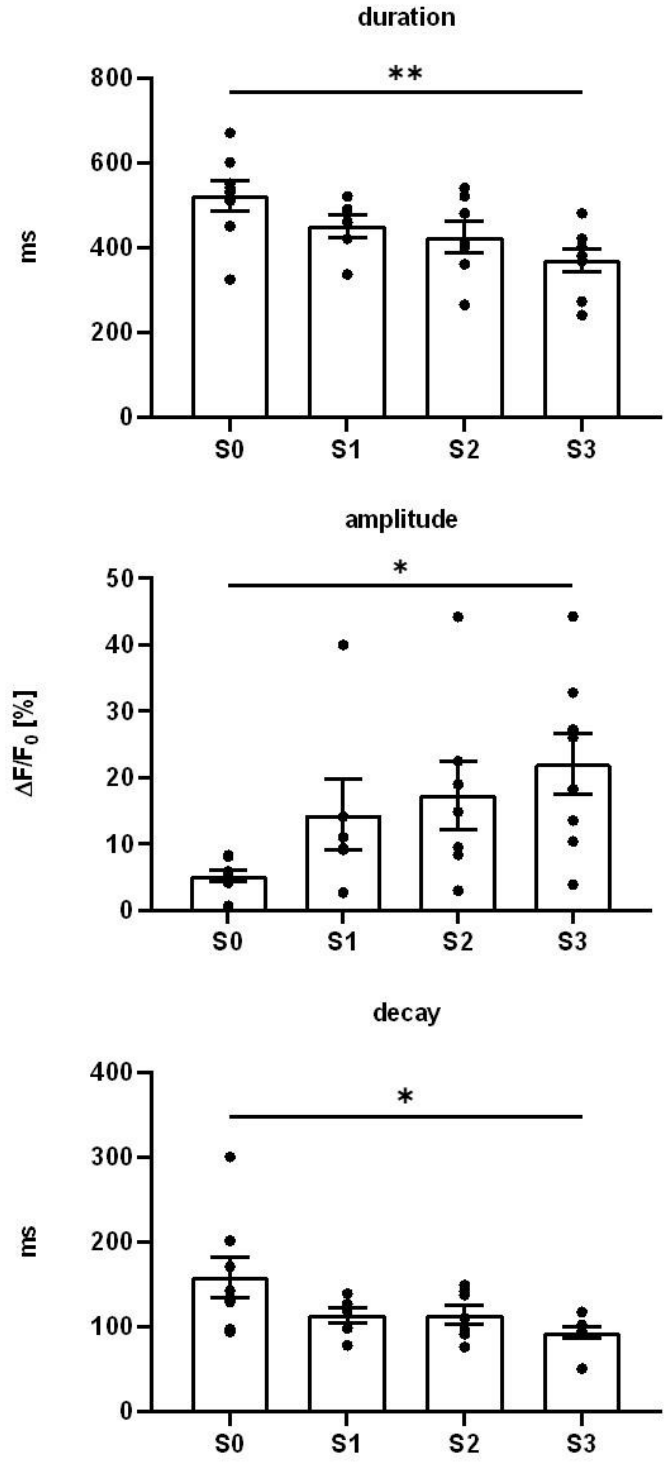

Figure 18. Ca^{2+} - transient quantification analysis

From top to bottom: Ca^{2+}- transient duration, amplitude, and exponential decay (τ) in four groups of EHTs (S0, n = 8; S1, n = 6; S2, n = 7; S3, n = 8). One Way ANOVA, Dunnett's multiple comparison test, *p < 0.05, **p < 0.01. Figure modified from Lu et al., 2021 with permission.

3.4.3 Action potential analysis

Mature electrophysiological properties are central hallmarks of cardiomyocyte maturation. To access the electrophysiological parameters of EHT cardiomyocytes more accurately, we performed separate experiments using glass sharp electrodes. Also, unsurprisingly, the EHT stretched at higher intensity had a more negative resting potential (RMP) and longer AP duration, with some samples of S2 and S3 groups even reaching almost the physiological level (Figure 20). These also corresponded to an increase in the upstroke velocities (S3 13.5 ± 3 V/s; S0 7.8 ± 0.5 V/s) and the larger AP amplitude (S3 100 ± 8 mV; S0 68 ± 6 mV, n = 6).

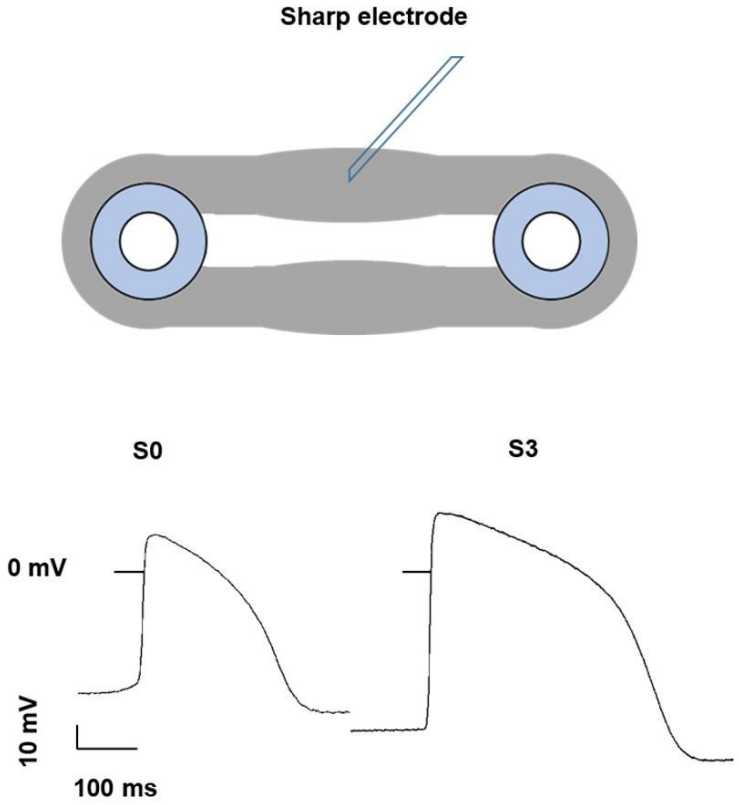

Figure 19. Representative action potentials

Exemplary action potential (AP) recording of EHTs in the S0 and S3 group. Adapted from Lu et al., 2021 with permission.

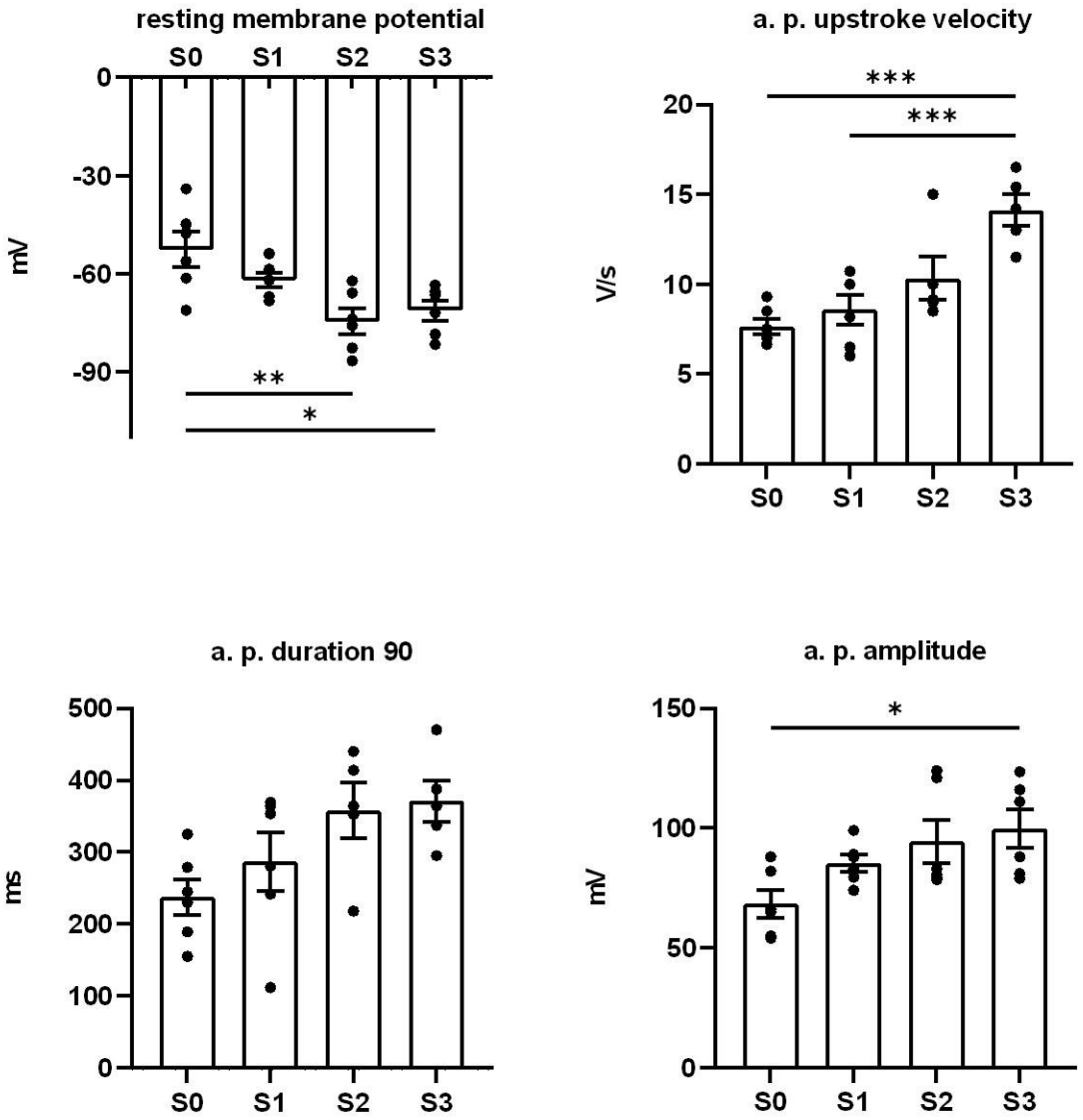

Figure 20. Action potential (AP) analysis

Measurement of resting membrane potential (RMP), AP upstroke velocity, AP duration at 90% repolarization, and AP amplitude (S0-S3, n = 6 for each group). One Way ANOVA, Tukey's multiple comparison test, *p < 0.05, **p < 0.01, *** p < 0.001. Figure based on Lu et al., 2021 with permission.

3.4.4 Effects of beta-adrenergic stimulation

Significant responses to beta-adrenergic agonists indicate phenotypic maturation, given the dependence of a functional adrenergic receptor system on intracellular calcium reserves and the presence of $Ca_V1.2$ channels and T-tubules (Ronaldson-Bouchard et al., 2018, Huebsch et al., 2016, Kaprielian et al., 2000). Stretch enhanced the positive lusitropic and inotropic responses to isoproterenol, as evidenced by greater contractile force, increased relaxation velocity, and shorter twitch duration (Figure 21 A-C).

A

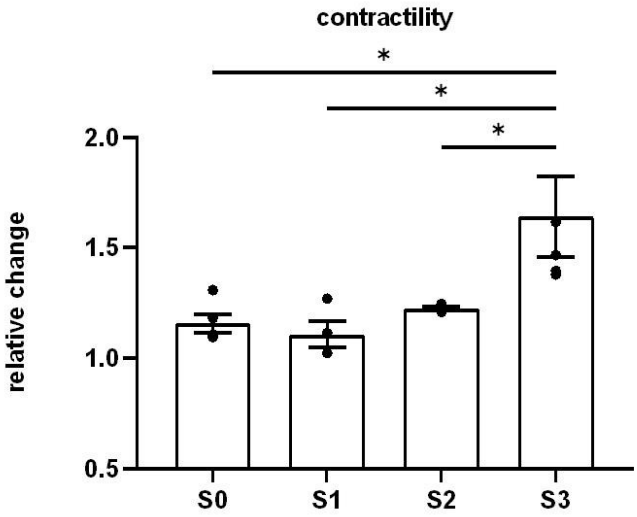

B

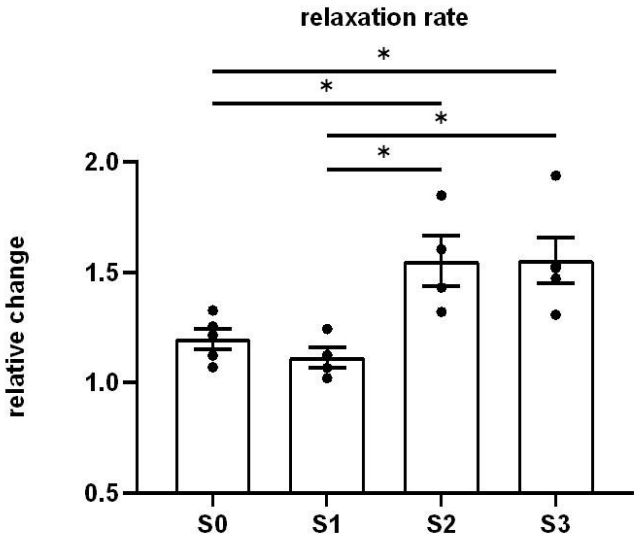

C

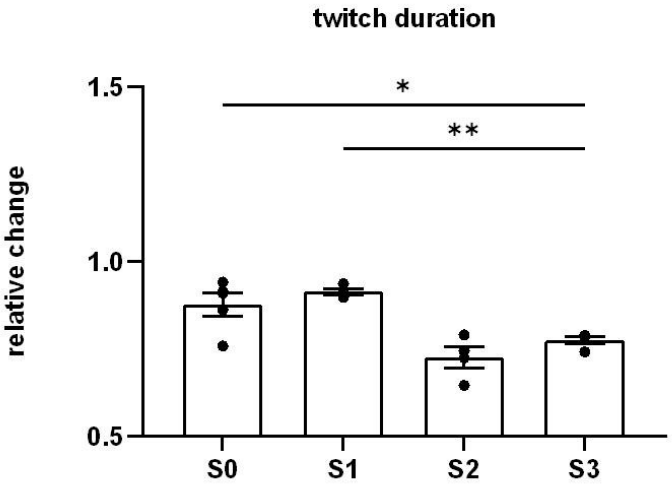

Figure 21. Adrenergic responsiveness of EHTs

Measurement of contractility (A), relaxation rate (B), and contraction duration (C) of EHTs subjected to 1 µmol/L isoprenaline. All values were normalized to pre-treatment values (S0-S3, n = 5). One Way ANOVA, Tukey's multiple comparison test, *p < 0.05, **p < 0.01. Figure based on Lu et al., 2021 with permission.

3.5 Stretch improves adult-specific gene expression in hiPSC-CMs

In addition to morphological and functional maturation, genetic changes are of major significance. Onwards we further studied the effect of progressive stretching on gene expression.

During human myocardium development, the production of the beta-myosin heavy chain (beta-MHC) improves, whereas that of the alpha-myosin heavy chain (alpha-MHC) declines. This occurs during the transition from the fetal heart to the adult heart, with beta-MHC being expressed predominately in the ventricle (Taegtmeyer et al., 2010, Xu et al., 2009).

According to the findings in qPCR experiments, higher intensely stretched EHT express a lower level of MYH6 and a higher level of MYH7. More significantly, the MYH7/MYH6 ratio in high-intensity stretched EHT was roughly 4.6 times greater than in static stretched or low-intensity stretched groups ($p = 0.001$, $n = 6\text{-}13$, Figure 22).

Interestingly, this was accompanied by a decrease in the mRNA expression of brain natriuretic peptide (NPPB, Figure 23), which also is considered to be a gene that responds to stress (Liang and Gardner, 1999).

In other selected genes (including structure, ion channels, and extracellular matrix) however, the role of stretching was not obvious (Figure 23). In order to obtain a more comprehensive and reliable gene expression profile, RNA sequencing was therefore further performed.

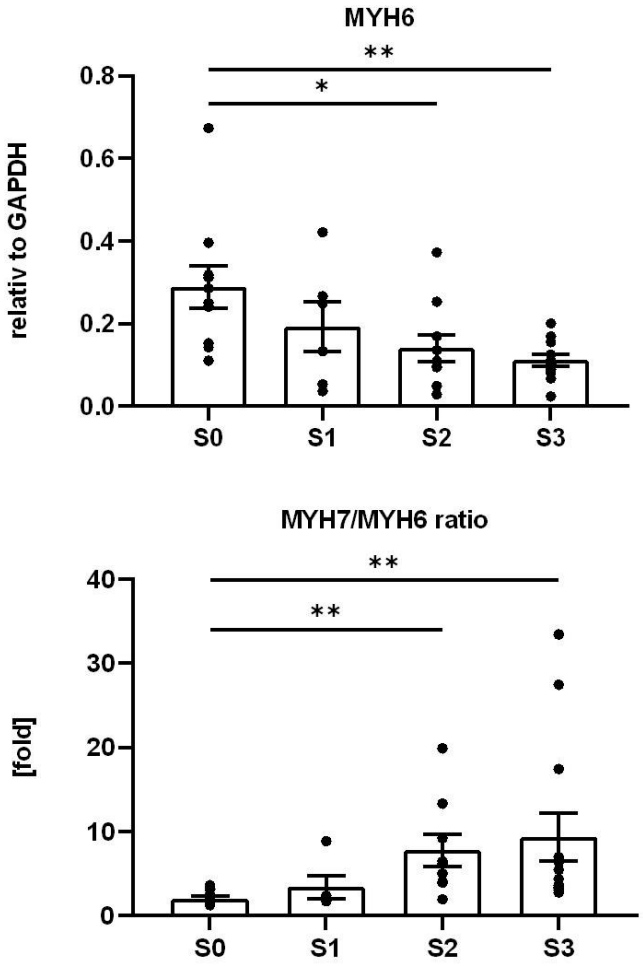

Figure 22. Shifting of myosin isoform expression

qPCR analysis of MYH6 expression and the ratio of MYH7/MYH6 in all four groups of EHTs. One-way ANOVA, Tukey's multiple comparison test. *p < 0.05, **p<0.01. Adapted from Lu et al., 2021 with permission.

Table 2. Primer sequences for qRT-PCR*

	5'- Sequence	3'- Sequence
MYH6	GCCCTTTGACATTCGCACTG	GGTTTCAGCAATGAC-CTTGCC
MYH7	GTATGGCAAGACAG-TGACCG	CGATCCTTGAGGTT-GTAGAGC
SCN5A	CTCTATGG-CAATCCACCCCAAG	CTGAGGACATA-CAAGGCGTTGG
KCNJ2	GTAAAGTCCACACCCGACA AC	CCAGCGAATGTCCACAC AC
ACTN2	ATGGCCTTGGACTCTGTGC	GGTGTTCAC-GATGTCTTCAGC
NRAP	GGCAAATGAGAGAGCC-TATTGG	CCTGGGTT-GCTCATAGTCTTC
MYOM2	CCTGGGAGAGA-CACACATTTG	CTTTGTACCACTGCAC-CACG
COL4A5	CCAGGAATAC-CAGGTCCTAAAGG	GGTCACCTGGAAGAC-CTACATC
MYL4	CACTGCCGACCAGATTGAA-GAG	CTCGGCATTGG-TAGGGTTCTG
VCAM1	GAGGAGTGAGGGGAC-CAATTC	CTAGGGAATGAG-TAGAGCTCCAC
SMPX	CCAATGTTA-GAGCCATCCAGGC	GAACACCCTCCTCCAC-TTCAG
TTN	GGATATGAGGCATCAA-TAGCCGG	CTCACTGGGCTTCACAG-TAGG
NPPB	TGGAAAC-GTCCGGGTTACAG	CTGATCCGGTCCATCTTC CT
CACNA1C	GCCGCTGCAGGAGAG-TTTTA	CCCACATGTGCAAGAC-CACA
SERCA	CATCAAGCACAC-TGATCCCGT	CCACTCCCA-TAGCTTTCCCAG
GAPDH	CATCTTCCAGGAGCGA-GATC	GTTCACACCCATGAC-GAACATG

*Table adapted from Lu et al., 2021 with permission.

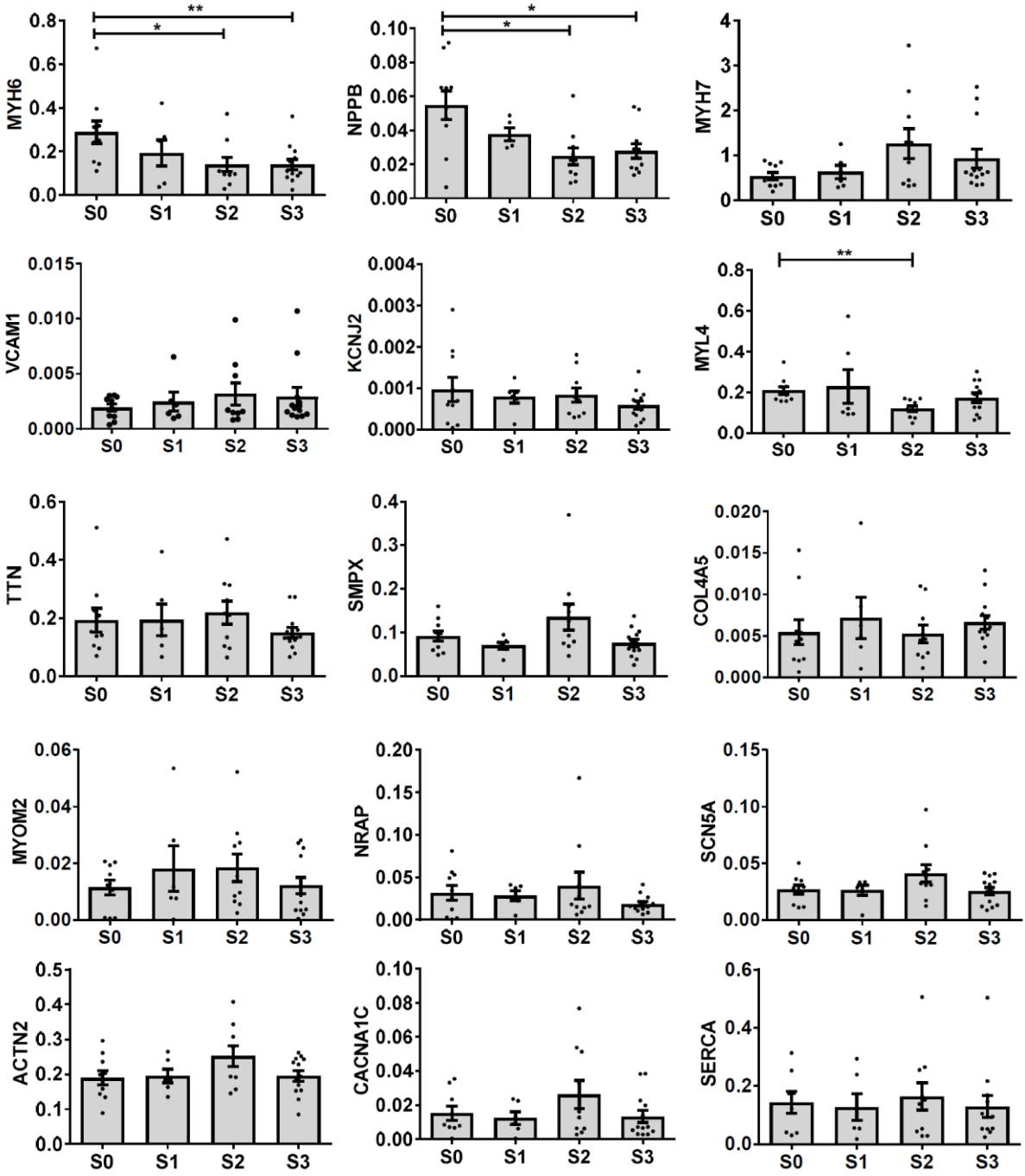

Figure 23. qRT-PCR Data

Stretch conditioning alters the expression of myosin isoforms (MYH6: Myosin Heavy Chain 6; MYL4: Myosin Light Chain 4) and NPPB (Natriuretic Peptide B, or brain natriuretic peptide). Bar plots (Y-axis) indicate the mRNA abundance of analyzed genes relative to glyceraldehyde 3-phosphate dehydrogenase (GAPDH) in EHTs after three weeks stretch. **p < 0.01, unpaired t-test of S0 and S2, S3 groups. Figure modified from Lu et al., 2021 with permission.

To investigate the maturity of stretched EHTs, an unbiased collection of genes that are typically expressed in adults as opposed to embryonic cardiomyocytes was utilized (Tiburcy et al., 2017). An improvement in cardiomyocyte maturation may be deduced from the fact that the average transcript abundance of these genes was 2.1 times greater in stretch conditioned (S3) EHTs compared to statically cultivated (S0) EHTs (Figure 24).

The expression of different genes was evaluated to identify specific maturation processes in terms of ion channels, contractility, metabolism, and also an extracellular matrix. In this context, RNA sequencing revealed a significant upregulation of genes associated with excitation/contraction coupling (Figure 24 B1).

Together with the increase in structural proteins (e.g., Titin, Myosin light chain 2, and Myosin heavy chain 2), the expression of Calsequestrin, which is responsible for calcium storage in the sarcoplasmic reticulum (SR), and Ryanodine receptor 2 (RYR2), which is responsible for Calcium-induced calcium release (CICR), and sarcoplasmic/endoplasmic reticulum calcium ATPase 2 and 3, was also found to be significantly higher.

In aspects of metabolic activities (Figure 24 B2), upregulation of cytochrome enzymes (CYP26A1 and CYP27A1), beta-oxidation (PPAR-a), and reduced activity of anaerobic glycolysis (Lactate dehydrogenase A, LDHA) are key indicators of metabolic shifting. In parallel, the progressive stretch also affects other non-cardiomyocyte cell markers (Figure 24 B3) , such as fibroblasts (e.g., PDGFRA, DDR2) and endothelial cells (CDH5).

All this shows the interactions between different cell types and the importance of non-cardiomyocyte cell types and the extracellular matrix for the myocardial tissue (Figure 25).

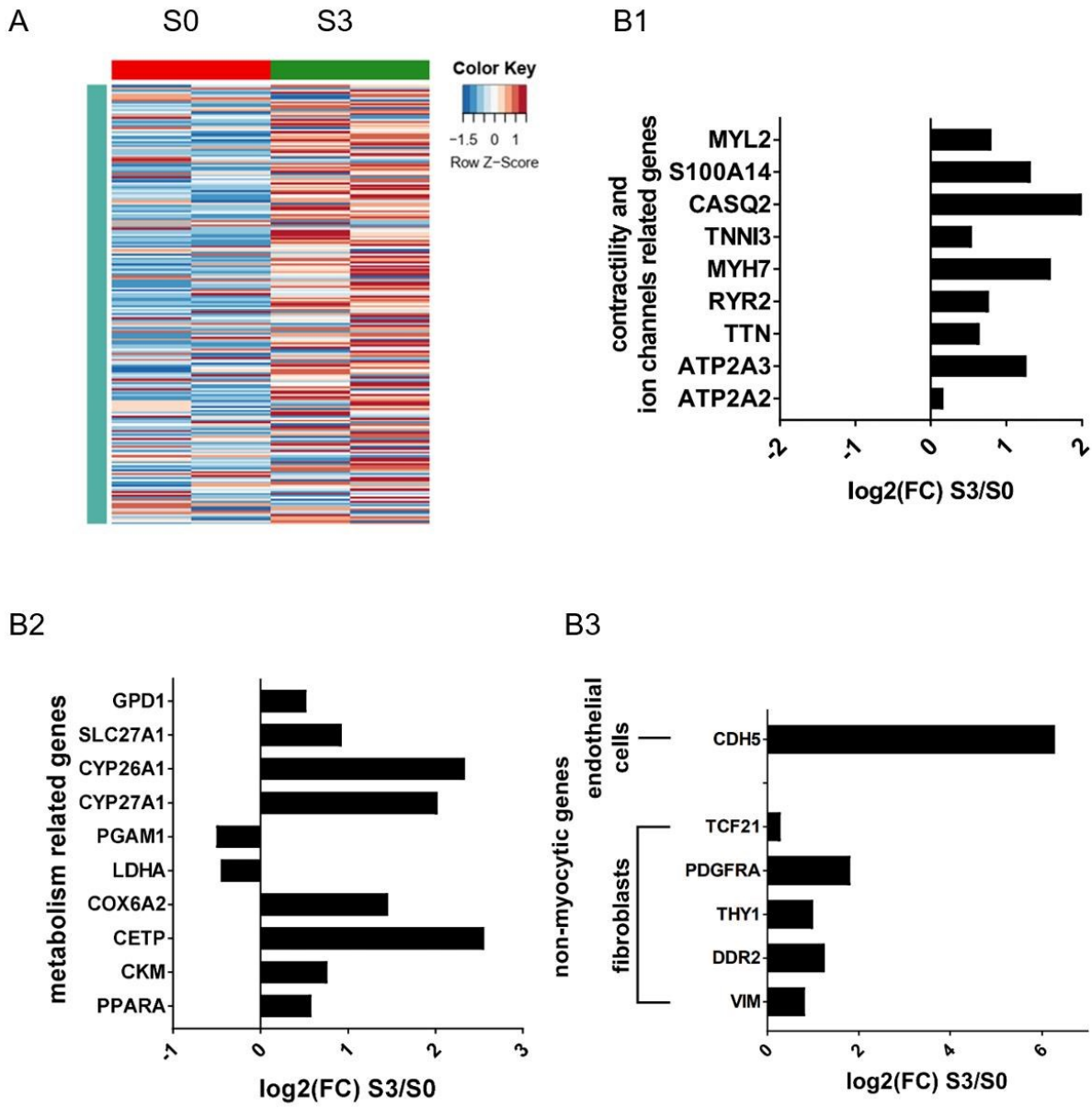

Figure 24. Explorative RNA sequencing

(A) Heatmap of transcripts in EHTs reveals the change in mRNA abundance between statically stretched EHTs (S0, upper red bar) and strongly stretched EHTs (S3, upper green bar). There were based on the 218 genes identified as specifically expressed in adult vs. embryonic cardiomyocytes (Tiburcy et al.,2020). (B1-B3) mRNA expression alteration in statically stretched EHTs (S0) and strongly stretched EHTs (S3) of genes related to cardiac contractility and ion channels (B1), metabolism (B2), or indicative of stretch responses of non-myocytic cell types (B3). Data was provided as means of log2 values of relative mRNA abundance. As an explorative test, no statistics were conducted due to the limited sample size (n=2). Figure modified from Lu et al., 2021, with permission.

3.6 Stretch promotes cellular growth and myofibril alignment

The cell size of immature cardiomyocytes differs significantly from that of mature cardiomyocytes. EHTs with progressive stretching underwent enormous changes in cell size and morphology. The most intuitive change is the macroscopic size elongation of the higher stretched EHTs, which is more than three times longer than that of the static stretched group (S3 vs. S0, Figure 25A). This was also directly tied to the expansion of cardiomyocyte length (Figure 26A).

At the same time, neither the total actinin positive cross-section area nor its contributions to tissue cross-section size were substantially affected by any stretch conditioning (about 40-50% among all stretch conditions, n = 2-6, n.s.; Figure 25C). With immunohistochemical staining and software calculation, the cardiomyocyte's cell length and cross-sectional area were also accessed (Figure 26 A-B).

Based on the data above, it was calculated that progressive stretching more than doubled the estimated volume of cardiomyocytes (mean length x mean cross-section, S0/S1: 3050 μm^3; S2/S3: 6270 μm^3), which coincides to the corresponding increase in EHT muscular mass (tissue length multiplied by actinin positive cross-section, S0: 1.3 mm^3, S3: 2.7 mm^3; Figure 25 A, C).

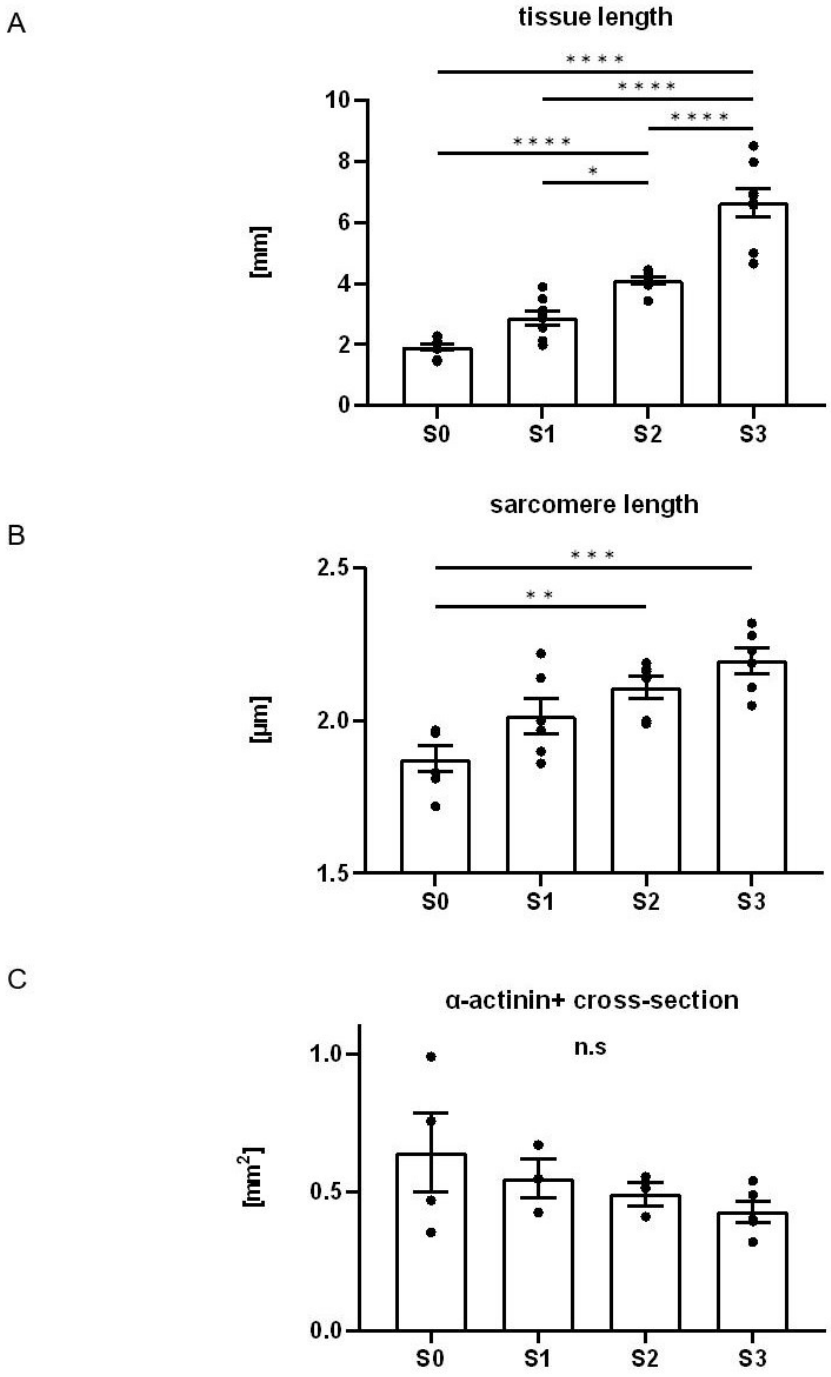

Figure 25. Morphological parameters of EHTs

From top to bottom are the following morphological parameters after three weeks of stretch: (A) EHT slack length (S0-S3, n = 8 for each group), (B) sarcomere length (mean values of n = 6 for each group), and (C) α-actinin positive cross-section area (n = 6 for S0 and S3, n = 4 for S1 and S2). One-way ANOVA, Tukey's multiple comparison test. *p < 0.05, **p < 0.01, ***p < 0.001, ****p < 0.0001. Figure modified from Lu et al., 2021 with permission.

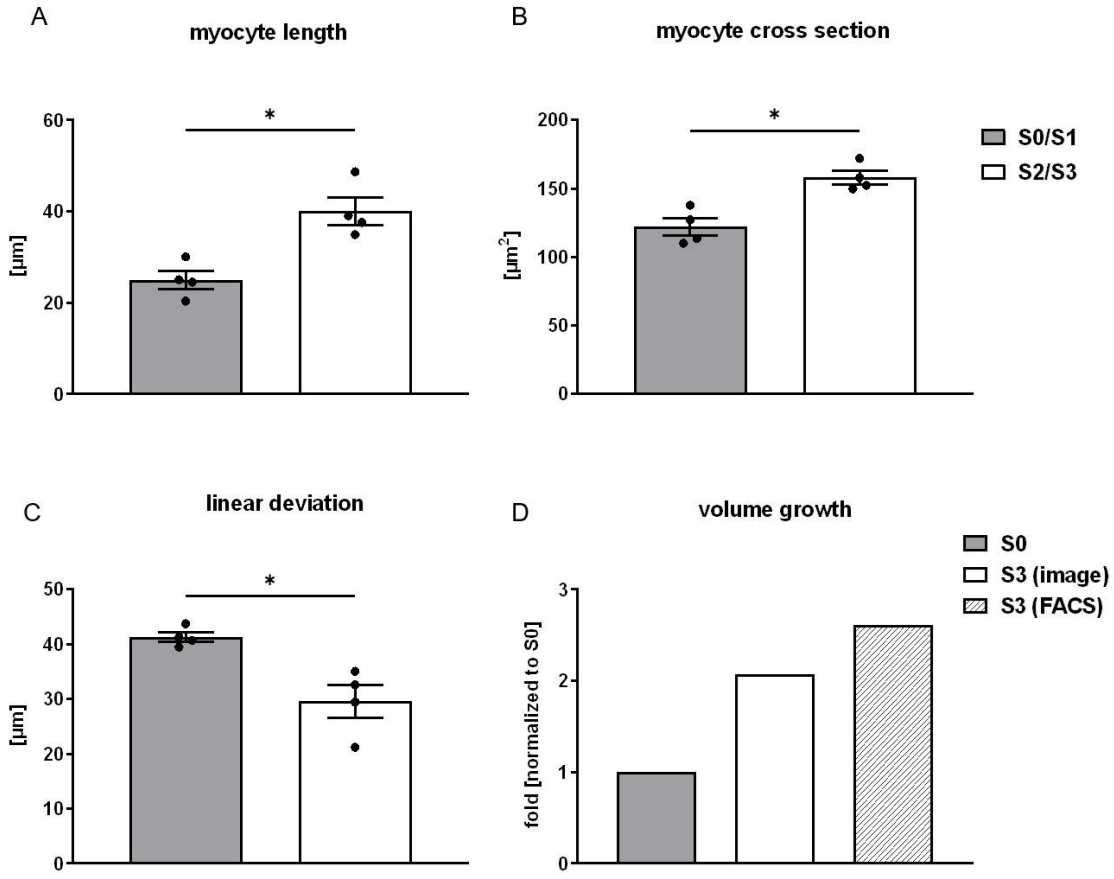

Figure 26. Morphological analysis of cardiomyocytes

(A) - (C) present the morphological parameters of hiPSC-CM after EHT was stretched for three weeks. Due to the sample size, two groups were categorized: S0 + S1 for the low-stretch group, and S2 + S3 for the high-stretch group (mean values of n = 4 for each group). The cell volume growth (D) is estimated values based on two different experimental methods. (A)-(C) Mann-Whitney test, *p < 0.05. Figure modified from Lu et al., 2021 with permission.

To further characterize the cardiomyocyte volume alteration, the verification was performed using flow cytometry. The forward scatter (FSC) intensity is related to the cell diameter and is caused mostly by light diffraction around the cell (Tzur et al., 2011). The ratio of cell size to laser wavelength alters scattering behavior. The analysis of forward scatter (FSC) enables cell size categorization.

Two parameters, forward scatter area (FSC-A) and forward scatter height (FSC-H), were chosen to evaluate the size of cardiomyocytes under different stretching conditions. Cardiac muscle troponin T (cTnT), which is typically well expressed in adult cardiomyocytes, was selected as the FACS marker. Human vascular endothelial cells which did not presumably express cTNT were utilized as a negative control (Figure 27, Figure 28). As shown by the histogram, the rightward shift of FSC-A and FSC-H (red peak) perfectly demonstrates the cell size increase. The red peak indicates a substantial increase from S0 to S3 in both FSC-A and FSC-H (Figure 27). Given that the force of progressive stretching acts largely in one direction, it is quite natural to hypothesize that this action also has a profound impact on the arrangement/alignment of cardiomyocytes.

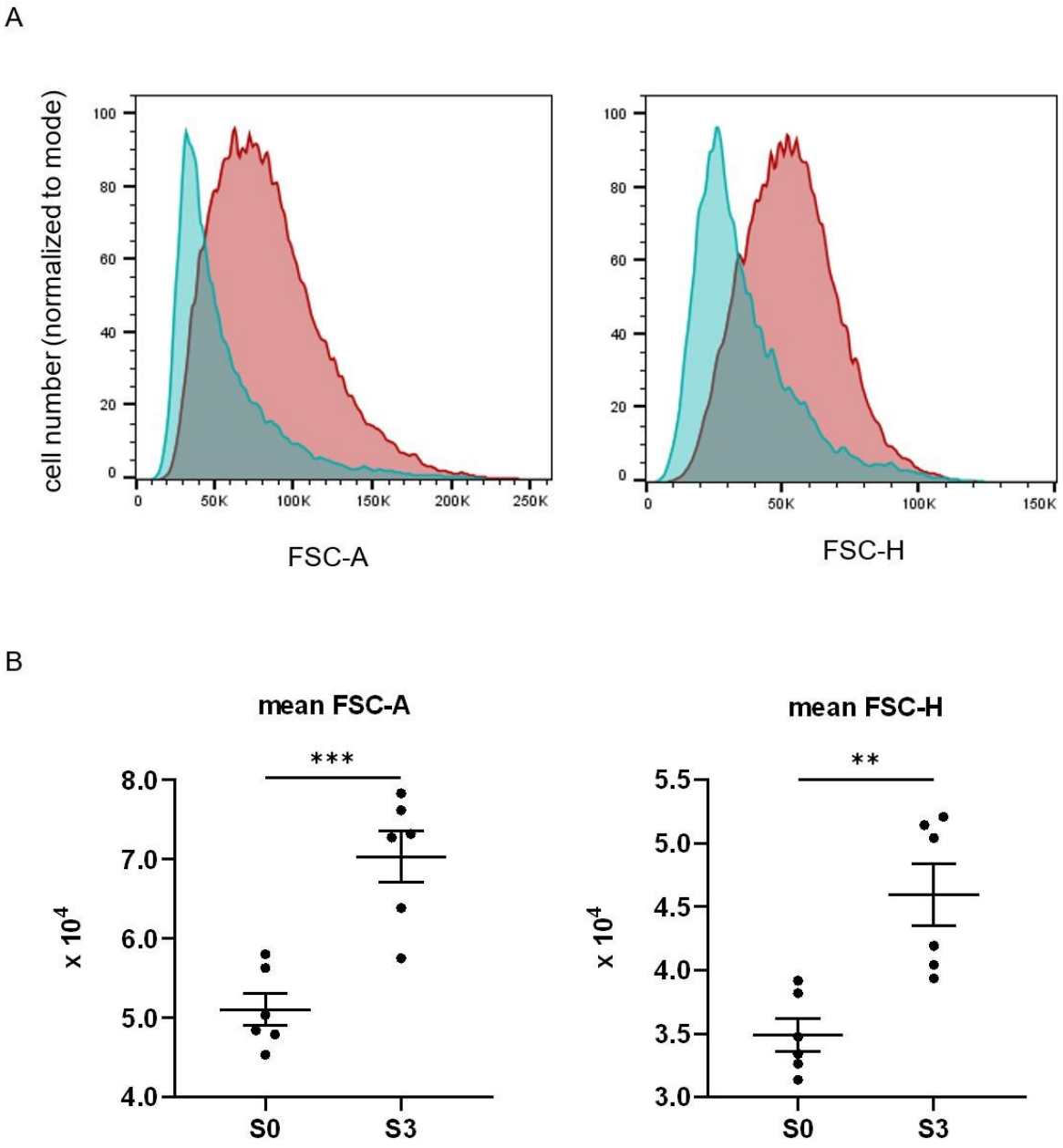

Figure 27. Flow cytometrical cell volume analysis

(A) Representative histogram of mean forward scatter area (mean FSC-A), forward scatter height (FSC-H) shifting. Cells were stained with cardiac muscle troponin T (cTnT). The cyan peak indicates cTnT positive cardiomyocyte from the S0 group, and the red peak indicates cTnT positive cardiomyocyte from the S3 group. (B) Cardiomyocyte volume analysis in terms of mean FSC-A and mean FSC-H, n=6 for S0 and S3. unpaired t-test, *p < 0.05, **p<0.01, ***p<0.001. Figure modified from Lu et al., 2021, with permission.

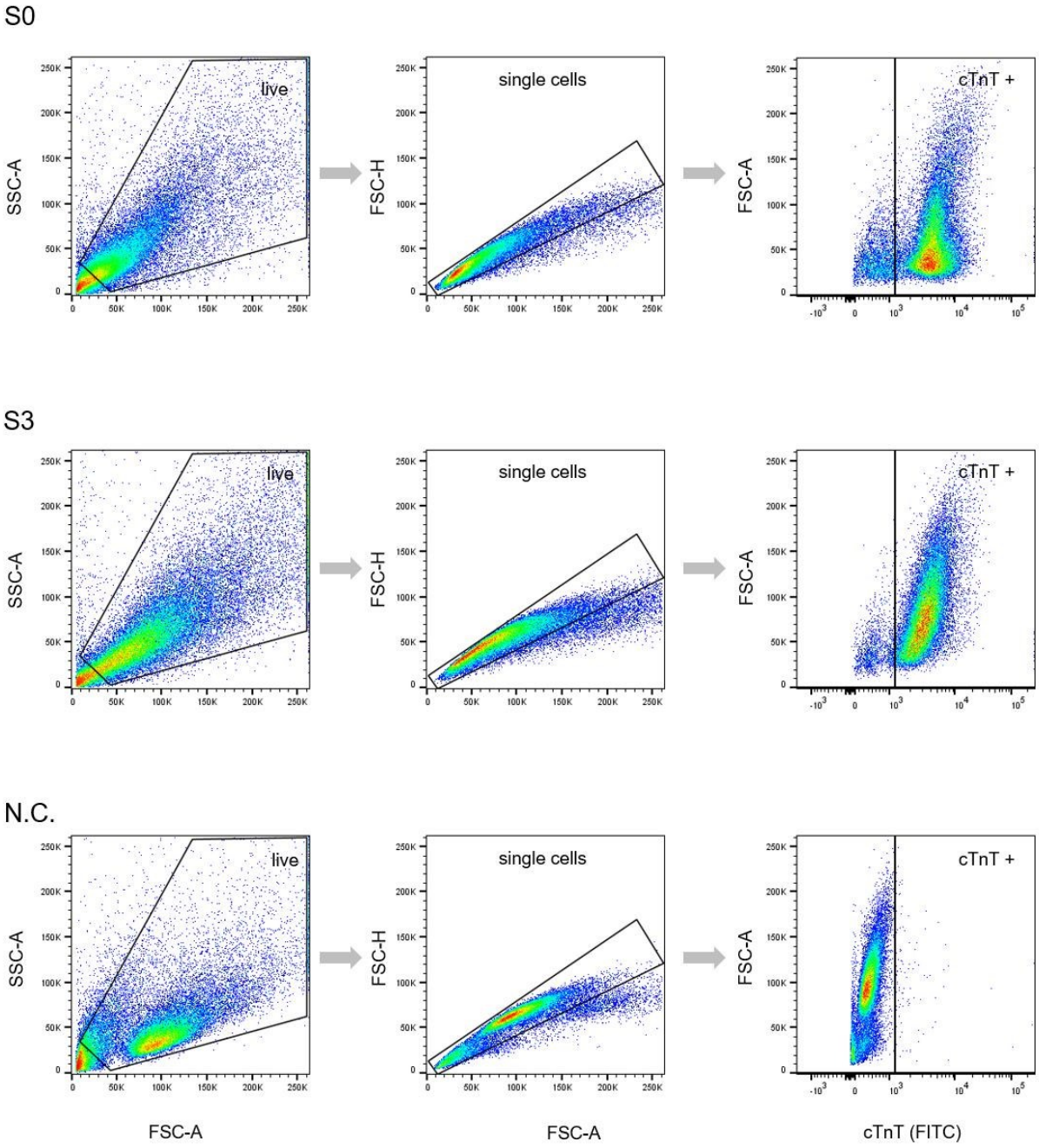

Figure 28. Gating strategy of flow cytometrical cell volume analysis

Representative flow-cytometric analysis of the dissociated cells after 21 days of stretch. S0 (first line) for static stretch, S3 (second line) for high stretch, N.C (third line) for negative control (human vascular epithelial cells). Dissociated cells were stained with cardiac muscle troponin T (cTnT).

Furthermore, the sarcomere length was also extended, which went from about 1.87 µm (S0) to about 2.19 µm (S3) (Figure 25B), which nears the physiological levels (2.2 µm). Such characteristics may play a part in the physiological force/length dependence of stretch-conditioned EHTs, which was shown to be similar to the Frank-Starling relationship (Figure 14). With computer processing, it is recognized that the progressively stretched EHT has a smaller axis dispersion as well as a much neater and more homogeneous cell alignment (Figure 26C, Figure 30). The difference in cellular alignment and abundance was also evident in the immunohistochemical graphs. The majority of cardiomyocytes with densely populated, and linearly arranged cross striations were identified in stretched tissues (S1-S3) by confocal as well as second harmonic generation microscopy (Figure 29), whilst cardiomyocytes exhibited scattered distribution as well as sparsity cross striations in static-stretched tissues (S0).

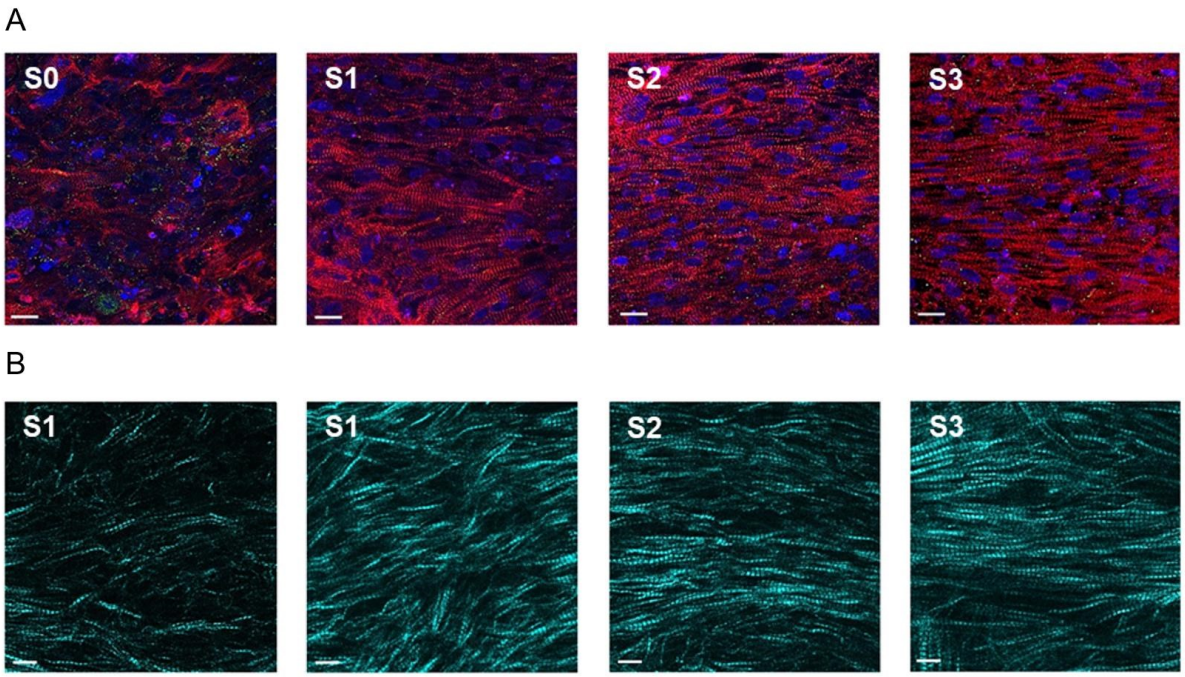

Figure 29. Images of myofibril alignment maturation

(A) Immunofluorescence images of the longitudinal section of EHTs after three weeks of progressive stretching (S0-S3, from static to high stretch conditions). Red for alpha-actinin green for connexin43, and blue for the nuclei. Scale bar: 10 µm. (B) Images of second harmonic generation of stretch conditioned EHTs revealing the alignment and density of myofibrils and sarcomeres. Scale bar: 10 µm. Figure modified from Lu et al., 2021 with permission.

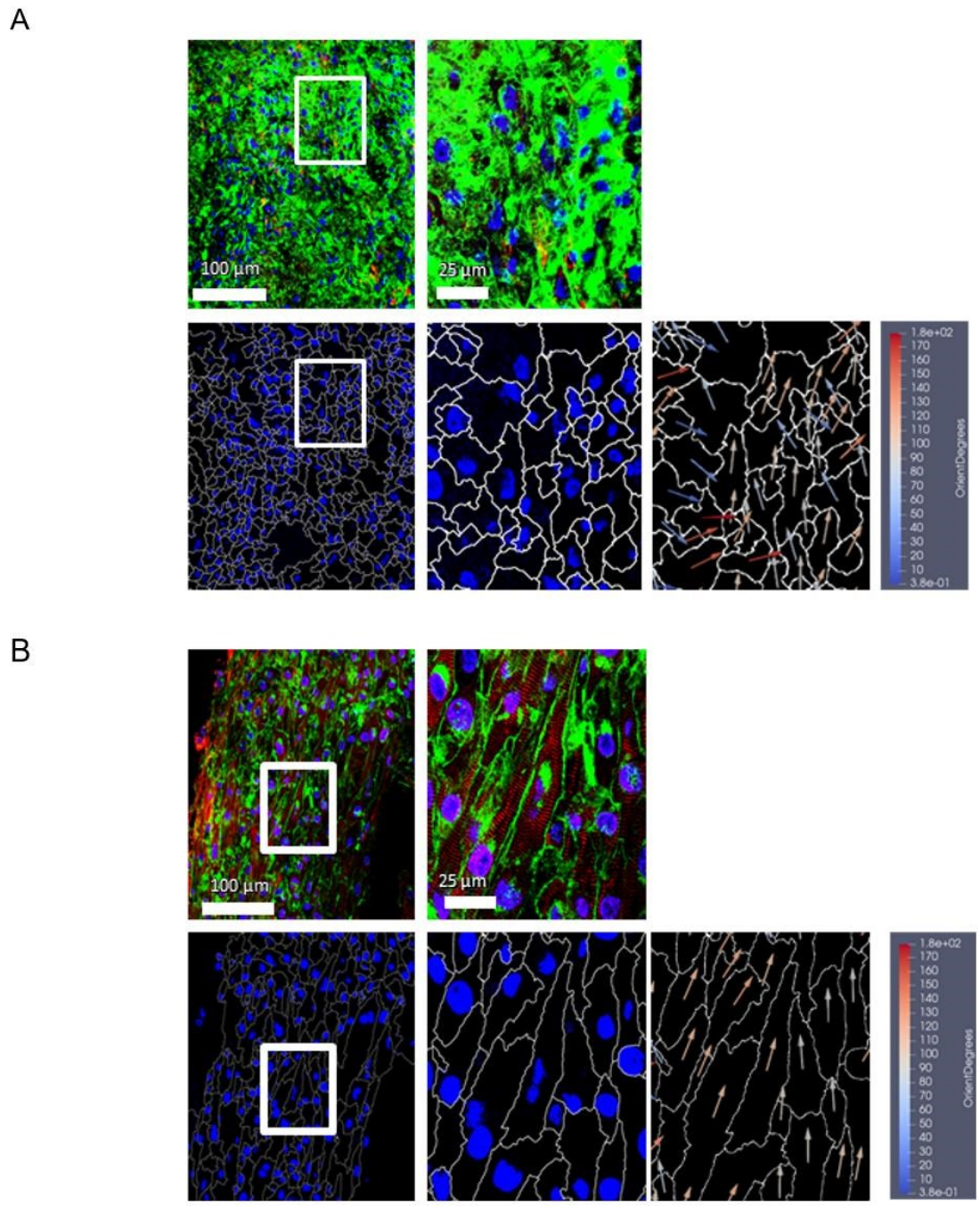

Figure 30. Computational study of hiPSC-CM structure and alignment.

Representative confocal immunofluorescence images of EHTs after three weeks of stretch conditioning. (A) for static stretched and (B) for high stretched EHTs. The upper panels display longitudinal sections with enlarged views of the boxed regions. Green (WGA) was stained for extracellular matrix and cell membranes, red for alpha-actinin, and blue for the nuclei. The respective cell borders (white) and nuclei (blue) identified by automatic image processing are displayed in the panels at the bottom. Arrows represent the direction of the main axis of cardiomyocytes. Figure modified from Lu et al., 2021 with permission.

Microscopy at high magnification showed a larger proportional area of alpha-actinin positive myofibrils in myocyte cross-sections and a tighter assembly of cardiomyocytes in progressively stretched compared to static stretched EHTs (Figure 31). The growth of myofibril density and structure, as well as strong mechanical cellular connection, may well be considered the structural basis for the increase in contractility caused by progressive stretch conditioning.

A

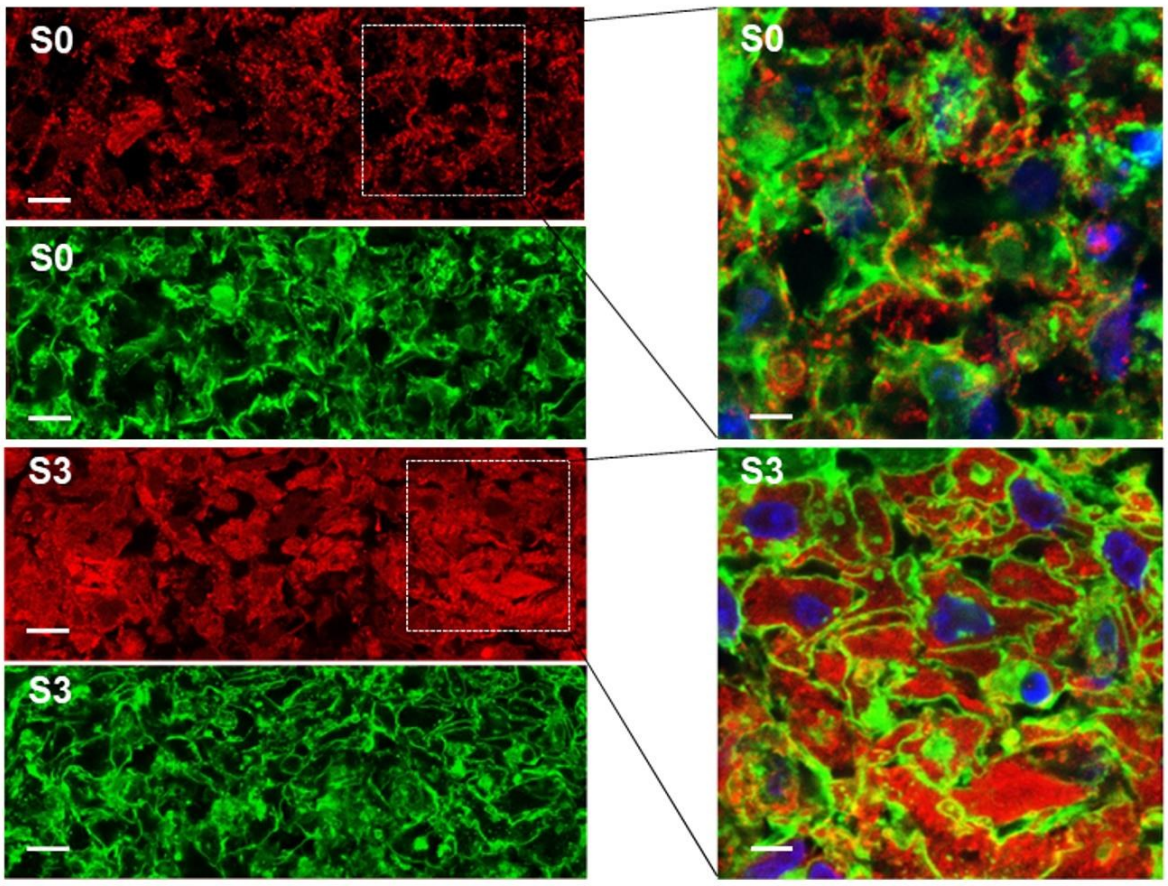

B

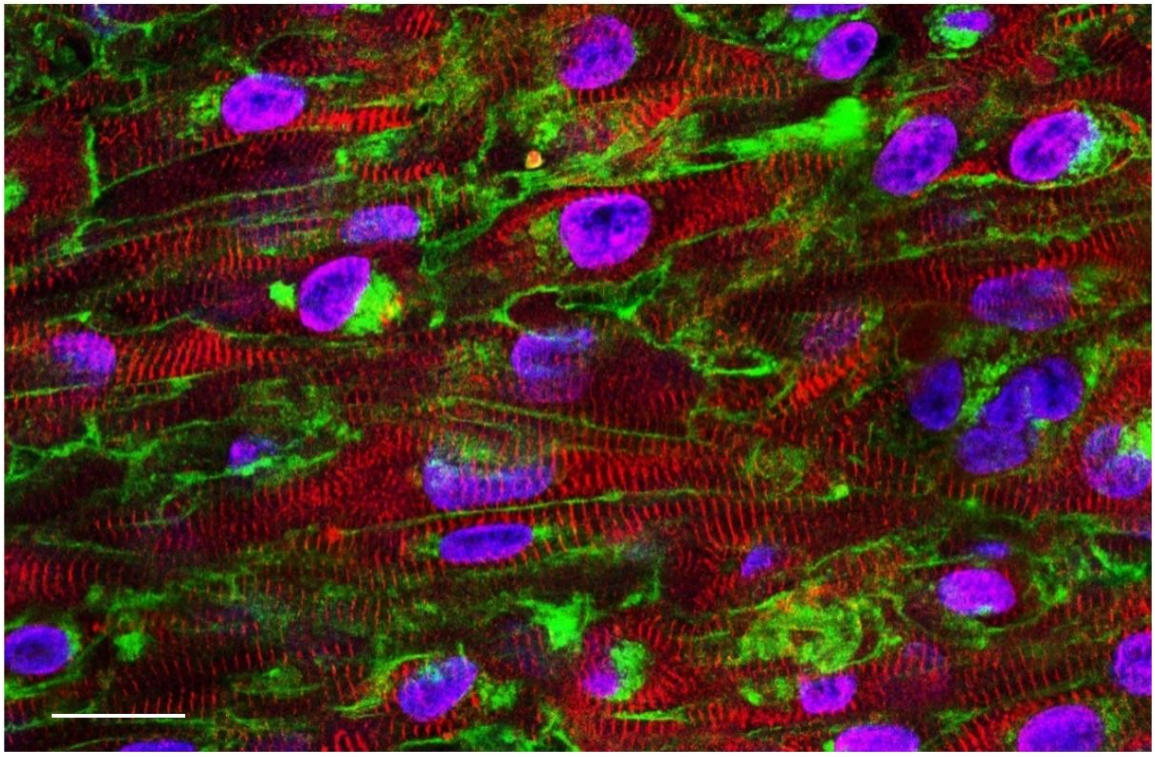

Figure 31. High-magnification fluorescence images of stretched hiPSC- CMs

(A) Cross-sections of EHTs (S0 for static, S3 for high stretched) at high magnification. WGA-negative areas correspond to cell-free areas (predominant in S0) or cytosol cross-sections (predominant in S3). Scale bar left: 10 µm, scale bar right: 5 µm. (B) Longitudinal section of S3-conditions EHT at high magnification, scale bar: 10 µm. (A) and (B) stained for alpha-actinin (red), WGA (green), and DNA (blue) after three weeks of stretch conditioning. Figure modified from Lu et al., 2021 with permission.

4. DISCUSSION

For years, scientists dedicated numerous efforts to the path to mature stem cell-induced cardiomyocytes and tissues. With the development of innovative technologies, such as pluripotent induced stem cells, 3D printing, and novel extracellular matrices, induced cardiomyocytes are increasingly moving toward a more mature stage. A suitable biomechanical condition is essential for cardiomyocyte development and functional maintenance. In vivo, cardiac organogenesis occurs under proper biomechanical strain (Taber, 1998). It functions effectively within a certain hemodynamic load range and fails in acute or chronic overload circumstances. Nevertheless, the implementation of this complex process in vitro has been an intensely investigated problem. More specifically, the physiological hypertrophy of cardiomyocytes, which is a characteristic of postnatal cardiac development, needs to have its size adjusted and be guided by the appropriate biomechanical stresses in order to function properly (Taber and Perucchio, 2001, Taber, 2001).

In our recent work, we demonstrated that mimicking tissue mechanics by the application of unidirectional stress was regarded as a significant prerequisite for the preservation of adult human heart tissue in culture (Fischer et al., 2019). This same reliable biomimetic culture system was employed for the purpose of inducing EHT maturation in order to better simulate the above conditions. This biomimetic culture system not only provides the electrical stimulation and oxygen supply required by the myocardium but, more importantly, is able to adjust the preload and compliance in accordance with the tissue growth. By using a renewed formulation and applying several different stretching forces to the EHTs, we have been able to demonstrate the key impact of progressive stretching on EHT maturation. With this strategy, we were able to demonstrate that EHTs derived from hiPSC-CMs direct response to progressive stretch along with elongation and linear alignment of CMs, increased density and structure of myofibrils, and excitation-contraction characteristics that resembled those of human adult myocardium, which include positive force-frequency and force-stretch relationships.

Detailed studies have shown that human cardiomyocytes lose the potential for cell division since postnatal, but heart weight still increases by hypertrophy until adulthood (Li et al., 1996, Oparil et al., 1984). As such, hypertrophy is the primary cellular activity responsible for the postnatal volume increase of single cardiomyocytes (Oparil et al., 1984). Different from the pathological hypertrophy remodeling caused by excessive

stress, the myocardial development that occurs during this phase is an adaptation strategy that improves heart size and function (Gibb and Hill, 2018). Thus, proper mechanical loading is definitely required for the completion of cardiomyocyte differentiation and maturation following their origin from stem cells.

4.1 Biomechanical approaches

In view of the overwhelming significance of biomechanical load, many investigators try to incorporate appropriate conditions in bioreactors designed to improve the maturation of artificial myocardium (Karbassi et al., 2020, Guo and Pu, 2020, Besser et al., 2018). Numerous studies evaluating various mechanical loading strategies on two-dimensional or three-dimensional EHTs have verified this concept, which includes substrate mechanics (Tallawi et al., 2015), static stress (Abilez et al., 2018, Hirt et al., 2012), and cyclic stretch (Zhang et al., 2017, Ruan et al., 2015, Mihic et al., 2014). Yet it suffers from various deficiencies. Firstly, passive stretching relies only on the force generated by the continuous compaction (referring to the smaller size and the tightening of the intercellular spaces) of the tissue during its growth in order to stimulate its growth. This tension generated by intercellular connections is frail compared to external forces. Therefore, the passively stretched tissue will not be mechanically stimulated to the maximum extent. Cyclic external stimulation solves the first problem by enabling the stimulus to become more powerful. However, both methods above have a major limitation, which makes them fundamentally different from the progressive stretching method. Both approaches have limited the final size of the EHTs from the experiment beginning, leading to the undeniable result that the physical size of the tissue will remain the same at the end of the training period. That is contradictory to the process of postnatal myocardial development. In contrast, the progressive stretching approach in this study ultimately resulted a 3-fold increase in the EHTs´ length (Figure 26 A) without consistently increasing the strain (Figure 9B, S0-S2). It also enhanced the contraction force of EHTs by a factor of 5 and contributed to the normalization of the sarcomere length (Figure 9C, Figure 26). Therefore, this presented method provides a fundamentally novel concept to enlarge the physical dimension of the tissue. It may be beneficial for later application in clinical treatment.

In order to accommodate progressive stretching and to provide a convenient protocol for EHTs construction, a completely redesigned methodology for manufacturing EHTs

was developed. Using commercially available small-molecule differentiation media, approximately 70% of iPSC from our cell line (MRIi004-A) were successfully induced into double-positive (alpha-actinin, cTnT positive) beating cardiomyocytes. The obtained cardiomyocytes were not purified by additional techniques (e.g., lactic acid nutrition (Tohyama et al., 2013)), and no additional cell types were added (e.g., fibroblasts, endothelial cells), thus greatly simplifying the cell acquisition process.

After differentiation, the unpurified populations of cells were dissociated into single-cell suspensions and then sufficiently mixed with a multitude of extracellular matrices and growth factors. The cell mixtures were carefully dripped onto the filter for the first compaction. This two-step design is intended to accelerate tissue solidification, which minimizes the effect of natural tissue shrinkage and gives the EHTs sufficient stability to withstand subsequent external stretching. In addition, our method omitted using the preconstructed scaffold (Rastogi and Kandasubramanian, 2019, Lee et al., 2019, Koivisto et al., 2019), leaving the mechanical support utterly reliant on the previously mixed hydrogel and the endogenous secreted extracellular matrix from the cell populations (especially the non-myocyte population). Thus, a high cell density could be employed to produce a more compact structure, which enabled more rapid development of intercellular connections and the conduction of electrical and mechanical signals, thereby providing a solid foundation for subsequent progressive stretching.

4.2 Application of multi-factorial biomimetic conditions to cardiac tissue engineering

Aiming to establish a superior milieu for EHTs maturation, many studies have applied further approaches to keep myocardial tissue viable and to promote its differentiation and growth in vitro. As a reference point for stretch conditioning, we selected EHT production and maintenance settings incorporating many newly described maturation promoters.

Given that thyroid hormone and glucocorticoid are essential for cardiogenesis and fetal cardiac development (Rog-Zielinska et al., 2013, Klein and Ojamaa, 2001). Parikh et al. developed a protocol that combined those effects to enhance T-tubule development as well as mature excitation-contraction coupling in hiPSC-CMs (Parikh et al., 2017). By replacing glucose in the culture medium with lactose or galactose and adding small

molecules such as fatty acids, researchers not only enriched the fraction of cardiomyocytes (Tohyama et al., 2013) but also improved the number of mitochondria and total oxidative capacity in hiPSC-CM (Horikoshi et al., 2019, Correia et al., 2018). Accordingly, we employed a serum-free medium for EHT maintenance (Tiburcy et al., 2017) and hormonal supplementation with evidence-based support for additional maturation promotion (Huang et al., 2020, Parikh et al., 2017).

Similar to adequate mechanical stimulation, also triggered electrical excitation has been found to significantly improve cardiomyocyte differentiation (Hirt et al., 2014). This is surprising because stem cell-derived EHTs typically display spontaneous rhythmic excitation. However, additional external pacing permits synchronized electrical and mechanical stimuli. Morgan's group first created a bioreactor system that allowed them to electro-mechanically stimulate EHTs (originated from neonatal rat cardiac cells entrapped in fibrin gel) for two weeks. Field electrical stimulation was applied with a delay to external stretching of the tissue and thus mimicked isovolumic contraction. Delayed combined stimulation resulted in statistically higher SERCA2a and troponin T expression levels and greater Akt1 expression compared to static culture, mechanical stimulation only, and electrical stimulation alone (Morgan and Black, 2014b, Morgan and Black, 2014a). A further biomimetic approach by Miklas and colleagues focused on the significance of diastolic tension. The group designed a reactor platform capable of electrical field stimulation in conjunction with static strain. Static strain generated by 5 % elongation of EHTs in combination with 1 Hz electrical stimulation improved sarcomere linear alignment and Cx43 expression after only three days of culture compared to either mechanical or electrical stimulation alone. Upregulated expression of atrial natriuretic peptide (ANP) and brain natriuretic peptide (BNP) indicated responses to increased preload in the electro-mechanically stimulated group (Miklas et al., 2014b, Miklas et al., 2014a). In this thesis, continuous pacing was performed at a normal heart rate (1 Hz), and we noticed a slowing of spontaneous beating rate, consistent 1:1 pacing at 1 Hz, and a steady decrease of stimulus threshold (Figure 10) as evidence of electrical maturation.

In quiescent cultures, oxygen availability is low due to its slow diffusion through an unstirred medium layer. Consequently, Radisic et al. fabricated a bioreactor with perfusion which was capable of administrating pulsatile fluid flow at physiologically relevant shear stresses and flow rates to EHTs made of neonatal rat cardiomyocytes and fibroblasts (Radisic et al., 2008, Brown et al., 2008). Under this condition, cardiomyocytes also

exhibited improvements in cell length and diameter, and this approach appears to be essential for the generation of large-scale myocardial therapeutic patches (Valls-Margarit et al., 2019). In our previous work, the preservation of adult multicellular preparations also required agitation to accommodate oxygen requirements (Fischer et al., 2019), and corresponding measures (perfusion or oxygenation) have been demonstrated to drastically increase the shape and function of iPSC-derived cardiac bundles (Jackman et al., 2016). In my work, our real-time assessment of contractility gives clear proof that the O_2 requirements of highly contractile EHTs are not sufficiently met by stationary incubation and are considerably more prominent in stretch-conditioned tissues (Figure 11). The increased oxygen consumption in stretch-conditioned EHTs is further manifested by a higher mitochondrial abundance and a more linear mitochondrial network (Figure 12). Some other methods, such as prolonged incubation, were also shown to be effective for maturation. iPSC-CMs gradually mature in long-term culture and – during many months - develop larger cell volumes, better myofibril alignment, and β-adrenergic response, as well as induced expression of adult marker genes such as Cx43 (Connexin 43), troponin I, and MYH7 (Myosin Heavy Chain 7) (Lundy et al., 2013). Due to the experimental duration, it was not applied in our work.

Consequently, the extensive implementation of features favoring myocardial tissue maturation appeared to be a promising concept for developing a new biomimetic bioreactor. Notably, the other maturation conditions given to all EHTs in this study have already enabled a relatively elevated level of maturation. Certain other parameters, such as the distribution of connexins, T-tubule formation, and the proportion of cross-sectional area occupied by cardiomyocytes, did not change substantially, and remained at the same levels. This might be attributed to too short a culture period, undifferentiated cell populations, and the absence of certain hormones.

4.3 Progressive stretch enhances the EHT maturity in different aspects

Considered as one of the major functional indicators of cardiomyocytes, contractility directly reflects their maturation. As the most significant change, a huge increase in EHT contraction force can be visualized with the help of real-time force monitoring. Compared to the slight increase in static stretching (S0), the EHT of progressive stretching (S3, 11.3 mN/mm²) outperformed almost all of the most recently reported tissues (< 5

mN/mm²) (Ronaldson-Bouchard et al., 2018, Tiburcy et al., 2017, Moretti et al., 2013, Radisic et al., 2004) and thus nearly attained the active force development of the human adult heart (15 mN/mm^2) (Grossman et al., 1975). Moreover, the enormous alteration in contractility is inseparable from the maturation of a series of structural and functional parameters, such as cell size, linear orientation, electrical properties, calcium signaling, etc.

Improvements in cell size and sarcomere length were observed in the immunohistochemical image (Figure 26-27) (2.2 µm, identical to adult cardiomyocytes; Lundy et al., 2013) and further verified by the flow cytometry results (Figure 28). Compared with other studies, the utilization of flow cytometry to verify the cell volume increase is highly plausible. It is primarily because the cells are in a fixed arrangement in the tissue, and the external forces acting on the cells are not entirely eliminated when the tissue is fixed. In contrast, with flow cytometry, the viable EHT tissue must first be dissociated into a single-cell suspension, which implies that the cardiomyocyte will lose the attachment to the extracellular matrix and become sphere-like again. The cell volume obtained at this point is more accurate. Yet it is obvious that the cardiomyocytes after only three weeks of training cannot reach the same size dimensions as the adult ventricular cardiomyocytes. Both results revealed that the increase of EHT length is attributed to the longitudinal growth and hypertrophy of cardiomyocytes rather than to a reversible elastic deformation. In parallel, no significant wall stress (diastolic load) alteration was found at low and moderate stretching rates (S1, S2), which further supports the direct correlation between progressive stretching and cell growth. Nevertheless, the more frequent tearing condition in the high-speed stretch group implies that such an increase in diastolic stress is unstable. Therefore this speed is probably already exceeding the maximum growth rate of cardiomyocytes.

A subject's elastic modulus measures its resistance to elastic deformation (i.e., temporary deformation) in response to external forces. We observed an enhancement of the elastic modulus of EHTs after progressive stretching. In the high-speed stretch group, the elastic modulus (S3, 4.5 kPa) has been capable of approaching the same level of healthy human myocardium (5-7 kPa (Ghista et al., 1975)) or porcine myocardium (5.8 kPa (Momtahan et al., 2015)). Momtahan et al. proved that less than 25% of myocardial tissue elasticity is derived from the extracellular matrix under physiological conditions, whereas more originates from the cardiomyocytes themselves (Momtahan et al., 2015). However, EHTs with pre-assembled scaffolds usually exhibit relatively high stiffness,

with this excess mechanical contribution actually due to the adhesion of cardiomyocytes to the extracellular matrix. In this pattern, cardiomyocytes do not fully act on their own stiffness but rather attach more to the extracellular matrix (McCain et al., 2014). Such a condition tends to impede mechanical force transmission between cells, thus leading to a non-physiological mechanical stimulus (McCain et al., 2012). One prominent feature of our model is to eliminate the influence of the extracellular scaffold or matrix on mechanical force transmission. By decreasing the proportion of the extracellular matrix and increasing the cell density in the suspension, we enabled cardiomyocytes themselves to generate the predominant part of EHT elasticity. Therefore, our method promoted the generation of active (systolic) and passive (diastolic) forces of EHTs within a physiological ratio of 9/1 in the elastic situation inside BMCCs and of 9,5/1 under optimal preload and an isometric contraction in an organ bath. These data from EHTs agree closely with the relation of maximal systolic/end-diastolic wall stress of the human heart (10.2 ± 1.7) (Hood et al., 1968), therefore confirming that EHTs exhibit comparable capabilities to adapt changes from external distension into improvements of sarcomere length.

In stretched EHTs, a switch of myosin heavy chain isoform expression (alpha-MHC to beta-MHC) was identified, which might be interpreted as evidence of cardiogenesis progression (Xu et al., 2009). Despite the fact that other genes chosen for rt-PCR gave limited evidence of maturity of stretched EHTs, a comprehensive evaluation using RNA-seq demonstrated a considerable upregulation of genes that had been validated as markers of maturation (Tiburcy et al., 2017). These genes are known to be involved in signal pathways of excitation/contraction coupling (including ion channels), metabolism, oxidative phosphorylation, and in the differentiation of non-myocyte cell types (e.g., fibroblasts and endothelial cells). Given that the second approach corresponds to a characteristic fingerprint of cardiomyocyte gene expression and therefore is generally acknowledged for assessing cardiogenesis, we may conclude that stretch-conditioned hiPSC-CMs exhibit a more mature transcriptional program.

Unexpectedly, we identified a distinct suppression of brain natriuretic peptide (BNP) activity at all degrees of stretch, which appears to contradict the mechano-sensitive upregulation of BNP observed in heart failure and in EHTs with low compliance or isometrical conditions (Leonard et al., 2018, Hirt et al., 2012, Magga et al., 1997). This further confirms that the EHTs undergoing progressive stretching in BMCC are not overextended, which is fundamentally opposed to the mechanical overload of the myocardium occurring in pathological dilatation heart disease. Assessments of diastolic preloading

were also consistent with this interpretation since they showed no (S1, S2) or only slight (S3) elevation in diastolic tensions. Collectively, such data in EHTs shows that systolic instead of diastolic stress could be the primary trigger for BNP production, which corroborates experiments conducted in humans (Maeder et al., 2010, Guterl et al., 2007). Accordingly, EHTs subjected to a specific biomechanical strain may be a helpful model for studying the unidentified mechano-transduction of different natriuretic peptides.

4.4 Hypothesis on progressive stretching mechanism

Despite the extensive studies regarding the effects of biomechanical stimulation on EHTs, the underlying molecular mechanisms and the signaling pathways remain unknown. As the maturation process of EHT simulates myocardial development, we hypothesize that progressive stretching acts in a similar pattern to the physiological hypertrophy of the postnatal heart. Stretching changes the shape of the cell, and changes in the shape of protein complexes allow cells to recognize mechanical stress. For a better understanding, two models have been established to describe mechanosensory and -transduction: the localized model and the decentralized model (Buyandelger et al., 2014). The localized model postulates that shift in the cellular membranes are instantly detected and communicated to other areas of the cell. On the contrary, the decentralized model suggests that every force applied to the cell surface would induce deformations of cytoskeletal structures and can be detected at great distances from the impact site. As cardiomyocytes are packed with various structural proteins, and the applied force is relatively strong, it is evident that the second model is more suitable for explaining mechanical perception and transduction. A large number of mechanosensitive receptors or proteins exist at different cell levels (e.g., at the cell membrane level, in the cardiac Z-line, at the sarcoplasmic reticulum level, etc.), which trigger various signaling pathways in response to mechanosensitive stimuli and initiate physiological hypertrophy-like growth. Since we assume that the applied biomechanical condition will neither provoke prenatal proliferation nor trigger pathological hypertrophy, we emphasize mechanisms of exercise-induced physiological myocardial growth.

Transient receptor potential channels (TRP) potentially operate as calcium and other cation-permeable stretch-sensitive signaling mediators among all kinds of cells. In contrast to ion channels gated by voltage, TRP channels do not possess the normal voltage sensor (Ramsey et al., 2006). Yet, TRP channels are gated in a polymodal activation

pattern and can sense mechanical, chemical, thermal, and local cellular environmental stimuli (Clapham, 2003). Then the calcium current activated by mechanical stretch can downstream activate growth signals in the heart via, for instance, calcineurin nuclear factor of activated T- cells (NFAT) - signaling pathways. TRPC1, TRPC 4 to TRPC6 from the canonical subfamily (TRPC) are also identified to be directly activated by stretching and may thus be involved in mechano-sensing and downstream signaling to trigger hypertrophic heart development (Seth et al., 2009, Spassova et al., 2006, Maroto et al., 2005).

As the largest known protein, titin has a large abundance in striated muscle. It straddles the whole Z line, provides mechanical stability, and interacts with more than 20 proteins with mechanosensory function. Titin has two isoforms in the human heart, N2B and N2BA. Dysregulation of these two isoforms leads to dilated cardiomyopathy (Wu et al., 2002). In particular, the N2B subunit specifically binds to FHL1/FHL2 proteins, which in turn activates downstream RAF, MEK1/2, and ERK2, thereby activating the growth factor-mediated G-protein signaling pathway and thus altering gene expression in the nucleus (Herman et al., 2012, Linke, 2008).

A further family of relevant membrane proteins are Integrins, which allow direct sensing and transduction of mechanical stimuli via their direct attachment to the cell membrane. Integrins are transmembrane proteins that promote adhesion between cells and the extracellular matrix (ECM). Following ligand binding, integrins initiate signaling pathways that regulate physiological signals, including control of the cell cycle and formation of the cellular cytoskeleton (Giancotti and Ruoslahti, 1999). They are heterodimers composed of alpha and beta subunits that cross the plasma membrane and adhere to extracellular matrix molecules, which include collagen and laminin. Integrins can use their beta subunits across the cell membrane to transmit extracellular matrix-conducted mechanical stimuli into cells and deliver them to downstream enzyme complexes, such as RHO/GTPase and PI3K. Studies have shown that the removal of beta subunits of cardiac integrins causes more severe cardiac fibrosis as well as pathological hypertrophy of the heart, revealing the vital function of integrins in mechanotransduction and mechano-regulation (Shai et al., 2002).

These mechanoreceptors are possibly involved in the sensing of progressive stretch, and they can be coupled to various effector molecules triggering hypertrophy or tissue differentiation. In the downstream, for example, ERK1/2 (also known as MAPK) can be

activated by many mechanical stimuli, including all three proteins mentioned above. It again activates many transcription factors, such as ELK1 (ETS Like-1 protein Elk-1), which functions as a transcription activator and promotes cell proliferation. Furthermore, ERK1/2 acts also as a protector against pathological hypertrophy. Inhibition of the ERK1/2 pathway causes more pathological myocardial dilatation under the same mechanical conditions (Purcell et al., 2007). Although the molecular mechanism of progressive stretching is not yet fully elucidated nowadays, the hypothesis of signaling pathways grounded on physiological hypertrophy provides a reliable direction for future studies.

As it has been shown for physiological hypertrophy, it may be envisaged that stretching directly activates TRPC channels, which drive the inward flow of extracellular calcium ions. Cell deformation was simultaneously sensed by integrins (through the extracellular matrix) and titin (through Z-line) which redirect signals to PI3K, which activates ERK1/2, establishing an important signaling pathway for cell growth.

4.5 Limitations

Even though progressive stretching has yielded very positive outcomes as described above, there are still limitations that are noteworthy to explore. A simplified cell formulation was claimed to be simpler and easier to fabricate, but the possible single-cell population still cannot accurately mimic the population of cells present in mature myocardial tissue. It was our intention to omit additional complexity which would have been introduced by incorporating purified fibroblasts into the cell mixture used for EHT generation. There was also a decrease in the purity of cardiomyocytes compared to other studies. Our approach to EHT assembly was based on the assumption that the population of non-myocytic cells contained in the cell suspension after initial differentiation would contain sufficient fibroblast-like cells to adequately form a new extracellular matrix. Indeed, previous studies demonstrated that the percentage of non-cardiomyocytes (the vast majority of which are fibroblasts) was largely maintained between 25-35% after the use of supporting cells to assemble EHT (34.4% fibroblasts, (Nunes et al., 2013); 25% input fibroblasts, (Ronaldson-Bouchard et al., 2018)). This proportion is well within the range of non-myocytic cells identified in our study (30%). However, in vitro differentiation of hiPSCs typically yields a broad spectrum of different cell types whose influence on the formation of compact myocardial tissue in our approach is unknown. Although

the functionality of the myocardial tissue has been improved by progressive stretching, the effect of this residual 30% non-cardiac cell population still needs to be further analyzed.

To accelerate the growth of cardiomyocytes in vitro, we followed a serum-free culture solution protocol, which was also non-physiological in certain aspects. The nutritional supplementation aspect needs to be further explored.

A significant fraction of the EHTs in the highest speed group (S3) showed structural instability and was even torn apart, even though they equally exhibited the maximum contraction force. As such, this velocity of distension appears to reflect the highest rate of myocyte growth that can be achieved under the present conditions. Besides the fact that this stretch speed may exceed the growth rate of the cardiomyocytes, instability of the extracellular matrix (lacking supporting cells) and insufficient energy supply may contribute to the occurrence of rupture.

Although we used a very common columnar/ring 3D structure and the overall EHT length was improved relative to previous studies, and there is a sufficient base for non-clinical applications such as conducting a series of experiments for drug testing, the entire length of only one centimeter or less is still a long way off for therapeutic applications. As such, for the generation of myocardial patches with suitable dimensions for therapeutic tissue replacement, this may be a severe restriction that needs to be resolved in view of the limited cultivation period. Some recent new studies, such as the planar reticular EHT structure, have provided good inspiration (Querdel et al., 2021).

In this context, combining progressive stretching with other well-known approaches, such as expanding the initial EHT volume using bioprinting techniques, supplementation of fibroblasts or even endothelial cells, as well as more extensive hormonal stimulation may further advance the maturation potential of EHT.

4.6 Prospects

In this work, an innovative approach to improve maturation, as well as the growth of engineered heart tissue, is presented. To fulfill our objective, we have proposed a new methodology of tissue assembly and biomimetic culture that prevent tissue shrinkage as well as induce myofibrils with contractility and compliance that are almost comparable to those of human myocardium. By implementing external progressive stretch, we

demonstrate the biological importance of tissue forces that govern postnatal heart development. Therefore, progressive stretch also establishes the framework conditions for bioreactors in which the size of EHTs needs to be increased. By upsizing the EHTs, this model gives a promising platform for the investigation of the myocardial growth process and pathological remodeling. Furthermore, with the improved maturity of the EHT, a more accurate assessment of the long-term drug efficacy is also expected. Focusing on the longer term, a potentially greater purpose for EHTs is therapeutic transplantation to replace damaged myocardial tissue. However, the small size and feeble contractility of EHT implants directly limit the possibility of this application. By using progressive stretching, this study offers a promising opportunity to expand the size and contractility of EHT, laying a solid foundation for therapeutic implant development. With the help of this approach, implants can be ramped up to accommodate different tissue sizes using patient-specific iPS cells, which opens up new avenues for cardiac regeneration medicine.

References

ABILEZ, O. J., TZATZALOS, E., YANG, H., ZHAO, M. T., JUNG, G., ZOLLNER, A. M., TIBURCY, M., RIEGLER, J., MATSA, E., SHUKLA, P., ZHUGE, Y., CHOUR, T., CHEN, V. C., BURRIDGE, P. W., KARAKIKES, I., KUHL, E., BERNSTEIN, D., COUTURE, L. A., GOLD, J. D., ZIMMERMANN, W. H. & WU, J. C. 2018. Passive Stretch Induces Structural and Functional Maturation of Engineered Heart Muscle as Predicted by Computational Modeling. *Stem Cells,* 36**,** 265-277.

AKHYARI, P., FEDAK, P. W., WEISEL, R. D., LEE, T. Y., VERMA, S., MICKLE, D. A. & LI, R. K. 2002. Mechanical stretch regimen enhances the formation of bioengineered autologous cardiac muscle grafts. *Circulation,* 106**,** I137-42.

ALLEN, D. G. & KENTISH, J. C. 1985. The cellular basis of the length-tension relation in cardiac muscle. *J Mol Cell Cardiol,* 17**,** 821-40.

ALPERT, N. R., LEAVITT, B. J., ITTLEMAN, F. P., HASENFUSS, G., PIESKE, B. & MULIERI, L. A. 1998. A mechanistic analysis of the force-frequency relation in non-failing and progressively failing human myocardium. *Basic Res Cardiol,* 93 Suppl 1**,** 23-32.

AUMAN, H. J., COLEMAN, H., RILEY, H. E., OLALE, F., TSAI, H. J. & YELON, D. 2007. Functional modulation of cardiac form through regionally confined cell shape changes. *PLoS Biol,* 5**,** e53.

BARTMAN, T. & HOVE, J. 2005. Mechanics and function in heart morphogenesis. *Dev Dyn,* 233**,** 373-81.

BARTMAN, T., WALSH, E. C., WEN, K. K., MCKANE, M., REN, J., ALEXANDER, J., RUBENSTEIN, P. A. & STAINIER, D. Y. 2004. Early myocardial function affects endocardial cushion development in zebrafish. *PLoS Biol,* 2**,** E129.

BESSER, R. R., ISHAHAK, M., MAYO, V., CARBONERO, D., CLAURE, I. & AGARWAL, A. 2018. Engineered Microenvironments for Maturation of Stem Cell Derived Cardiac Myocytes. *Theranostics,* 8**,** 124-140.

BOUDOU, T., LEGANT, W. R., MU, A., BOROCHIN, M. A., THAVANDIRAN, N., RADISIC, M., ZANDSTRA, P. W., EPSTEIN, J. A., MARGULIES, K. B. & CHEN, C. S. 2012. A microfabricated platform to measure and manipulate the mechanics of engineered cardiac microtissues. *Tissue Eng Part A,* 18**,** 910-9.

BRANDENBURGER, M., WENZEL, J., BOGDAN, R., RICHARDT, D., NGUEMO, F., REPPEL, M., HESCHELER, J., TERLAU, H. & DENDORFER, A. 2012. Organotypic slice culture from human adult ventricular myocardium. *Cardiovasc Res,* 93**,** 50-9.

BROWN, M. A., IYER, R. K. & RADISIC, M. 2008. Pulsatile perfusion bioreactor for cardiac tissue engineering. *Biotechnol Prog,* 24**,** 907-20.

BUYANDELGER, B., MANSFIELD, C. & KNOLL, R. 2014. Mechano-signaling in heart failure. *Pflugers Arch,* 466**,** 1093-9.

CASHMAN, T. J., JOSOWITZ, R., GELB, B. D., LI, R. A., DUBOIS, N. C. & COSTA, K. D. 2016. Construction of Defined Human Engineered Cardiac Tissues to Study Mechanisms of Cardiac Cell Therapy. *J Vis Exp***,** e53447.

CHEN, G., GULBRANSON, D. R., HOU, Z., BOLIN, J. M., RUOTTI, V., PROBASCO, M. D., SMUGA-OTTO, K., HOWDEN, S. E., DIOL, N. R., PROPSON, N. E., WAGNER, R., LEE, G. O., ANTOSIEWICZ-BOURGET, J., TENG, J. M. & THOMSON, J. A. 2011. Chemically defined conditions for human iPSC derivation and culture. *Nat Methods,* 8**,** 424-9.

CLAPHAM, D. E. 2003. TRP channels as cellular sensors. *Nature,* 426**,** 517-24.

CORREIA, C., KOSHKIN, A., DUARTE, P., HU, D., CARIDO, M., SEBASTIAO, M. J., GOMES-ALVES, P., ELLIOTT, D. A., DOMIAN, I. J., TEIXEIRA, A. P., ALVES, P. M. & SERRA, M. 2018. 3D aggregate culture improves metabolic maturation of human pluripotent stem cell derived cardiomyocytes. *Biotechnol Bioeng,* 115**,** 630-644.

CROZATIER, B. 1998. Force-frequency relations in nonfailing and failing animal myocardium. *Basic Res Cardiol,* 93 Suppl 1**,** 46-50.

DAMON, B. J., REMOND, M. C., BIGELOW, M. R., TRUSK, T. C., XIE, W., PERUCCHIO, R., SEDMERA, D., DENSLOW, S. & THOMPSON, R. P. 2009. Patterns of muscular strain in the embryonic heart wall. *Dev Dyn,* 238**,** 1535-46.

DIETZEL, S., PIRCHER, J., NEKOLLA, A. K., GULL, M., BRANDLI, A. W., POHL, U. & REHBERG, M. 2014. Label-free determination of hemodynamic parameters in the microcirculaton with third harmonic generation microscopy. *PLoS One,* 9**,** e99615.

ENDOH, M. 2004. Force-frequency relationship in intact mammalian ventricular myocardium: physiological and pathophysiological relevance. *Eur J Pharmacol,* 500**,** 73-86.

FINK, C., ERGUN, S., KRALISCH, D., REMMERS, U., WEIL, J. & ESCHENHAGEN, T. 2000. Chronic stretch of engineered heart tissue induces hypertrophy and functional improvement. *FASEB J,* 14**,** 669-79.

FISCHER, C., MILTING, H., FEIN, E., REISER, E., LU, K., SEIDEL, T., SCHINNER, C., SCHWARZMAYR, T., SCHRAMM, R., TOMASI, R., HUSSE, B., CAO-EHLKER, X., POHL, U. & DENDORFER, A. 2019. Long-term functional and structural preservation of precision-cut human myocardium under continuous electromechanical stimulation in vitro. *Nat Commun,* 10**,** 117.

GALIE, P. A., BYFIELD, F. J., CHEN, C. S., KRESH, J. Y. & JANMEY, P. A. 2015. Mechanically stimulated contraction of engineered cardiac constructs using a microcantilever. *IEEE Trans Biomed Eng,* 62**,** 438-42.

GEACH, T. J., HIRST, E. M. & ZIMMERMAN, L. B. 2015. Contractile activity is required for Z-disc sarcomere maturation in vivo. *Genesis,* 53**,** 299-307.

GERSHLAK, J. R., RESNIKOFF, J. I., SULLIVAN, K. E., WILLIAMS, C., WANG, R. M. & BLACK, L. D., 3RD 2013. Mesenchymal stem cells ability to generate traction stress in response to substrate stiffness is modulated by the changing extracellular matrix composition of the heart during development. *Biochem Biophys Res Commun,* 439**,** 161-6.

GHISTA, D. N., SANDLER, H. & VAYO, W. H. 1975. Elastic modulus of the human intact left ventricle--determination and physiological interpretation. *Med Biol Eng,* 13**,** 151-61.

GIANCOTTI, F. G. & RUOSLAHTI, E. 1999. Integrin signaling. *Science,* 285**,** 1028-32.

GIBB, A. A. & HILL, B. G. 2018. Metabolic Coordination of Physiological and Pathological Cardiac Remodeling. *Circ Res,* 123**,** 107-128.

GROSSMAN, W., JONES, D. & MCLAURIN, L. P. 1975. Wall stress and patterns of hypertrophy in the human left ventricle. *J Clin Invest,* 56**,** 56-64.

GUO, Y. & PU, W. T. 2020. Cardiomyocyte Maturation: New Phase in Development. *Circ Res,* 126**,** 1086-1106.

GUTERL, K. A., HAGGART, C. R., JANSSEN, P. M. & HOLMES, J. W. 2007. Isometric contraction induces rapid myocyte remodeling in cultured rat right ventricular papillary muscles. *Am J Physiol Heart Circ Physiol,* 293**,** H3707-12.

HERMAN, D. S., LAM, L., TAYLOR, M. R., WANG, L., TEEKAKIRIKUL, P., CHRISTODOULOU, D., CONNER, L., DEPALMA, S. R., MCDONOUGH, B., SPARKS, E., TEODORESCU, D. L., CIRINO, A. L., BANNER, N. R., PENNELL, D. J., GRAW, S., MERLO, M., DI LENARDA, A., SINAGRA, G., BOS, J. M., ACKERMAN, M. J., MITCHELL, R. N.,

MURRY, C. E., LAKDAWALA, N. K., HO, C. Y., BARTON, P. J., COOK, S. A., MESTRONI, L., SEIDMAN, J. G. & SEIDMAN, C. E. 2012. Truncations of titin causing dilated cardiomyopathy. *N Engl J Med,* 366**,** 619-28.

HIRT, M. N., BOEDDINGHAUS, J., MITCHELL, A., SCHAAF, S., BORNCHEN, C., MULLER, C., SCHULZ, H., HUBNER, N., STENZIG, J., STOEHR, A., NEUBER, C., EDER, A., LUTHER, P. K., HANSEN, A. & ESCHENHAGEN, T. 2014. Functional improvement and maturation of rat and human engineered heart tissue by chronic electrical stimulation. *J Mol Cell Cardiol,* 74**,** 151-61.

HIRT, M. N., SORENSEN, N. A., BARTHOLDT, L. M., BOEDDINGHAUS, J., SCHAAF, S., EDER, A., VOLLERT, I., STOHR, A., SCHULZE, T., WITTEN, A., STOLL, M., HANSEN, A. & ESCHENHAGEN, T. 2012. Increased afterload induces pathological cardiac hypertrophy: a new in vitro model. *Basic Res Cardiol,* 107**,** 307.

HOLUBARSCH, C., RUF, T., GOLDSTEIN, D. J., ASHTON, R. C., NICKL, W., PIESKE, B., PIOCH, K., LUDEMANN, J., WIESNER, S., HASENFUSS, G., POSIVAL, H., JUST, H. & BURKHOFF, D. 1996. Existence of the Frank-Starling mechanism in the failing human heart. Investigations on the organ, tissue, and sarcomere levels. *Circulation,* 94**,** 683-9.

HOOD, W. P., JR., RACKLEY, C. E. & ROLETT, E. L. 1968. Wall stress in the normal and hypertrophied human left ventricle. *Am J Cardiol,* 22**,** 550-8.

HORIKOSHI, Y., YAN, Y., TERASHVILI, M., WELLS, C., HORIKOSHI, H., FUJITA, S., BOSNJAK, Z. J. & BAI, X. 2019. Fatty Acid-Treated Induced Pluripotent Stem Cell-Derived Human Cardiomyocytes Exhibit Adult Cardiomyocyte-Like Energy Metabolism Phenotypes. *Cells,* 8.

HOVE, J. R., KOSTER, R. W., FOROUHAR, A. S., ACEVEDO-BOLTON, G., FRASER, S. E. & GHARIB, M. 2003. Intracardiac fluid forces are an essential epigenetic factor for embryonic cardiogenesis. *Nature,* 421**,** 172-7.

HUANG, C. Y., PERES MORENO MAIA-JOCA, R., ONG, C. S., WILSON, I., DISILVESTRE, D., TOMASELLI, G. F. & REICH, D. H. 2020. Enhancement of human iPSC-derived cardiomyocyte maturation by chemical conditioning in a 3D environment. *J Mol Cell Cardiol,* 138**,** 1-11.

HUEBSCH, N., LOSKILL, P., DEVESHWAR, N., SPENCER, C. I., JUDGE, L. M., MANDEGAR, M. A., FOX, C. B., MOHAMED, T. M., MA, Z., MATHUR, A., SHEEHAN, A. M., TRUONG, A., SAXTON, M., YOO, J., SRIVASTAVA, D., DESAI, T. A., SO, P. L., HEALY, K. E. & CONKLIN, B. R. 2016. Miniaturized iPS-Cell-Derived Cardiac Muscles for Physiologically Relevant Drug Response Analyses. *Sci Rep,* 6**,** 24726.

HUXLEY, A. F. & NIEDERGERKE, R. 1954. Structural changes in muscle during contraction; interference microscopy of living muscle fibres. *Nature,* 173**,** 971-3.

HUXLEY, H. & HANSON, J. 1954. Changes in the cross-striations of muscle during contraction and stretch and their structural interpretation. *Nature,* 173**,** 973-6.

HUXLEY, H. E. 1969. The mechanism of muscular contraction. *Science,* 164**,** 1356-65.

INTENGAN, H. D., THIBAULT, G., LI, J. S. & SCHIFFRIN, E. L. 1999. Resistance artery mechanics, structure, and extracellular components in spontaneously hypertensive rats : effects of angiotensin receptor antagonism and converting enzyme inhibition. *Circulation,* 100**,** 2267-75.

IVEY, M. J., KUWABARA, J. T., PAI, J. T., MOORE, R. E., SUN, Z. & TALLQUIST, M. D. 2018. Resident fibroblast expansion during cardiac growth and remodeling. *J Mol Cell Cardiol,* 114**,** 161-174.

JACKMAN, C. P., CARLSON, A. L. & BURSAC, N. 2016. Dynamic culture yields engineered myocardium with near-adult functional output. *Biomaterials,* 111**,** 66-79.

JACOT, J. G., KITA-MATSUO, H., WEI, K. A., CHEN, H. S., OMENS, J. H., MERCOLA, M. & MCCULLOCH, A. D. 2010. Cardiac myocyte force development during differentiation and maturation. *Ann N Y Acad Sci,* 1188**,** 121-7.

KAPRIELIAN, R. R., STEVENSON, S., ROTHERY, S. M., CULLEN, M. J. & SEVERS, N. J. 2000. Distinct patterns of dystrophin organization in myocyte sarcolemma and transverse tubules of normal and diseased human myocardium. *Circulation,* 101**,** 2586-94.

KARBASSI, E., FENIX, A., MARCHIANO, S., MURAOKA, N., NAKAMURA, K., YANG, X. & MURRY, C. E. 2020. Cardiomyocyte maturation: advances in knowledge and implications for regenerative medicine. *Nat Rev Cardiol,* 17**,** 341-359.

KLEIN, I. & OJAMAA, K. 2001. Thyroid hormone and the cardiovascular system. *N Engl J Med,* 344**,** 501-9.

KOBIRUMAKI-SHIMOZAWA, F., INOUE, T., SHINTANI, S. A., OYAMA, K., TERUI, T., MINAMISAWA, S., ISHIWATA, S. & FUKUDA, N. 2014. Cardiac thin filament regulation and the Frank-Starling mechanism. *J Physiol Sci,* 64**,** 221-32.

KOIVISTO, J. T., GERING, C., KARVINEN, J., MARIA CHERIAN, R., BELAY, B., HYTTINEN, J., AALTO-SETALA, K., KELLOMAKI, M. & PARRAGA, J. 2019. Mechanically Biomimetic Gelatin-Gellan Gum Hydrogels for 3D Culture of Beating Human Cardiomyocytes. *ACS Appl Mater Interfaces,* 11**,** 20589-20602.

KOWALSKI, W. J., PEKKAN, K., TINNEY, J. P. & KELLER, B. B. 2014. Investigating developmental cardiovascular biomechanics and the origins of congenital heart defects. *Front Physiol,* 5**,** 408.

LATACHA, K. S., REMOND, M. C., RAMASUBRAMANIAN, A., CHEN, A. Y., ELSON, E. L. & TABER, L. A. 2005. Role of actin polymerization in bending of the early heart tube. *Dev Dyn,* 233**,** 1272-86.

LEE, A., HUDSON, A. R., SHIWARSKI, D. J., TASHMAN, J. W., HINTON, T. J., YERNENI, S., BLILEY, J. M., CAMPBELL, P. G. & FEINBERG, A. W. 2019. 3D bioprinting of collagen to rebuild components of the human heart. *Science,* 365**,** 482-487.

LEGANT, W. R., PATHAK, A., YANG, M. T., DESHPANDE, V. S., MCMEEKING, R. M. & CHEN, C. S. 2009. Microfabricated tissue gauges to measure and manipulate forces from 3D microtissues. *Proc Natl Acad Sci U S A,* 106**,** 10097-102.

LEONARD, A., BERTERO, A., POWERS, J. D., BEUSSMAN, K. M., BHANDARI, S., REGNIER, M., MURRY, C. E. & SNIADECKI, N. J. 2018. Afterload promotes maturation of human induced pluripotent stem cell derived cardiomyocytes in engineered heart tissues. *J Mol Cell Cardiol,* 118**,** 147-158.

LI, F., WANG, X., CAPASSO, J. M. & GERDES, A. M. 1996. Rapid transition of cardiac myocytes from hyperplasia to hypertrophy during postnatal development. *J Mol Cell Cardiol,* 28**,** 1737-46.

LIANG, F. & GARDNER, D. G. 1999. Mechanical strain activates BNP gene transcription through a p38/NF-kappaB-dependent mechanism. *J Clin Invest,* 104**,** 1603-12.

LINDSEY, S. E., BUTCHER, J. T. & YALCIN, H. C. 2014. Mechanical regulation of cardiac development. *Front Physiol,* 5**,** 318.

LINKE, W. A. 2008. Sense and stretchability: the role of titin and titin-associated proteins in myocardial stress-sensing and mechanical dysfunction. *Cardiovasc Res,* 77**,** 637-48.

LU, K., SEIDEL, T., CAO-EHLKER, X., DORN, T., BATCHA, A. M. N., SCHNEIDER, C. M., SEMMLER, M., VOLK, T., MORETTI, A., DENDORFER, A. & TOMASI, R. 2021. Progressive stretch enhances growth and maturation of 3D stem-cell-derived myocardium. *Theranostics,* 11**,** 6138-6153.

LUNDY, S. D., ZHU, W. Z., REGNIER, M. & LAFLAMME, M. A. 2013. Structural and functional maturation of cardiomyocytes derived from human pluripotent stem cells. *Stem Cells Dev,* 22**,** 1991-2002.

MAEDER, M. T., MARIANI, J. A. & KAYE, D. M. 2010. Hemodynamic determinants of myocardial B-type natriuretic peptide release: relative contributions of systolic and diastolic wall stress. *Hypertension,* 56**,** 682-9.

MAGGA, J., VUOLTEENAHO, O., TOKOLA, H., MARTTILA, M. & RUSKOAHO, H. 1997. Involvement of transcriptional and posttranscriptional mechanisms in cardiac overload-induced increase of B-type natriuretic peptide gene expression. *Circ Res,* 81**,** 694-702.

MANASEK, F. J., BURNSIDE, M. B. & WATERMAN, R. E. 1972. Myocardial cell shape change as a mechanism of embryonic heart looping. *Dev Biol,* 29**,** 349-71.

MANNER, J. 2009. The anatomy of cardiac looping: a step towards the understanding of the morphogenesis of several forms of congenital cardiac malformations. *Clin Anat,* 22**,** 21-35.

MAROTO, R., RASO, A., WOOD, T. G., KUROSKY, A., MARTINAC, B. & HAMILL, O. P. 2005. TRPC1 forms the stretch-activated cation channel in vertebrate cells. *Nat Cell Biol,* 7**,** 179-85.

MCCAIN, M. L., LEE, H., ARATYN-SCHAUS, Y., KLEBER, A. G. & PARKER, K. K. 2012. Cooperative coupling of cell-matrix and cell-cell adhesions in cardiac muscle. *Proc Natl Acad Sci U S A,* 109**,** 9881-6.

MCCAIN, M. L., YUAN, H., PASQUALINI, F. S., CAMPBELL, P. H. & PARKER, K. K. 2014. Matrix elasticity regulates the optimal cardiac myocyte shape for contractility. *Am J Physiol Heart Circ Physiol,* 306**,** H1525-39.

MIHIC, A., LI, J., MIYAGI, Y., GAGLIARDI, M., LI, S. H., ZU, J., WEISEL, R. D., KELLER, G. & LI, R. K. 2014. The effect of cyclic stretch on maturation and 3D tissue formation of human embryonic stem cell-derived cardiomyocytes. *Biomaterials,* 35**,** 2798-808.

MIKLAS, J. W., NUNES, S. S., SOFLA, A., REIS, L. A., PAHNKE, A., XIAO, Y., LASCHINGER, C. & RADISIC, M. 2014a. Bioreactor for modulation of cardiac microtissue phenotype by combined static stretch and electrical stimulation. *Biofabrication,* 6**,** 024113.

MIKLAS, J. W., NUNES, S. S., ZHANG, B. & RADISIC, M. 2014b. Design and fabrication of biological wires. *Methods Mol Biol,* 1181**,** 157-65.

MIRONOV, V., VISCONTI, R. P. & MARKWALD, R. R. 2005. On the role of shear stress in cardiogenesis. *Endothelium,* 12**,** 259-61.

MOMTAHAN, N., POORNEJAD, N., STRUK, J. A., CASTLETON, A. A., HERROD, B. J., VANCE, B. R., EATOUGH, J. P., ROEDER, B. L., REYNOLDS, P. R. & COOK, A. D. 2015. Automation of Pressure Control Improves Whole Porcine Heart Decellularization. *Tissue Eng Part C Methods,* 21**,** 1148-61.

MORETTI, A., LAUGWITZ, K. L., DORN, T., SINNECKER, D. & MUMMERY, C. 2013. Pluripotent stem cell models of human heart disease. *Cold Spring Harb Perspect Med,* 3.

MORGAN, K. Y. & BLACK, L. D., 3RD 2014a. Creation of a bioreactor for the application of variable amplitude mechanical stimulation of fibrin gel-based engineered cardiac tissue. *Methods Mol Biol,* 1181**,** 177-87.

MORGAN, K. Y. & BLACK, L. D., 3RD 2014b. Mimicking isovolumic contraction with combined electromechanical stimulation improves the development of engineered cardiac constructs. *Tissue Eng Part A,* 20**,** 1654-67.

MOSS, R. L. & FITZSIMONS, D. P. 2002. Frank-Starling relationship: long on importance, short on mechanism. *Circ Res,* 90**,** 11-3.

MULIERI, L. A., HASENFUSS, G., LEAVITT, B., ALLEN, P. D. & ALPERT, N. R. 1992. Altered myocardial force-frequency relation in human heart failure. *Circulation,* 85**,** 1743-50.

NAKAMURA, M. & SADOSHIMA, J. 2018. Mechanisms of physiological and pathological cardiac hypertrophy. *Nat Rev Cardiol,* 15**,** 387-407.

NOEL, E. S., VERHOEVEN, M., LAGENDIJK, A. K., TESSADORI, F., SMITH, K., CHOORAPOIKAYIL, S., DEN HERTOG, J. & BAKKERS, J. 2013. A Nodal-independent and tissue-intrinsic mechanism controls heart-looping chirality. *Nat Commun,* 4**,** 2754.

NUNES, S. S., MIKLAS, J. W., LIU, J., ASCHAR-SOBBI, R., XIAO, Y., ZHANG, B., JIANG, J., MASSE, S., GAGLIARDI, M., HSIEH, A., THAVANDIRAN, N., LAFLAMME, M. A., NANTHAKUMAR, K., GROSS, G. J., BACKX, P. H., KELLER, G. & RADISIC, M. 2013. Biowire: a platform for maturation of human pluripotent stem cell-derived cardiomyocytes. *Nat Methods,* 10**,** 781-7.

OPARIL, S., BISHOP, S. P. & CLUBB, F. J., JR. 1984. Myocardial cell hypertrophy or hyperplasia. *Hypertension,* 6**,** III38-43.

PARADIS, A. N., GAY, M. S. & ZHANG, L. 2014. Binucleation of cardiomyocytes: the transition from a proliferative to a terminally differentiated state. *Drug Discov Today,* 19**,** 602-9.

PARIKH, S. S., BLACKWELL, D. J., GOMEZ-HURTADO, N., FRISK, M., WANG, L., KIM, K., DAHL, C. P., FIANE, A., TONNESSEN, T., KRYSHTAL, D. O., LOUCH, W. E. & KNOLLMANN, B. C. 2017. Thyroid and Glucocorticoid Hormones Promote Functional T-Tubule Development in Human-Induced Pluripotent Stem Cell-Derived Cardiomyocytes. *Circ Res,* 121**,** 1323-1330.

PURCELL, N. H., WILKINS, B. J., YORK, A., SABA-EL-LEIL, M. K., MELOCHE, S., ROBBINS, J. & MOLKENTIN, J. D. 2007. Genetic inhibition of cardiac ERK1/2 promotes stress-induced apoptosis and heart failure but has no effect on hypertrophy in vivo. *Proc Natl Acad Sci U S A,* 104**,** 14074-9.

QUERDEL, E., REINSCH, M., CASTRO, L., KOSE, D., BAHR, A., REICH, S., GEERTZ, B., ULMER, B., SCHULZE, M., LEMOINE, M. D., KRAUSE, T., LEMME, M., SANI, J., SHIBAMIYA, A., STUDEMANN, T., KOHNE, M., BIBRA, C. V., HORNASCHEWITZ, N., PECHA, S., NEJAHSIE, Y., MANNHARDT, I., CHRIST, T., REICHENSPURNER, H., HANSEN, A., KLYMIUK, N., KRANE, M., KUPATT, C., ESCHENHAGEN, T. & WEINBERGER, F. 2021. Human Engineered Heart Tissue Patches Remuscularize the Injured Heart in a Dose-Dependent Manner. *Circulation,* 143**,** 1991-2006.

RADISIC, M., MARSANO, A., MAIDHOF, R., WANG, Y. & VUNJAK-NOVAKOVIC, G. 2008. Cardiac tissue engineering using perfusion bioreactor systems. *Nat Protoc,* 3**,** 719-38.

RADISIC, M., PARK, H., SHING, H., CONSI, T., SCHOEN, F. J., LANGER, R., FREED, L. E. & VUNJAK-NOVAKOVIC, G. 2004. Functional assembly of engineered myocardium by electrical stimulation of cardiac myocytes cultured on scaffolds. *Proc Natl Acad Sci U S A,* 101**,** 18129-34.

RAMSEY, I. S., MORAN, M. M., CHONG, J. A. & CLAPHAM, D. E. 2006. A voltage-gated proton-selective channel lacking the pore domain. *Nature,* 440**,** 1213-6.

RASTOGI, P. & KANDASUBRAMANIAN, B. 2019. Review of alginate-based hydrogel bioprinting for application in tissue engineering. *Biofabrication,* 11**,** 042001.

ROG-ZIELINSKA, E. A., THOMSON, A., KENYON, C. J., BROWNSTEIN, D. G., MORAN, C. M., SZUMSKA, D., MICHAILIDOU, Z., RICHARDSON, J., OWEN, E., WATT, A., MORRISON, H., FORRESTER, L. M., BHATTACHARYA, S., HOLMES, M. C. & CHAPMAN, K. E. 2013. Glucocorticoid receptor is required for foetal heart maturation. *Hum Mol Genet,* 22**,** 3269-82.

RONALDSON-BOUCHARD, K., MA, S. P., YEAGER, K., CHEN, T., SONG, L., SIRABELLA, D., MORIKAWA, K., TELES, D., YAZAWA, M. & VUNJAK-NOVAKOVIC, G. 2018.

Advanced maturation of human cardiac tissue grown from pluripotent stem cells. *Nature,* 556**,** 239-243.

RUAN, J. L., TULLOCH, N. L., RAZUMOVA, M. V., SAIGET, M., MUSKHELI, V., PABON, L., REINECKE, H., REGNIER, M. & MURRY, C. E. 2016. Mechanical Stress Conditioning and Electrical Stimulation Promote Contractility and Force Maturation of Induced Pluripotent Stem Cell-Derived Human Cardiac Tissue. *Circulation,* 134**,** 1557-1567.

RUAN, J. L., TULLOCH, N. L., SAIGET, M., PAIGE, S. L., RAZUMOVA, M. V., REGNIER, M., TUNG, K. C., KELLER, G., PABON, L., REINECKE, H. & MURRY, C. E. 2015. Mechanical Stress Promotes Maturation of Human Myocardium From Pluripotent Stem Cell-Derived Progenitors. *Stem Cells,* 33**,** 2148-57.

SEDMERA, D., PEXIEDER, T., RYCHTEROVA, V., HU, N. & CLARK, E. B. 1999. Remodeling of chick embryonic ventricular myoarchitecture under experimentally changed loading conditions. *Anat Rec,* 254**,** 238-52.

SEIDEL, T., SANKARANKUTTY, A. C. & SACHSE, F. B. 2017. Remodeling of the transverse tubular system after myocardial infarction in rabbit correlates with local fibrosis: A potential role of biomechanics. *Prog Biophys Mol Biol,* 130**,** 302-314.

SETH, M., ZHANG, Z. S., MAO, L., GRAHAM, V., BURCH, J., STIBER, J., TSIOKAS, L., WINN, M., ABRAMOWITZ, J., ROCKMAN, H. A., BIRNBAUMER, L. & ROSENBERG, P. 2009. TRPC1 channels are critical for hypertrophic signaling in the heart. *Circ Res,* 105**,** 1023-30.

SHAI, S. Y., HARPF, A. E., BABBITT, C. J., JORDAN, M. C., FISHBEIN, M. C., CHEN, J., OMURA, M., LEIL, T. A., BECKER, K. D., JIANG, M., SMITH, D. J., CHERRY, S. R., LOFTUS, J. C. & ROSS, R. S. 2002. Cardiac myocyte-specific excision of the beta1 integrin gene results in myocardial fibrosis and cardiac failure. *Circ Res,* 90**,** 458-64.

SPASSOVA, M. A., HEWAVITHARANA, T., XU, W., SOBOLOFF, J. & GILL, D. L. 2006. A common mechanism underlies stretch activation and receptor activation of TRPC6 channels. *Proc Natl Acad Sci U S A,* 103**,** 16586-91.

STEPHENSON, D. G., STEWART, A. W. & WILSON, G. J. 1989. Dissociation of force from myofibrillar MgATPase and stiffness at short sarcomere lengths in rat and toad skeletal muscle. *J Physiol,* 410**,** 351-66.

STEPHENSON, D. G. & WILLIAMS, D. A. 1982. Effects of sarcomere length on the force-pCa relation in fast- and slow-twitch skinned muscle fibres from the rat. *J Physiol,* 333**,** 637-53.

TABER, L. A. 1998. Mechanical aspects of cardiac development. *Prog Biophys Mol Biol,* 69**,** 237-55.

TABER, L. A. 2001. Biomechanics of cardiovascular development. *Annu Rev Biomed Eng,* 3**,** 1-25.

TABER, L. A. & PERUCCHIO, R. 2001. Stress-strain relations in embryonic chick heart. *Am J Physiol Heart Circ Physiol,* 281**,** H463-6.

TAEGTMEYER, H., SEN, S. & VELA, D. 2010. Return to the fetal gene program: a suggested metabolic link to gene expression in the heart. *Ann N Y Acad Sci,* 1188**,** 191-8.

TALLAWI, M., RAI, R., BOCCACCINI, A. R. & AIFANTIS, K. E. 2015. Effect of substrate mechanics on cardiomyocyte maturation and growth. *Tissue Eng Part B Rev,* 21**,** 157-65.

TAO, G., LEVAY, A. K., PEACOCK, J. D., HUK, D. J., BOTH, S. N., PURCELL, N. H., PINTO, J. R., GALANTOWICZ, M. L., KOCH, M., LUCCHESI, P. A., BIRK, D. E. & LINCOLN, J. 2012. Collagen XIV is important for growth and structural integrity of the myocardium. *J Mol Cell Cardiol,* 53**,** 626-38.

TIBURCY, M., DIDIE, M., BOY, O., CHRISTALLA, P., DOKER, S., NAITO, H., KARIKKINETH, B. C., EL-ARMOUCHE, A., GRIMM, M., NOSE, M., ESCHENHAGEN, T., ZIESENISS, A., KATSCHINKSI, D. M., HAMDANI, N., LINKE, W. A., YIN, X., MAYR, M. & ZIMMERMANN, W. H. 2011. Terminal differentiation, advanced organotypic maturation, and modeling of hypertrophic growth in engineered heart tissue. *Circ Res,* 109**,** 1105-14.

TIBURCY, M., HUDSON, J. E., BALFANZ, P., SCHLICK, S., MEYER, T., CHANG LIAO, M. L., LEVENT, E., RAAD, F., ZEIDLER, S., WINGENDER, E., RIEGLER, J., WANG, M., GOLD, J. D., KEHAT, I., WETTWER, E., RAVENS, U., DIERICKX, P., VAN LAAKE, L. W., GOUMANS, M. J., KHADJEH, S., TOISCHER, K., HASENFUSS, G., COUTURE, L. A., UNGER, A., LINKE, W. A., ARAKI, T., NEEL, B., KELLER, G., GEPSTEIN, L., WU, J. C. & ZIMMERMANN, W. H. 2017. Defined Engineered Human Myocardium With Advanced Maturation for Applications in Heart Failure Modeling and Repair. *Circulation,* 135**,** 1832-1847.

TOHYAMA, S., HATTORI, F., SANO, M., HISHIKI, T., NAGAHATA, Y., MATSUURA, T., HASHIMOTO, H., SUZUKI, T., YAMASHITA, H., SATOH, Y., EGASHIRA, T., SEKI, T., MURAOKA, N., YAMAKAWA, H., OHGINO, Y., TANAKA, T., YOICHI, M., YUASA, S., MURATA, M., SUEMATSU, M. & FUKUDA, K. 2013. Distinct metabolic flow enables large-scale purification of mouse and human pluripotent stem cell-derived cardiomyocytes. *Cell Stem Cell,* 12**,** 127-37.

TOISCHER, K., ROKITA, A. G., UNSOLD, B., ZHU, W., KARARIGAS, G., SOSSALLA, S., REUTER, S. P., BECKER, A., TEUCHER, N., SEIDLER, T., GREBE, C., PREUSS, L., GUPTA, S. N., SCHMIDT, K., LEHNART, S. E., KRUGER, M., LINKE, W. A., BACKS, J., REGITZ-ZAGROSEK, V., SCHAFER, K., FIELD, L. J., MAIER, L. S. & HASENFUSS, G. 2010. Differential cardiac remodeling in preload versus afterload. *Circulation,* 122**,** 993-1003.

TZUR, A., MOORE, J. K., JORGENSEN, P., SHAPIRO, H. M. & KIRSCHNER, M. W. 2011. Optimizing optical flow cytometry for cell volume-based sorting and analysis. *PLoS One,* 6**,** e16053.

USMAN, A., GANDHI, J. & GUPTA, G. 2020. Physiology, Bowditch Effect. *StatPearls.* Treasure Island (FL).

VAHL, C. F., TIMEK, T., BONZ, A., KOCHSIEK, N., FUCHS, H., SCHAFFER, L., ROSENBERG, M., DILLMANN, R. & HAGL, S. 1997. Myocardial length-force relationship in end stage dilated cardiomyopathy and normal human myocardium: analysis of intact and skinned left ventricular trabeculae obtained during 11 heart transplantations. *Basic Res Cardiol,* 92**,** 261-70.

VALLS-MARGARIT, M., IGLESIAS-GARCIA, O., DI GUGLIELMO, C., SARLABOUS, L., TADEVOSYAN, K., PAOLI, R., COMELLES, J., BLANCO-ALMAZAN, D., JIMENEZ-DELGADO, S., CASTILLO-FERNANDEZ, O., SAMITIER, J., JANE, R., MARTINEZ, E. & RAYA, A. 2019. Engineered Macroscale Cardiac Constructs Elicit Human Myocardial Tissue-like Functionality. *Stem Cell Reports,* 13**,** 207-220.

WIEGERINCK, R. F., COJOC, A., ZEIDENWEBER, C. M., DING, G., SHEN, M., JOYNER, R. W., FERNANDEZ, J. D., KANTER, K. R., KIRSHBOM, P. M., KOGON, B. E. & WAGNER, M. B. 2009. Force frequency relationship of the human ventricle increases during early postnatal development. *Pediatr Res,* 65**,** 414-9.

WU, Y., BELL, S. P., TROMBITAS, K., WITT, C. C., LABEIT, S., LEWINTER, M. M. & GRANZIER, H. 2002. Changes in titin isoform expression in pacing-induced cardiac failure give rise to increased passive muscle stiffness. *Circulation,* 106**,** 1384-9.

WYCZALKOWSKI, M. A., CHEN, Z., FILAS, B. A., VARNER, V. D. & TABER, L. A. 2012. Computational models for mechanics of morphogenesis. *Birth Defects Res C Embryo Today,* 96**,** 132-52.

XU, X. Q., SOO, S. Y., SUN, W. & ZWEIGERDT, R. 2009. Global expression profile of highly enriched cardiomyocytes derived from human embryonic stem cells. *Stem Cells,* 27**,** 2163-74.

ZHANG, W., KONG, C. W., TONG, M. H., CHOOI, W. H., HUANG, N., LI, R. A. & CHAN, B. P. 2017. Maturation of human embryonic stem cell-derived cardiomyocytes (hESC-CMs) in 3D collagen matrix: Effects of niche cell supplementation and mechanical stimulation. *Acta Biomater,* 49**,** 204-217.

ZIMMERMANN, W. H., FINK, C., KRALISCH, D., REMMERS, U., WEIL, J. & ESCHENHAGEN, T. 2000. Three-dimensional engineered heart tissue from neonatal rat cardiac myocytes. *Biotechnol Bioeng,* 68**,** 106-14.

ZIMMERMANN, W. H., SCHNEIDERBANGER, K., SCHUBERT, P., DIDIE, M., MUNZEL, F., HEUBACH, J. F., KOSTIN, S., NEUHUBER, W. L. & ESCHENHAGEN, T. 2002. Tissue engineering of a differentiated cardiac muscle construct. *Circ Res,* 90**,** 223-30.

Acknowledgments

First of all, I would like to offer my sincerest gratitude to my supervisor, dear Prof. Dr. med. Andreas Dendorfer, who guided me throughout my whole doctoral study. The old Chinese Proverbs " One should treat his mentor with reverence as his father " is certainly not an exaggeration here to express my thanks. Prof. Dendorfer has always supported me both scholastically and in my life. I could always ask him in the first place without hesitation. The meetings and conversations were vital in inspiring me to consider new ideas and structure a comprehensive consideration from different points of view. I will always appreciate his recognition of my work and generous support throughout the past years.

My most profound thanks also go to Dr. med. Roland Tomasi. Without his effort in carrying out experiments, processing data, and reviewing the manuscript, I could not complete the publications efficiently and successfully. I would also like to thank PD Dr. med. Thomas Seidel for supporting the bioimaging and giving me valuable advice on reviewing and submitting the manuscript. I need to give my incredible acknowledgements to Prof. Dr. Alessandra Moretti and her research group for providing the induced pluripotent stem cells, which made this project possible in any case. Her valuable experience and inspirative advice have made my whole experiments and submission much more straightforward. I want to thank Dr. Xiaochun Cao-Ehlker for her help in establishing the iPS cell culture method, as well as the outstanding lab technicians Claudia Fahney and Meiping Wu for their kindness and patience in supporting me with all laboratory techniques. I really appreciate the support and advice from my Co-supervisor, Prof. Dr. Christian Schulz. I also thank PD Dr. rer. nat Steffen Dietzel and Dr. rer. nat. Andreas Thomae for their time and patience in teaching me with the confocal microscope.

I would like to express my thankfulness to the Förderprogramm für Forschung und Lehre (FöFoLe) for providing me the 18 months of financial support and all the well-organized seminars, workshops, and events. It is my extraordinary pleasure to be enrolled in this program and meet with its professional teaching faculties. Living and studying abroad is a challenging but fantastic experience. I am grateful for all my dear companions, lovely group members and colleagues - Tingting Wu, Zakir Chew, Jiawei Ying, Ting Jiang, Marie Semmler, Zheming Liu, Jiehua Qiu, Zhe Zhang, Lulu Liu, Huaqian Wang, and every friend, who have always believed in me, encouraged me, and supported me, especially during my most frustrating moments. My study and life here surely would not

be this productive and colorful without their company. The picnics by the river, trips to beautiful cities, eating hotpots, drinking all kinds of beer, and playing tabletop games with you guys are the most enjoyable times for me. I will never forget the wonderful time we spent together, and it will be my most precious memory.

Last but not least, I would like to express my most sincere gratitude to my parents and my wife for their constant and unconditional understanding, love, and support. Without you, I could never have accomplished what I have today.

Affidavit

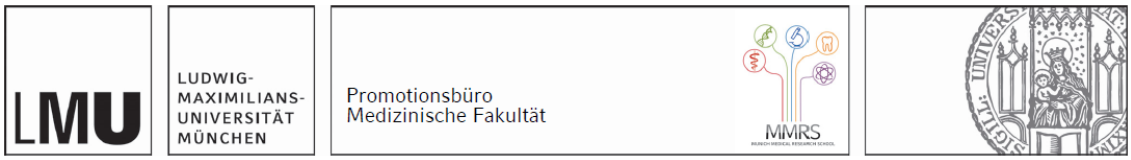

Eidesstattliche Versicherung

Lu, Kun

Name, Vorname

Ich erkläre hiermit an Eides statt, dass ich die vorliegende Dissertation mit dem Titel:

Maturation of human-induced pluripotent stem cell-based myocardium by biomechanical stimulation of three-dimensional tissue cultures

selbständig verfasst, mich außer der angegebenen keiner weiteren Hilfsmittel bedient und alle Erkenntnisse, die aus dem Schrifttum ganz oder annähernd übernommen sind, als solche kenntlich gemacht und nach ihrer Herkunft unter Bezeichnung der Fundstelle einzeln nachgewiesen habe.

Ich erkläre des Weiteren, dass die hier vorgelegte Dissertation nicht in gleicher oder in ähnlicher Form bei einer anderen Stelle zur Erlangung eines akademischen Grades eingereicht wurde.

München, 25.06.2023 **Lu, Kun**

Ort, Datum

Unterschrift Doktorand

List of publications

Original articles

1. **Lu K**, Seidel T, Cao-Ehlker X, Dorn T, Batcha AMN, Schneider CM, Semmler M, Volk T, Moretti A, Dendorfer A, Tomasi R. Progressive stretch enhances growth and maturation of 3D stem-cell-derived myocardium. **Theranostics**. 2021 Apr 15;11(13):6138-6153. doi: 10.7150/thno.54999. PMID: 33995650; PMCID: PMC8120210. (IF_{2020} 11.5). The dissertation has been partially published in this paper.
2. Fischer C, Milting H, Fein E, Reiser E, **Lu K**, Seidel T, Schinner C, Schwarzmayr T, Schramm R, Tomasi R, Husse B, Cao-Ehlker X, Pohl U, Dendorfer A. Long-term functional and structural preservation of precision-cut human myocardium under continuous electromechanical stimulation in vitro. **Nat Commun.** 2019 Jan 10;10(1):117. doi: 10.1038/s41467-018-08003-1. PMID: 30631059; PMCID: PMC6328583. (IF_{2020} 14.9)
3. Poch CM, Foo KS, De Angelis MT, Jennbacken K, Santamaria G, Bähr A, Wang QD, Reiter F, Hornaschewitz N, Zawada D, Bozoglu T, My I, Meier A, Dorn T, Hege S, Lehtinen ML, Tsoi YL, Hovdal D, Hyllner J, Schwarz S, Sudhop S, Jurisch V, Sini M, Fellows MD, Cummings M, Clarke J, Baptista R, Eroglu E, Wolf E, Klymiuk N, **Lu K,** Tomasi R, Dendorfer A, Gaspari M, Parrotta E, Cuda G, Krane M, Sinnecker D, Hoppmann P, Kupatt C, Fritsche-Danielson R, Moretti A, Chien KR, Laugwitz KL. Migratory and anti-fibrotic programmes define the regenerative potential of human cardiac progenitors. **Nat Cell Biol.** 2022 May;24(5):659-671. doi: 10.1038/s41556-022-00899-8. Epub 2022 May 12. PMID: 35550611; PMCID: PMC9106586. (IF_{2021} 28.2)
4. Hamers J, Sen P, Merkus D, Seidel T, **Lu K**, Dendorfer A. Preparation of Human Myocardial Tissue for Long-Term Cultivation. **J Vis Exp.** 2022 Jun 2;(184). doi: 10.3791/63964. PMID: 35723462. (IF_{2021} 1.4)
5. Cao-Ehlker X, Fischer C, **Lu K**, Bruegmann T, Sasse P, Dendorfer A, Tomasi R. Optimized Conditions for the Long-Term Maintenance of Precision-Cut Murine Myocardium in Biomimetic Tissue Culture. **Bioengineering (Basel)**. 2023 Jan 28;10(2):171. doi: 10.3390/bioengineering10020171. PMID: 36829664; PMCID: PMC9952453. (IF_{2022} 5.0)

Conference contributions

1. **Lu K,** Tomasi R, Cao-Ehlker X, Dendorfer A. (2019): The effect of progressive stretch on human-engineered heart tissue maturation. EMBL Symposium Mechanical Forces in Development 2019, 03-06.07.2019, Heidelberg, Germany
2. Schneidereit D, Sulistio AA, Bröllochs A, **Lu K**, Distler T, Schürmann S, Detsch R, Dendorfer A, Boccaccini AR, Friedrich O. (2018) 3D Tissue Substructure: Using Multi-Photon Excitation to Reveal Cellular 3D Morphology of Natural and Engineered Tissue in Depth, Annual Conference of the International Society for Biofabrication (ISBF), 28-31.10.2018 Würzburg, Germany
3. **Lu K,** Cao-Ehlker X, Tomasi R, Schneider CM, Dendorfer A. (2018): The effect of progressive stretch on human-engineered heart tissue maturation. MHA Summer Meeting 2018, 19.07.2018, Starnberger See, Germany